FORMATION OF AMMONIUM NITRATE AEROSOLS BY GAS-PHASE REACTION OF AMMONIA AND NITROGEN DIOXIDE

By

WALID SALEH BOU-HAMRA

Bachelor of Chemical Engineering
Kuwait University
Kuwait
1981

Master of Science
Oklahoma State University
Stillwater, Oklahoma
1985

Submitted to the Faculty of the
Graduate College of the
Oklahoma State University
in partial fulfillment of
the requirements for
the Degree of
DOCTOR OF PHILOSOPHY
December, 1988

FORMATION OF AMMONIUM NITRATE AEROSOLS BY
GAS-PHASE REACTION OF AMMONIA
AND NITROGEN DIOXIDE

Thesis Approved:

Mayis Seapan
Thesis Adviser

M. S. Rockley

Robert S. Robinson Jr.

Harry L. Fuller

Norman N. Durham
Dean of the Graduate College

ABSTRACT

With the increased emissions of nitrogen oxides, atmospheric nitrate aerosols have become a great concern. The presence of total nitrate in the atmosphere is as much as 25% of the total aerosol pollutants, in which ammonium nitrate is always in equilibrium with ammonia and nitric acid. Although ammonium nitrate is a major pollutant in the atmosphere, very limited data exists on its concentrations and size distributions and mechanisms of formation. The aim of this work was to study the formation and growth of ammonium nitrate aerosols from the gas-phase reaction of nitrogen dioxide and ammonia in air, with the specific objective to identify the mechanisms of aerosol formation and growth. The NO_2-NH_3 reaction was studied in a laminar flow aerosol reactor. A TSI differential Mobility Particle Sizer (DMPS), interfaced with an IBM/XT personal computer, was used to measure the size distributions in the range of 0.01-1.0 μm. The concentrations of the reactants after mixing were in the range of 0.5-14 ppm. The reaction was studied at the atmospheric pressure and in the temperature range of 4.4-21.0 °C (40-70 °F).

Ammonium nitrate aerosols form by the homogeneous nucleation and grow by the condensation of the monomeric NH_4NO_3 and to a lesser extent by the adsorption of NH_3 and HNO_3 vapors on the particle surface followed by the surface reaction of the adsorbed species. A number distribution equation, based on the condensation equation, fits the measured data well. This indicates that the condensation of ammonium

nitrate is the dominant particle growth process. The evolution of the size distributions shows that the growth by volume reaction is not possible and coagulation is not significant in the reaction conditions under study. The experimental critical particle diameter was found to be in the range of 0.018-0.052 μm. The results showed an average particle diameter in the range of 0.2-0.4 μm at the reaction conditions under study. As expected the critical particle size decreased and the concentration increased when the temperature was decreased.

ACKNOWLEDGMENTS

I wish to express my sincere gratitude and deep appreciation to my major adviser, Dr. Mayis Seapan, for his concern, help, and encouragement throughout my graduate work. I am also grateful to the other committee members, Drs. R. L. Robinson, Jr. G. Foutch, and M. Rockley for their assistance, and invaluable advice during the course of this work. I would also like to thank the School of Chemical Engineering of Oklahoma State University for providing me the opportunity, space, and supplies to conduct this research. My deep appreciation belongs to the Embassy of Kuwait and Kuwait University for their finanical and emotional support.

Finally, I wish to thank my parents and my wife for their love and encouragment throughout this study.

TABLE OF CONTENTS

LIST OF TABLES

LIST OF FIGURES

Figure Page

Figure Page

Figure Page

NOMENCLATURE

A	parameter in equation [25]
B	parameter in equation [25]
C	parameter in equation [25]
C_1	Cunningham slip correction factor
D	diffusivity of molecules, $cm^2\ s^{-1}$
D_P	particle diameter, cm
$\overline{D}_{pg}$	median diameter (defined as the diameter for which exactly one-half of the particles are smaller and one-half are larger than the median size)
e	elementary unit of charge (4.803×10^{-10} $erg^{1/2}$ $cm^{1/2}$)
E	electrical field strength, volts cm^{-1}
g^*	number of vapor molecules in an embryo or nucleus of a critical size, molecule
ΔG_T^o	change in Gibbs free energy
I_m^r	a reference value of the rate of change in the particle mass
J	nucleation rate, $cm^{-3}\ s^{-1}$
J_c	rate of increase in the number of molecules on the particle, molecule $cm^{-2}\ s^{-1}$
k	Boltzmann constant, 1.38×10^{-16} dyne cm K^{-1} $molecule^{-1}$
K_1	dissociation constant of the ammonium nitrate
L	length between the sample exit slit and the aerosol inlet slit in EC (44.44 cm)
m	mass of one particle, g
m_1	mass of a molecule, g $molecule^{-1}$
n_i	number of moles of species i at any time

n_i^o	initial moles of species i at any time
n_i^r	reacted moles of species i at any time
N_1	equilibrium concentration of clusters at the critical size, molecule cm^{-3}
N_{np}	concentration of particles of diameter D_p carrying n_p charges
N_o	concentration of particles carrying zero units of charges
P	partial pressure, atm (or dyne cm^{-2})
p_o	vapor pressure, dyne cm^{-2}
p_1	partial pressure of NO_2, atm.
p_2	partial pressure of NH_3, atm.
p_3	partial pressure of HNO_3, atm.
p_4	partial pressure of H_2O, atm.
p_5	partial pressure of N_2, atm.
p_6	partial pressure of NH_4NO_3, atm.
q_t	total flow inside the EC $cm^3\ s^{-1}$
q_s	sample aerosol outlet flowrate $cm^3\ s^{-1}$
q_a	aerosol inlet flowrate $cm^3\ s^{-1}$
r_1	inner electrode radius (for EC r_1 = 0.937 cm)
r_2	outer electrode radius (for EC r_2 = 1.958 cm)
r*	radius of the critical size
R	gas law constant
S	supersatruation ratio
t	time, s
T	absolute temperature, K
v_m	molecular volume of the monomer, cm^3 molecule^{-1}
v_l	volume of a molecule in the liquid phase, cm^3 molecule^{-1}
v_e	electrical velocity component, cm s^{-1}
V	voltage on the center electrode of the EC, volts

x	mole fraction of ammonium nitrate in an aqueous solution
Z_p	electrical particle mobility, cm^2 volts^{-1} s^{-1}
α_1, α_2	constants
β_1, β_2	constants
$\beta(K_n)$	correction factor in terms of Knudsen number
λ	mean free path of gas (for air at 1 atm., $\lambda = 0.653 \times 10^{-5}$ cm)
μ	dimensionless particle mass, $\mu = m/\rho_p\lambda^3$
μ_1	gas viscosity (for air at 1 atm. and 20 °C, $\mu_1 = 1.83 \times 10^{-6}$ poise)
ρ_p	particle density, g cm^{-3}
σ	surface tension, dyne cm^{-1}
σ_g	geometric standard deviation
τ	dimensionless time = $tI_m^r/\rho_p\lambda^3$

CHAPTER I

INTRODUCTION

The formation and growth of aerosols by gas-phase reactions are important both in industrial processes and in the atmosphere. The gas-phase reactions produce monomeric species which nucleate to form stable particles. As soon as the particles form, they grow by different mechanisms. One important gas-phase reaction, responsible for the production of solid particles, is that between ammonia and nitrogen dioxide to produce ammonium nitrate. The importance of this reaction comes from its applications in atmospheric studies as well as in industry. This reaction can take place naturally in the atmosphere to produce ammonium nitrate particles. Ammonium nitrate can also form and deposit in different sections of industrial plants where ammonia and nitrogen oxides exist together. For instance, ammonium nitrate forms and deposits in the nitrous oxide gas compressors of nitric acid plants (Mearns and Ofosu-Asiedu, 1984a). Another example is in the injection of NH_3 in fume stacks to eliminate the NO_x emissions.

The major product of the reaction between NH_3 and NO_2 is ammonium nitrate (NH_4NO_3) (Falk, 1955). This product is of a great concern because of its effects on earth's radiation energy balance, its adverse effects on human health, and its role in reducing atmospheric visibility. The presence of ammonium nitrate in the atmosphere has been identified in several urban and rural areas. Most studies suggest that

atmospheric ammonium nitrate is in equilibrium with its precursors, NH_3 and HNO_3. The harmful effect of ammonium nitrate aerosols rises from the small particle size and number concentration that it has in the atmosphere.

The chemical reaction between NH_3 and NO_2 was reported as early as 1906 (Besson and Rosset, 1906). Later investigations of the NH_3-NO_2 system were concerned with the stoichiometry and kinetics of this reaction (Falk, 1955; and Mearns and Ofosu-Asiedu, 1984a,b). Only a few studies were conducted on the formation of ammonium nitrate aerosols (Olszyna et al., 1974; and Kodas et al., 1986). These investigations considered the formation of ammonium nitrate either from the reaction of ozone and ammonia or from the irradiation of a mixture of NO_2, NH_3, C_3H_6 and air. However, formation of aerosols from the direct reaction of NH_3 and NO_2 has not been studied. An understanding of the mechanisms of particle formation and growth of this system in an aerosol reactor can bridge the gap between the reaction kinetics and the complex chemical systems of the atmosphere.

The objective of this work is to study the mechanisms of formation and growth of ammonium nitrate aerosols from the reaction of ammonia and nitrogen dioxide in an initially dry air. A laminar flow aerosol reactor was used in this project and the measured total number concentration and particle size distributions were used to examine the dynamics of the ammonium nitrate aerosols. A simulation model based on the reaction kinetics and general aerosol dynamics was developed and used to verify the particle formation and growth mechanisms.

In this work the gas-phase reaction of ammonia and nitrogen dioxide was carried out at atmospheric pressure in the temperature range of

4.4-21 °C (40-70 °F). The concentrations of the reactants, after mixing, were in the range of 0.5-14 ppm and the residence time was in the range of 3-30 s. A Thermal System Incorporation (TSI) Differential Mobility Particle Sizer (DMPS) interfaced with an IBM/XT personal computer was used to measure the total number concentrations and the size distributions of the aerosols in the particle size range of 0.01-1.0 μm.

The results of this study showed that the primary mechanisms for formation and growth of ammonium nitrate aerosols are the homogeneous nucleation followed by the condensation of ammonium nitrate vapor on the freshly nucleated particles.

A number distribution function, based on the condensation equation, provided a good fit to the measured size distributions. These findings assured that the condensation of ammonium nitrate was the dominant particle growth process. The evolution of the size distributions showed that coagulation was not significant in the reaction conditions under study. The experimental critical particle size was found to be in the range of 0.018-0.052 μm. The median diameter and the geometric standard deviation used to fit the measured size distribution were in the range of 0.1-0.35 μm and 1.5-2.0, respectively.

CHAPTER II

SCIENTIFIC DISCUSSION

This chapter briefly reviews some of the experimental and theoretical studies available in the literature, which are concerned with ammonium nitrate aerosols. The review is presented in four sections. The first section reviews the experimental measurements of the total concentration and size distribution of ammonium nitrate in the atmosphere and in laboratory experiments. The second section presents the stoichiometry and kinetics of the reaction of ammonia and nitrogen dioxide. The third section briefly discusses the theoretical models dealing with the aerosol dynamics. Finally, the fourth section presents some of the thermodynamic and physical properties of ammonium nitrate.

2.1 Experimental Data on Ammonium Nitrate

Several investigators have measured the concentration and size distribution of total nitrate in the atmosphere (Kadowaki, 1977; Moskowitz, 1977; Apple, et al., 1980; Forrest, et al., 1980; Greenfelt, 1980; Appel, et al., 1981; Shaw, et al., 1982; Forrest, et al., 1982; Cadle, et al., 1982; and Yoshizumi, et al., 1985). A major observation from these studies is that the atmospheric nitrate consists mainly of two compounds. The volatile ammonium nitrate (NH_4NO_3), which has a size distribution in the fine particle size range (0.01-1.0 μm), and the nonvolatile sodium nitrate ($NaNO_3$), which has a size distribution in the

course particle size range (1.0-30 μm). As reported in some of these studies, the size distribution of ammonium nitrate measured in the winter differs from that measured in the summer (Cadle, 1982; Yoshizumi, et al., 1985). The measurements taken in the winter showed a higher number concentration of ammonium nitrate than those taken in the summer. The seasonal variation in the ammonium nitrate concentration and aerosol size distribution have been related to the dependence of NH_4NO_3 vapor pressure on temperature.

There are several works that studied the formation and characterization of aerosols by chemical reactions in laboratory flow reactors (de Pena, et al., 1973; Olszyna, et al., 1974; Dahlin, et al., 1981; Henry, et al., 1983; Vega and Peters, 1983; Tran and Seapan, 1984; and Kodas, et al., 1986). However, only a few studies were concerned with the formation of ammonium nitrate particles (de Pena, et al., 1973; Olszyna, et al., 1974; Kodas, et al., 1986; and Kodas and Friedlander, 1988). de Pena, et al., 1973; and Olszyna, et al., 1974 studied the formation of NH_4NO_3 by the reaction of NH_3 and O_3 at room temperature. Their experiments showed an initial induction time before any particles could form. After the product of $[NH_3]$ and $[O_3]$ reached 5.8×10^{27} $(molecules/cm^3)^2$, the nucleation of particles occurred only during a short period of time. As the reaction proceeded, the particles already present continued to grow and maintained a fairly uniform size, while the particle number density slowly decreased. Therefore, they suggested that the mechanism of the particle formation and growth was composed of four stages: induction period, particle nucleation, particle growth, and particle removal.

In the first study, de Pena, et al., 1973, reported that the

particles grew mainly by the condensation of the monomeric NH_4NO_3 on the particle surface and that most of the particles were lost to the wall. However, in their later study, Olszyna, et al., 1974, reported that the two possible routes of particle growth were the condensation of HNO_3 on the particles followed by the surface reaction with NH_3, and the second route was the condensation of NH_4NO_3 on the particles. Their study showed that the former route was the most dominant, with most of the monomer, HNO_3, being lost to the particle surface rather than to the walls.

Kodas, et al., 1986, studied the formation of ammonium nitrate particles by irradiation of NO_2, NH_3, C_3H_6 and air in a laminar core reactor. They used an Electrical Aerosol Analyzer (EAA) with an Optical Particle Counter (OPC) to measure the size distribution of the aerosols. They found that most of the monomers (HNO_3 in their case) formed by chemical reaction were lost to the wall. Their measurements showed an average particle diameter in the range of 0.01-0.05 μm with no particles larger than 0.09 μm formed. They concluded that coagulation was not important for total number concentrations less than 10^6 particle/cm^3 and residence times less than 30 seconds. The variation in their total concentration from different experiments having the same conditions was up to a factor of two.

2.2 Kinetics of the Ammonia-Nitrogen Dioxide Reaction

Falk, 1955, studied the stoichiometry and kinetics of the reaction of ammonia and nitrogen dioxide. He suggested that below 100 °C the stoichiometry of the reaction can be represented by:

$$2NO_2 + 2NH_3 \longrightarrow N_2 + H_2O + NH_4NO_3 \quad [1]$$

where ammonium nitrate particles (NH_4NO_3) are the major product of this reaction especially at low temperatures.

The reaction was thought to proceed by the following elementary steps, where two NO_2 molecules react first to form the reactive N_2O_4 species:

$$N_2O_4 + NH_3 \longrightarrow N_2O_4 \cdot NH_3 \quad [2]$$

$$N_2O_4 \cdot NH_3 \longrightarrow HNO_3 + NH_2 \cdot NO \quad [3]$$

$$HNO_3 + NH_3 \longrightarrow NH_4NO_3 \quad [4]$$

$$NH_2 \cdot NO \longrightarrow N_2 + H_2O \quad [5]$$

After H_2O is formed, the following steps also start to take part in the overall reaction:

$$N_2O_4 + H_2O \longrightarrow N_2O_4 \cdot H_2O \longrightarrow HNO_3 + HNO_2 \quad [6]$$

$$HNO_2 \longrightarrow OH + NO \quad [7]$$

$$OH + NH_3 \longrightarrow H_2O + NH_2 \quad [8]$$

$$NH_2 + NO \longrightarrow N_2 + H_2O \quad [9]$$

Falk, 1955 controlled the flowrates of NH_3 and/or NO_2 so that mixing was obtained only by diffusion. His experiments showed that the solid ammonium nitrate formed throughout the reactor. This indicated that the reaction was too slow to be diffusion controlled. He reported that the rate-controlling step was the collision between NH_3 and N_2O_4 molecules.

Tran and Seapan, 1984, analyzed the solid product of the NO_2-NH_3 reaction in air and their results showed that the major product was ammonium nitrate. They also detected low concentrations of ammonium nitrite with the ratio of nitrate to nitrite varying from 0.1% to 1% nitrite. This result agrees with the findings of Falk, 1955.

In a work similar to that of Falk (1954, 1955), Mearns and Ofosu-Asiedu (1984a, 1984b) studied the kinetics of the reaction between nitrogen oxides, ammonia, water vapor and oxygen. Their study considered very low concentrations of these reactants (128-430 Nm^{-2}) in nitrogen. Their experiments suggested that when only nitrogen dioxide and ammonia were present, such as at the beginning of the reaction between these two species, the reaction mechanism was described by:

$$2\ NO_2 \underset{k_2}{\overset{k_1}{\rightleftharpoons}} N_2O_4 \qquad [10]$$

$$N_2O_4 + NH_3 \xrightarrow{k_3} HNO_3 + NH_2 \cdot NO \qquad [11]$$

$$NH_2 \cdot NO \xrightarrow{k_4} N_2 + H_2O \qquad [5]$$

with the following overall stoichiometry:

$$NH_3 + 2NO_2 \longrightarrow N_2 + H_2O + HNO_3 \qquad [12]$$

However, when nitrogen dioxide, ammonia, and water were present initially, or after the formation of water as the reaction between ammonia and nitrogen dioxide proceeded, Mearns and Ofosu-Asiedu, 1984a, suggested the following reaction mechanism:

$$2NO_2 \underset{k_2}{\overset{k_1}{\rightleftharpoons}} N_2O_4 \qquad [10]$$

$$N_2O_4 + NH_3 \xrightarrow{k_3} HNO_3 + NH_2 \cdot NO \qquad [11]$$

$$N_2O_4 + H_2O \xrightarrow{k_5} HNO_3 + HNO_2 \qquad [13]$$

$$NH_3 + HNO_2 \underset{k_7}{\overset{k_6}{\rightleftharpoons}} NH_4NO_2\ (s) \qquad [14]$$

$$HNO_3 + NH_3 \underset{k_9}{\overset{k_8}{\rightleftharpoons}} NH_4NO_3\ (s) \qquad [4]$$

$$NH_2 \cdot NO \xrightarrow{k_4} N_2 + H_2O \qquad [5]$$

They suggested that the reaction between NH_3 and NO_2, either in the presence or the absence of other gases, can be considered to occur in two steps. The first step includes the reaction between NH_3 and NO_2 to form nitric acid. The second step starts when the solid ammonium nitrate begins to form. The solid nitrate forms when $P_{NH_3} \cdot P_{HNO_3} \geq K_1$, where K_1 is the dissociation constant of the nitrate according to reaction [15]:

$$NH_4NO_3\ (s) \rightleftharpoons HNO_3\ (g) + NH_3\ (g) \qquad [15]$$

The following equation gives the stoichiometry which describes the first step of the reaction (i.e. up to the formation of the nitrate):

$$NH_3 + 2\ NO_2 \longrightarrow N_2 + H_2O + HNO_3 \qquad [12]$$

with the rate of reaction given by:

$$\frac{-dP_{NO_2}}{dt} = 2\,\frac{dP_{HNO_3}}{dt} = k_a P_{NH_3} P^2_{NO_2} + k_b P_{H_2O} P^2_{NO_2} \qquad [16]$$

or

$$\frac{-dP_{NO_2}}{dt} = 2\,\frac{dP_{HNO_3}}{dt} = k_a P_{NH_3} P^2_{NO_2} + k_b P_{H_2O} P^2_{NO_2} - k_c P_{O_2} P^2_{NO} \qquad [17]$$

where equation [17] applies if oxygen and NO are initially present or added to the reactants.

The following equation gives the stoichiometry and rate of the reaction for the second step (i.e. after the formation of nitrate):

$$2NO_2 + 2NH_3 \longrightarrow N_2 + H_2O + NH_4NO_3 \qquad [1]$$

and

$$\frac{-dP_{NO_2}}{dt} = k_a P_{NH_3} P^2_{NO_2} + k_b P_{H_2O} P^2_{NO_2} - k_c P_{O_2} P^2_{NO} \qquad [18]$$

If there is no O_2 or NO initially present or added to the system, equation [18] reduces to equation [16].

They used the theoretical kinetic model, described by equations [17] and [18], to calculate a threshold partial pressure of ammonia below which no solid material formed regardless of the partial pressure of nitrogen dioxide and water vapor. This threshold partial pressure is given by:

$$p = 2\,(K_1)^{1/2} \qquad [19]$$

where K_1 is the equilibrium constant of reaction [15] given by

$$\ln K_1 = 34.685 - 21506.145/T \qquad [20]$$

where T is the absolute temperature in K and K_1 has the units of bar^2.

Their study showed that the concentrations of NO_2 and H_2O had an effect only on the induction time and had no influence on the magnitude of the threshold pressure of NH_3. The time for the onset of salt formation could be shortened by increasing the partial pressure of NO_2. For a given temperature and residence time, the threshold partial pressure of NH_3 increased as the partial pressure of NO_2 decreased. The presence of the water vapor accelerated the reaction rate and made it possible for the salt to form at lower NO_2 partial pressures.

The mechanisms of Falk (1954, 1955) and Mearns and Ofosu-Asiedu (1984a) are very similar and both consider the dinitrogen tetroxide (N_2O_4) to be the reactive species rather than the nitrogen dioxide (NO_2).

2.3 Aerosol Dynamic Models

Numerous theoretical studies, based on the classical nucleation theory, have been developed to model the aerosol dynamics in the atmosphere and in aerosol flow reactors. These studies include the work of Middleton, et al., 1976; Gelbard and Seinfeld, 1978, 1979, 1980; Dahlin, et al., 1981; Henry, et al., 1981; Vega and Peters, 1983; Warren and Seinfeld, 1984, 1985; Kodas, et al., 1986; Pratsinis, et al., 1986; Pilinis and Seinfeld, 1987; Kodas and Friedlander, 1988; and Russell et al., 1988. The General Dynamic Equation (GDE) of aerosol derived by

Gelbard and Seinfeld, 1978, 1979, 1980 was based on the population balance equation for particulate systems. The theoretical study of Pratsinis, et al., 1986 was based on the first three moments of the size distribution derived by Friedlander, 1977, 1983.

Dahlin, et al., 1981 applied a theoretical model to the anhydrous NH_3-HCl system. The experimental data of Su, 1979 were simulated in terms of the gas-phase reaction, homogeneous nucleation of the product, and the growth of particles by different growth mechanisms. The growth mechanisms considered were diffusion, surface reaction, and cluster scavenging. It was found that at low concentrations of reactants, the growth by monomer diffusion was the predominant mechanism. At high concentrations, cluster scavenging became more important. Coagulation was not important for the range of conditions in their study.

Henry,, et al., 1983 used the model of Dahlin, et al., 1981 to predict the experimental data of Gonzalez, 1980. They also examined the processes that affected the quality of data. These processes included the particle loss to the reactor walls at high residence times, sedimentation, thermophoresis, and deposition due to particle charge. They found that none of these processes had any effect on the experimental data. Their study of the temperature effect showed an increase in both the total number density and the total particle volume as the temperature decreased. This was explained by the increase in the nucleation rate with the decrease in temperature.

The study of Henry, et al., 1983 showed that as the residence time increased, the total number density and the total particle volume followed similar trends regardless of the temperature or the initial reactant concentrations. At very short residence times, the total

number and total volume of particles were zero due to the induction time that the particles needed to form. After the induction period, the total number and total volume of the particles increased extremely rapidly, indicating that nucleation occurred in a burst. After which, the existing particles grew rapidly.

Kodas, et al., 1986 used an extension of the model of Pratsinis, et al., 1986 to simulate the aerosol dynamics in a laminar flow reactor. The experimental data of ammonium nitrate were produced by irradiation of NH_3-NO_2-C_3H_6 in air. They considered nitric acid to be the monomer. The model predicted very small values for the ratio of HNO_3 in the aerosol to the total concentration of HNO_3 produced. The predicted low yield agreed with their experimental measurements and explained as losses of the product to the wall. They reported that particle growth occurred by surface reaction where the limiting step was the collision of the nitric acid molecules with the embryo and the rate of ammonium nitrate particle growth was determined by the monomer flux. The surface tension and rate of monomer formation were obtained by fitting the particle concentrations and the average particle diameter predicted by theory to the experimental data. An ammonium nitrate surface tension of 113 erg/cm^2 showed the best fit to their data.

2.4 Thermodynamic and Physical Properties

In general the atmospheric measurements have shown that atmospheric ammonium nitrate is in equilibrium with ammonia and nitric acid (Stelson, et al., 1979; and Stelson and Seinfeld, 1982). In many cases, the measured concentrations of ammonia and nitric acid agree with the concentrations predicted from the ammonium nitrate equilibrium

constant. However, in some urban and rural locations such equilibrium does not exist (Cadle, et al., 1982). The equilibrium of the NH_3-HNO_3-NH_4NO_3 system is very sensitive to temperature. The equilibrium constant (K_1) for the reaction represented by equation [15] equals the dissociation constant of ammonium nitrate. K_1 is related to the partial pressures of NH_3 and HNO_3 and to the standard Gibbs free energy change as shown in equations [21] and [22] respectively (Denbigh, 1971).

$$K_1 = P_{NH_3} \cdot P_{HNO_3} \qquad [21]$$

$$\ln K_1 = - \Delta G_T^o/(RT) \qquad [22]$$

Stelson, et al., 1979 used the thermodynamic data for NH_4NO_3 and integrated the van't Hoff equation to derive the following formula

$$\ln K_1 = 70.68 - 24090/T - 6.04 \ln(T/298) \qquad [23]$$

where K_1 and T have the units of ppm^2 and K, respectively.

Another formula, reported by Stelson, et al., 1979, which is in good agreement with equation [23], is that derived from the measured dissociation pressure of solid NH_4NO_3 of Brander, 1962. The formula is valid for the temperature range of 76 to 165 °C and is shown as follows, where the units are the same as in equation [23],

$$\ln K_1 = 62.296 - 21510/T \qquad [24]$$

Brandner, et al., 1962, experimentally measured the heats of vaporization of solid and liquid NH_4NO_3. These were found to be 42.7 and 39.9 kcal/g-mole respectively. These values agreed with the

literature values of the heats of dissociation calculated from thermodynamic data. This agreement supports the assumption that the solid NH_4NO_3 vaporizes by dissociation into ammonia and nitric acid (Mearns and Ofosu-Asiedu, 1984b). The standard free energies of formation for $NH_3(g)$, $HNO_3(g)$, and $NH_4NO_3(s)$ at 25 °C are -3.915, -17.690 and -43.98 kcal/g-mole respectively (Stelson, et al., 1979).

Falk, 1955 used his experimental data to predict the reaction rate constants k_a and k_b, which can be expressed in the form of an Arrhenius equation. For the first rate constant k_a, shown in equations [14, and 16] he reported an activation energy of 12.8 kcal/g-mole (53.55 kJ/mol) and an Arrhenius factor, A, of 2.94×10^{-3} m^6 $kmol^{-1}$ s^{-1} (5.018×10^{-6} atm^{-2} sec^{-1}) at the temperature range of 22-205 °C. For the second rate constant, k_b, he reported an activation energy of 7 kcal/g-mole (29.29 kJ/mol) and an Arrhenius factor of 0.481 m^6 $kmol^{-2}$ s^{-1} (8.219×10^{-4} atm^{-2} sec^{-1}) at the temperature range of 174-205 °C. Similarly, Mearns and Ofosu-Asiedu, 1984a used their data to predict the k_a and k_b. For k_a, they reported an activation energy of 10.75 kcal/g-mole (45 kJ/mol), and an Arrhenius factor of 1.534 m^6 $kmol^{-2}$ s^{-1} (2.618×10^{-3} atm^{-2} sec^{-1}) in the range of 60-203 °C. For k_b, they reported an activation energy of 5.784 kcal/g-mole (24.2 kJ/mol) and an A factor of 965.6 m^6 mol^{-2} s^{-1} (1.648 atm^{-2} sec^{-1}) at the temperature range of 85-175 °C. When the k-values of Falk, 1955 are used in the theoretical prediction of this work, they showed a better data-fit than the k-values of Mearns and Ofosu-Asiedu, 1984a as will be discussed in Chapter V.

Sacchetto, et al., 1981 determined the vapor pressure of water above an aqueous solution of ammonium nitrate using dew-point measurements. Their experimental data covered a temperature range of 45

to 100 °C with ammonium nitrate mole fractions of 0.0 to 0.35. The empirical correlation of the vapor pressure in kPa is:

$$\log p = (A/T) + B \log(T) + C \qquad [25]$$

where T is the absolute temperature in K and the parameters A, B and C are defined as follows

$$A = -2822.5 + 196\ x - 58\ x^2,$$

$$B = -4.0966,$$

and

$$C = 20.1054 - 1.195\ x \qquad [26]$$

where x is the mole fraction of ammonium nitrate in the solution.

In summary, the atmospheric measurements show that ammonium nitrate is one of the major pollutants in the atmosphere and usually exists in equilibrium with the atmospheric NH_3 and HNO_3. The temperature dependence of the vapor pressure of ammonium nitrate is considered to be responsible for the seasonal variations in total number concentrations and size distributions of the nitrate aerosols. The reaction kinetics of ammonium nitrate show that for solid nitrate to form, the partial pressure of HNO_3 needs to build up so that $P_{NH_3} \cdot P_{HNO_3} \geq K_1$. A review of the laboratory studies and the dynamics of aerosols shows that there are not enough experimental data on the total number concentrations and size distributions of ammonium nitrate aerosols and their dependency on different operating parameters such as temperature, residence time, etc. Furthermore, no systematic study has been conducted regarding the formation of NH_4NO_3 from the reaction of NO_2 with NH_3 in pure air, except for a preliminary study by Tran and Seapan, 1984.

Therefore, the aim of this project is to study the formation and

growth of ammonium nitrate aerosols from the reaction of nitrogen dioxide and ammonia in air with the specific objective to identify the mechanisms of aerosol formation and growth. The NO_2-NH_3 reaction is studied in a laminar flow aerosol reactor. Wide ranges of very low initial reactant concentrations, reaction temperature, and residence times are considered in this project. The experimental data are used to predict the critical nuclei size. The data are then fitted by a theoretical model, based on the reaction kinetics and the principles of the homogeneous nucleation theory. The measured and predicted results are used to present a better understanding of the formation of ammonium nitrate aerosols under different atmospheric conditions.

CHAPTER III

FUNDAMENTALS OF AEROSOL FORMATION AND GROWTH

This chapter will briefly describe the classical homogeneous nucleation theory and the General Dynamic Equation (GDE) for aerosol growth. These principles will later be used in Chapter V to discuss the theoretical model employed in this study.

The classical nucleation theory was originally proposed by Volmer and Weber, 1926. Several improvements have been made to the theory in the later years. Such developments include the work of Farkas, 1927; Volmer, 1929; Kaischew and Stranski, 1934; Becker and Doering, 1935; Volmer, 1939; Frenkel, 1955; Zeldovich, 1942; and Lothe and Pound, 1962. For more in-depth discussion of the classical theory, one can refer to Zettlemoyer, 1969; Springer, 1978; and Seinfeld, 1986.

The term nucleation refers to the formation of new particles from a continuous phase, such as a gas-phase. The homogeneous nucleation is the nucleation of vapor as embryos, or condensed nuclei, in the absence of foreign substances. The nucleation on a foreign substance or surface such as an ion or a solid salt particle is called heterogeneous nucleation (Seinfeld, 1986).

To understand the homogeneous nucleation theory, one needs to know about the thermodynamic equilibrium properties of small particles, saturation and supersaturation. These topics are discussed in detail in the references mentioned above. The supersaturation (S), defined as the

ratio of the partial pressure to the vapor pressure of the condensing species, is related to the critical size of particles via the following formula, which was originally derived by Thomson, 1870:

$$\ln S = 2\sigma v_1 / r^* kT \qquad [27]$$

where σ is the surface tension, r^* is the radius of the critical size, k is the Boltzmann constant and v_1 is the volume of a molecule in the liquid phase defined as (Springer, 1978):

$$v_1 = m_1 / \rho_1 \qquad [28]$$

where m_1 is the mass of one molecule and ρ_1 is the liquid phase density. The corresponding value of the number of molecules in an embryo or nucleus of critical size is defined as:

$$g^* = \frac{32\ \pi\ \sigma^3 v_1^2}{3(kT\ \ln S)^3} \qquad [29]$$

The rate at which new particles form is called the nucleation rate (J), given by:

$$J = \left[\frac{p_1}{(2\pi m_1 kT)^{1/2}}\right]\left[\frac{2\sigma^{1/2} v_1}{(kT)^{1/2}}\right] N_1 \exp\left[\frac{-16\ \pi\ \sigma^3 v_1^2}{3(kT)^3 (\ln S)^2}\right] \qquad [30]$$

where p_1 = partial pressure, dyne cm^{-2}.

m_1 = mass of a molecule, g $molecule^{-1}$.

σ = surface tension, dyne cm^{-1}.

v_1 = volume of a molecule, cm^3 $molecule^{-1}$.

k = Boltzmann constant, 1.380×10^{-16} dyne cm K^{-1} molecule^{-1}.

$N_1 = p_1/kT$, molecule cm^{-3}.

The first term in equation [30] is the flux of the monomers to a unit area, the second term is a correction factor and the third term (N_1) is the equilibrium concentration of clusters of the critical size (Seinfeld, 1986).

The rate of growth of a particle volume based on the condensation equation is given by:

$$\frac{dv}{dt} = I(D_p) = v_m J_c \qquad [31]$$

where v_m is the molecular volume of the monomer. J_c is the flow of molecules to the surface of a spherical particle, or the rate of increase in the number of molecules on the particle, given by the Maxwell equation (Seinfeld, 1986):

$$J_c = 2DD_p P^o(S - 1)/kT \qquad [32]$$

where D = diffusivity of the molecules, $cm^2\ s^{-1}$

D_p = particle diameter, cm.

P^o = vapor pressure, dyne cm^{-2}.

The growth in the particle diameter is given by

$$I_D(D_p) = \frac{dD_p}{dt} = \frac{dD_p}{dv}\frac{dv}{dt} = \frac{2}{\pi D_p^2} I(D_p) = \frac{4Dv_m P^o(S - 1)}{kTD_p} \qquad [33]$$

A special case of the continuous General Dynamic Equation (GDE), developed by Gelbard and Seinfeld, 1979, where coagulation is negligible

and nucleation is the only source of particles. For this case, the solution of the aerosol growth equation, based on the condensation equation and incorporating the log-normal aerosol distribution, is given by (Seinfeld, 1986):

$$n(D_p,t) = \frac{D_p}{(D_p^2 - 2A_D t)} \frac{N_o}{\sqrt{2\pi}\ \ln\sigma_g} \exp\left[-\frac{\ln^2((D_p^2-2A_D t)^{1/2}/\ \overline{D}_{pg})}{2\ \ln^2\sigma_g}\right] \qquad [34]$$

where $A_D = 4Dv_m P^o(S-1)/kT$

$\overline{D}_{pg}$ = median particle diameter (defined as the diameter for which exactly one-half of the particles are smaller and one-half are larger than the median size).

σ_g = geometric standard deviation

and N_o may be defined as

$$N_o = \int_{\sqrt{2A_D t}}^{\infty} n(D_p,t)\,dD_p \qquad [35]$$

Equation [34] can be used to determine the aerosol size distribution at different times, t.

As mentioned above, the aerosols can form either by a homogeneous or a heterogeneous nucleation. As soon as the particles form, they grow by different growth mechanisms. The two main growth mechanisms of the atmospheric aerosols are coagulation and gas-to-particle conversion. The latter mechanism is more dominant for particles in the fine size range (0.01-1.0 μm). Seinfeld, 1986 discussed the three major forms of the gas-to-particle conversion processes and their effects on the

evolution of the aerosol size distribution. The first gas-to-particle process is the diffusion-controlled growth, in which the rate-controlling step is the rate of diffusion of the vapor molecules to the particle surface. For this case, the rate of growth is given by:

$$I(\mu, \tau) = \mu^{1/3} S \beta(K_n) \qquad [36]$$

where μ and τ are dimensionless time and particle mass, defined as:

$$\tau = \frac{t I_m^r}{\rho_p \lambda^3}, \quad \text{and} \quad \mu = \frac{m}{\rho_p \lambda^3}$$

I_m^r is a reference value of the rate of change in the particle mass, ρ_p is the particle density, λ is the mean free path of the vapor, and m is the mass of one particle. S is the saturation ratio and $\beta(K_n)$ is a correction factor defined in terms of Knudsen number as:

$$\beta(K_n) = \frac{1 + K_n}{1 + 1.71K_n + 1.333K_n^2}$$

The second mechanism is the surface reaction-controlled growth, at which the rate-controlling step is the rate of the surface reaction between the adsorbed vapor molecules and the particle surface. The growth rate in this case is given as:

$$I(\mu, \tau) = S\mu^{2/3} \exp(-\omega\mu^{-1/3}) \qquad [37]$$

where μ, τ, and S are as defined above and ω is defined as:

$$\omega = \left(\frac{32\pi}{3}\right)^{1/3} \frac{\sigma \bar{v}}{RT}$$

where σ is the surface tension and $\bar{v}$ is the molar volume of the liquid phase.

The third gas-to-particle process is the volume reaction-controlled growth, in which the rate of growth is controlled uniformly by the conversion of dissolved A to a second species B throughout the volume of the particle. The rate of growth of this case is given by:

$$I(\mu, \tau) = S\mu \exp(-\omega\mu^{-1/3}) \qquad [38]$$

with the parameters as defined above.

As discussed by Seinfeld, 1986, the mechanism of the particle growth can be explained by following the evolution of the aerosol size distribution. He showed that for a diffusion-controlled growth, the smallest particles grow with a rate proportional to D_p^2 (square of the particle diameter) while the larger particles grow at a rate proportional to D_p. For the case of surface reaction-controlled growth, the large particles grow at a rate proportional to D_p^2. However, in the case of volume reaction-controlled growth, the large particles grow at a rate proportional to D_p^3. Therefore, the growth mechanism can be inferred by studying the dependence of the growth rate (I) on the particle diameter for both the small particles (free molecule regime) and the large particles (continuum regime).

This concept is explained further by Figure 1(a,b) which shows the size distributions resulting from the three growth mechanisms discussed above. The significance of the growth of the small and large particles

can be relatively indicated by the position of the peak of the distribution curves. For example, the volume reaction growth, for which the large particles grow at a rate proportional to D_p^3, has a main peak located at the largest particle diameter while diffusion growth with no vapor pressure over the particle surface shows a main peak located at the smallest particle diameter (as shown in Figure 1a where all the size distributions are taken at the same time τ). Figure 1b shows the spectra of these three cases when the total mass added to the aerosol phase equals seven times the initial aerosol mass. In this case, the growth by volume reaction also leads to a size distribution with more large particles than any other. This approach indicates that one can use the experimental evolution of the size distribution to explain the particle growth mechanism.

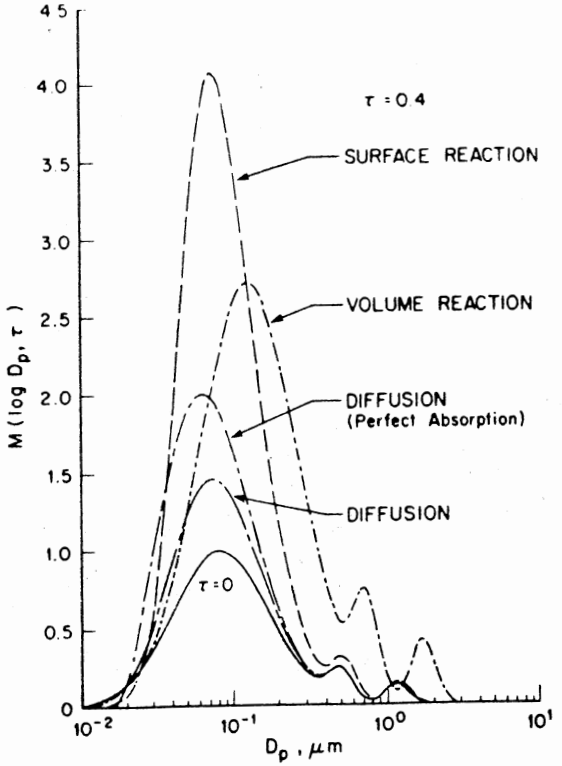

a.) At Dimensionless Time = 0.4 Resulting From Growth by Diffusion, With and Without Perfect Absorption, Surface Reaction, and Volume Reaction

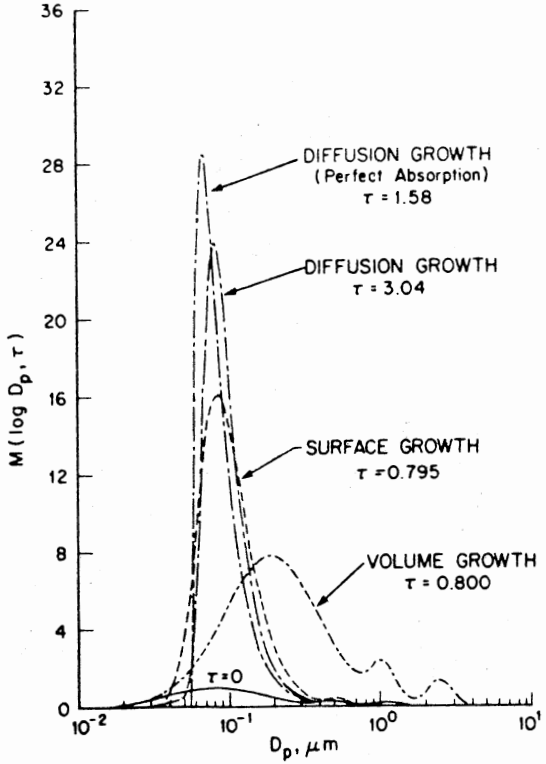

b.) At the Time When the Mass Added by the Gas-to-Particle Conversion is Seven Times the Initial Mass

Figure 1. Evolution of Aerosol Mass Distribution (Seinfeld and Bassett, 1982)

CHAPTER IV

APPARATUS AND EXPERIMENTAL PROCEDURES

4.1 Apparatus

The important components of the experimental system used in this project are shown schematically in Figures 2 and 3. Anhydrous gaseous mixtures of NH_3 and NO_2 (at 30-105 ppm) in air were purchased locally from Sooner Supply Company. Ultrahigh purity air (zero grade) was used to further dilute the NH_3 and NO_2 to the desired concentrations. The air was passed through an air drying filter trap (Regis Chemical Company, model 970014) to remove any water vapor or suspended particles that may exist in the line.

The reactant gases were mixed with the carrier gas in two separate gas proportioners (rotameters) (Air Products, model E22C-150MM43). These proportioners acted as flowmeters and were used to adjust the flowrates of the reactants to the desired values. During the experiments, the flowmeters were calibrated and their calibrations were checked regularly. Appendix A shows the calibration data of these flowmeters. Before entering the reactor, the reactant gases were passed through two high purity filters (Matheson, model 6184T4-FF) to remove particles larger than 0.003 μm. A routine check before each experiment assured that no foreign nuclei was present in either gas stream.

The reactor was a 70 mm ID x 75 mm OD x 850 mm long pyrex glass tube. In order to obtain a quick and efficient mixing inside the

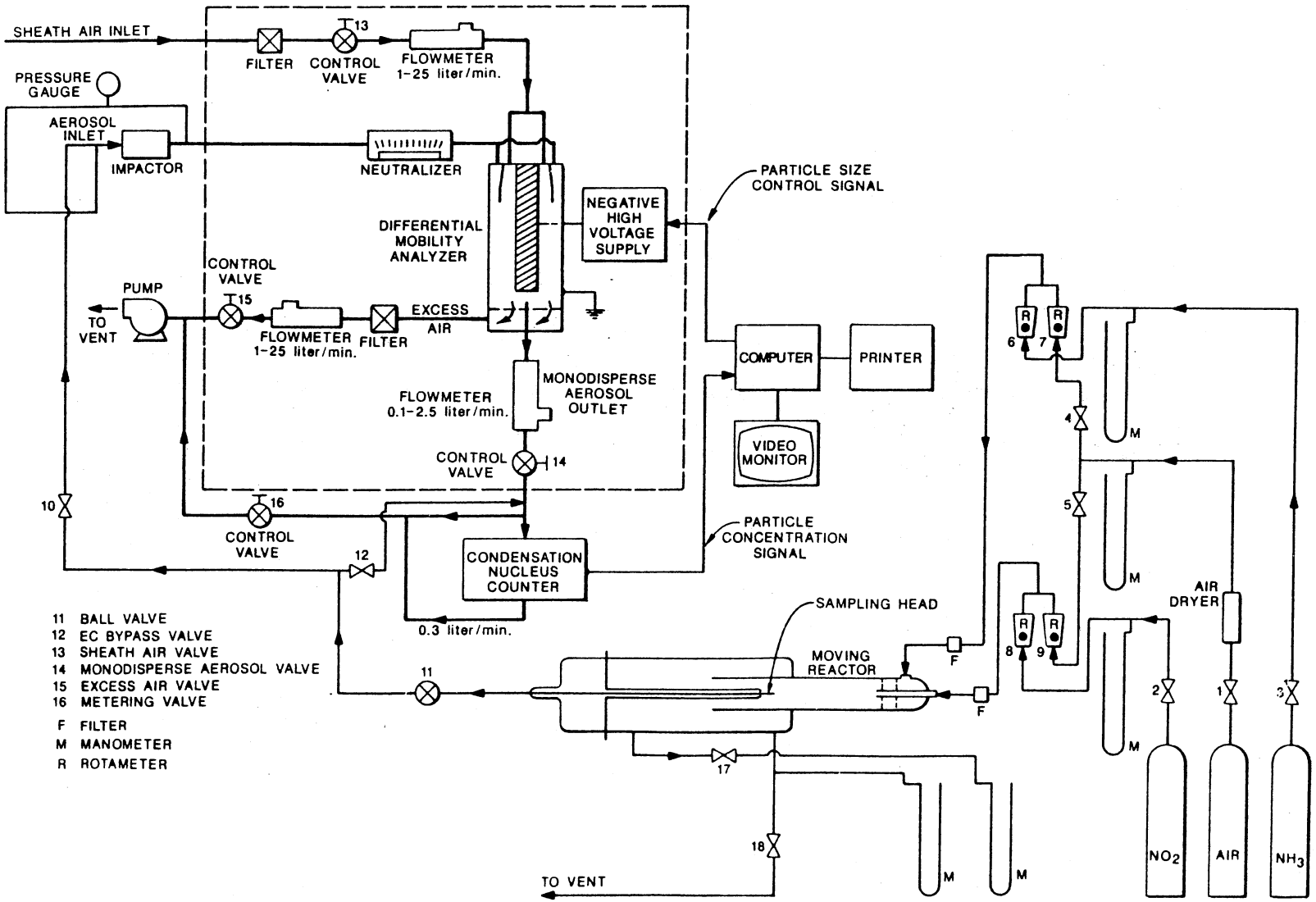

Figure 2. Schematic Diagram of the Experimental Apparatus

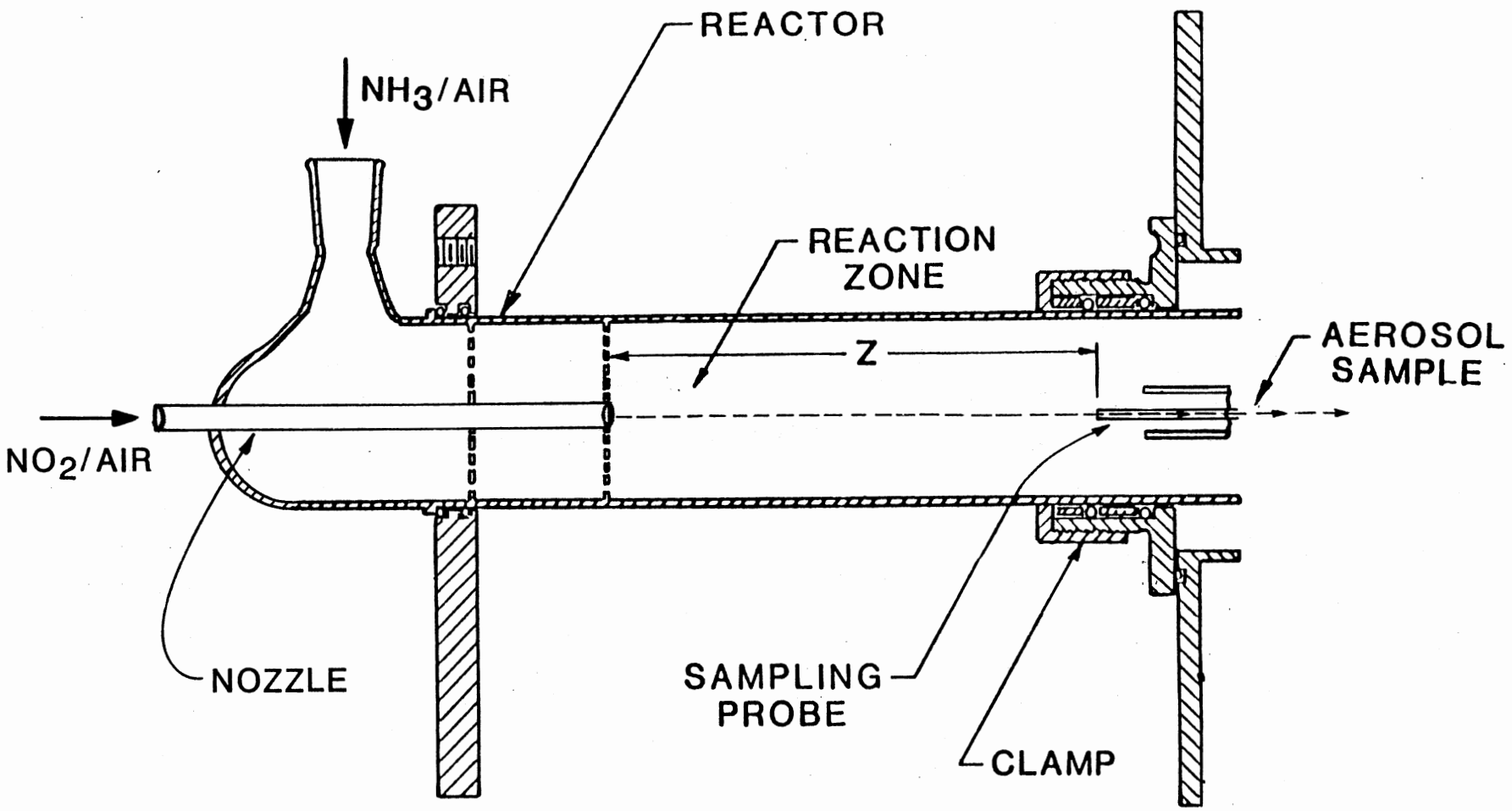

Figure 3. Aerosol Reactor

reactor a mixing head was used. The head consisted of two perforated pyrex plates which were installed at 93 mm and 141 mm distances respectively from the closed end of the reactor. The first disk had 62 holes of 3 mm diameter distributed on three circles, and the second disk had 72 holes of 1 mm diameter distributed on four circles. Figure 3 shows a schematic diagram of the aerosol reactor. The NO_2/Air stream was allowed to enter the reactor through a 5 mm ID x 7 mm OD x 290 mm long nozzle which passed through a 10 mm hole through both disks. The NH_3/Air stream was allowed to enter the reactor through a side inlet located 10 mm from the closed end of the reactor before the two perforated disks (as shown in Figure 3).

The reactor was supported on a sliding table and was connected to a steel chamber which was originally designed for an aerosol beam experiment (Seapan,, et al., 1982). The reactor could be moved to allow sampling from different reaction zones. The total flowrate was adjusted so that a laminar flow was always obtained in the reactor. The residence time could be varied by changing the total flowrate and the length of the reaction zone.

In this study, a TSI differential mobility particle sizer system (DMPS) was used to measure the particle size distributions in the 0.01-1.0 μm diameter range. The DMPS system consisted primarily of a condensation nucleus counter (TSI, model 3020), an electrostatic classifier (TSI, model 3071), an impactor (TSI, model 1030669), an aerosol neutralizer (TSI, model 3077), a data analysis and aerosol conditioning/transport package (TSI, model 3900-72I), and an IBM personal computer (IBM/XT) as shown in Figure 2.

In the DMPS system, the electrostatic classifier (EC) is used to

remove a predictable fraction of the particles entering within a narrow size range. The removed particles are then passed to the CNC to measure their concentrations. The size and amount of the airborne particles in the removed fraction depend on the voltage of the inner cylindrical electrode of the EC, which consists of two concentric cylindrical electrodes. Aerosols which enter the EC first pass through a Kr-85 neutralizer, which exposes the particles to a concentrated environment of charged (positive and negative) ions. The Boltzmann's equilibrium charge distribution describes the charge distribution on the particles.

The voltage supply of the center or inner electrode can be controlled manually or by the computer. The outer electrode is kept at the ground potential. When the charged particles enter the EC, they are attracted toward the center electrode, through the flow layer of the sheath air which enters with the aerosols. The trajectory of each particle depends on the flowrate, geometry, electric field, number of charges on the particle and the particle diameter. For more in-depth discussion of the description and performance of the DMPS, one can refer to Keady, et al., 1983.

A data inversion procedure is used in the software package of the DMPS to obtain the particle concentration as a function of particle diameter. A microcomputer which is interfaced with the DMPS performs these calculations. The data inversion and the hardware interfacing are developed and discussed in more detail by Hoppel, 1978; Fissan, et al., 1982; and Plomp, et al., 1982. The particle diameter can be calculated from the electrical mobility of the particles. The particle electrical mobility is defined as a measure of how fast an electrically-charged particle responds to an electric field.

Some of the principles of the data reduction inversion procedure are presented here, but for more in depth discussion one can refer to the above mentioned authors. The ratio of the concentration of particles of diameter D_p (cm) which carry n_p charges to the concentration of particles carrying zero units of charge is:

$$\frac{N_{n_p}}{N_o} = \exp(-n_p^2 e^2/D_p kT) \qquad [39]$$

where:

e = elementary unit of charge (4.803×10^{-10} $erg^{1/2}cm^{1/2}$)

k = Boltzmann's constant (1.38×10^{-16} erg/K)

T = absolute temperature (K).

The electrical mobility Z_p is defined as

$$Z_p = \frac{v_e}{E} \qquad [40]$$

where:

v_e = electrical velocity component (cm s^{-1})

E = electrical field strength (volts cm^{-1})

The particle diameter is related to the electrical mobility and to the number of charges carried by the particle as follows:

$$Z_p = \frac{n_p e C_1}{3\pi\mu_1 D_p} \qquad [41]$$

where:

μ_1 = gas viscosity (for air at 1 atm and 20 °C, $\mu_1 = 1.83 \times 10^{-6}$ poise)

C_1 = Cunningham slip correction factor

λ = mean free path of gas (for air at 1 atm, λ = 0.653×10^{-5} cm)

Thus, a relation between the particle diameter, the central electrode voltage, number of charges on the particle, flowrates, and geometry of the analyzer is given as:

$$D_p = \frac{2n_p e\, C_1\, V\, L}{3\mu[q_t - 1/2(q_s + q_a)\, \ln(r_2/r_1)]} \qquad [42]$$

where:

q_t = total flow inside the EC ($cm^3\ s^{-1}$)

q_s = sample aerosol outlet flowrate ($cm^3\ s^{-1}$)

q_a = aerosol inlet flowrate ($cm^3\ s^{-1}$)

r_2 = outer electrode radius (for EC it is 1.958 cm)

r_1 = inner electrode radius (for EC it is 0.937 cm)

V = voltage on the center electrode (volts)

L = length between the sample exit slit and the aerosol inlet slit (44.44 cm)

If the computer is used for sampling, it first sets the delay time necessary between a step change in the EC center rod voltage. The computer also sets the time for measuring the concentration. The sampling starts by outputting specific voltage to the inner rod of the EC. This allows particles with specific size (corresponding to the voltage on the inner rod and the particle electrical mobility) to exit to the CNC. If the particle concentrations are above 1000 particles/ml, the computer obtains the aerosol concentration from the standard linearized CNC output. The computer compares repeated concentration values until it obtains stable values and then steps to the next mobility channel and a new voltage is sent to the center rod of the EC. However, if the

concentration is below 1000 particles/ml, the computer counts directly the pulses from the CNC counter trigger output and calculates the concentration from the number of counts over a measured time period. The sampling continues from the lowest channel number corresponding to the smallest diameter (highest electrical mobility), to the highest channel number, passing through 40 mobility channels.

4.2 Experimental Procedure

The operational procedure for this study consists of two parts, the procedure for the particle generating system and the procedure for the particle measuring system. Appendix presents a detailed description of both procedures. Appendix C tabulates the health hazards of the chemicals involved in this experiment.

There are two different operating modes that the DMPS can work with. These are the overpressure mode, and the underpressure mode. In this study the underpressure mode is used because the experiments were conducted at atmospheric pressure. Before taking any measurement, certain preparations are required. This includes the preparation of the CNC (see Appendix B) and the calculation of the desired flowrates for the reactor and the EC.

In this study, a routine check for any foreign particles was performed before starting each experiment. Before sampling the reaction products by the DMPS, the reactor outlet was first connected to the CNC (bypassing the EC). The CNC was used to monitor the variation in the total number concentration of the product particles. Table I shows a typical tabulation of these results. In these measurements the CNC is also interfaced with the computer, and the program "COUNT" of the DMPS

software is used to record and store the total number concentration with time. When the CNC starts reading a constant concentration, the reactor outlet is connected to the EC for size distribution measurements. Tables II and III show the typical output of results for size distribution measurements. The number concentration versus size distribution data represented by the second and third columns of Table III was used to estimate the critical particle diameter. For example, in Table III, the first detected particle concentration was at a particle diameter of 0.019 μm, corresponding to a mobility channel number 5. Since this size is above the lowest detection limit of the DMPS, the particle size of 0.019 μm was considered to be the critical particle diameter for this experiment.

In this study two different sizes of the impactor nozzle were used as indicated in Table IV in Chapter V. The low temperature experiments were performed during the cold winter days of 1987 by leaving the room window open. For very low temperature (4 °C) experiments the room window was left open overnight.

During the experiments, a periodic maintenance of the DMPS system, as recommended and described in the DMPS operating manual, was conducted to ensure proper performance. This maintenance included calibrating the EC, regular checking of the EC calibration, cleaning of several parts of the EC, and periodic testing of the pressure drop through the system. The DMPS operating manual recommended testing for pressure drop every 40 operating hours. Due to the accumulation of aerosol deposits in the EC, which may cause electrical breakdown of the high voltage or error in the measurement of volumetric flowrates, the suggested maintenance schedule was strictly followed.

TABLE I

TYPICAL VARIATION OF THE TOTAL NUMBER DENSITY WITH TIME
(FOR RUN # 31)

TIME (Sec)	CONCENTRATION (particle/ml)	CONCENTRATION (particle/cu.ft)
0	0	0
30	.03	755
55	43	1.2E6
61	183	5.1E6
66	245	6.9E6
70	316	8.9E6
73	358	1.0E7
76	388	1.1E7
79	446	1.2E7
82	460	1.3E7
85	439	1.2E7
88	472	1.3E7
90	551	1.5E7
92	587	1.6E7
94	592	1.6E7
96	584	1.6E7
98	575	1.6E7
100	587	1.6E7
102	582	1.6E7
104	589	1.6E7
106	585	1.6E7
108	592	1.6E7
110	642	1.8E7
112	644	1.8E7
114	563	1.8E7
116	658	1.8E7
118	721	2.0E7
120	735	2.0E7
122	722	2.0E7
124	748	2.1E7
126	760	2.1E7
128	763	2.1E7
130	786	2.2E7
132	784	2.2E7
134	789	2.2E7
136	775	2.1E7
138	769	2.1E7
140	782	2.2E7
142	794	2.2E7
144	830	2.3E7
146	827	2.3E7
148	844	2.3E7
150	827	2.3E7
152	869	2.4E7

TABLE I (Continued)

TIME (Sec)	CONCENTRATION (particle/ml)	CONCENTRATION (particle/cu.ft)
156	917	2.5E7
158	911	2.5E7
160	944	2.6E7
162	937	2.6E7
163	1010	2.8E7
165	993	2.8E7
166	1056	2.9E7
167	1093	3.0E7
168	1094	3.0E7
169	1075	3.0E7
170	1061	3.0E7
171	1078	3.0E7
172	1136	3.2E7
173	1152	3.2E7
174	1125	3.1E7
175	1120	3.1E7
176	1095	3.1E7
177	1081	3.0E7
178	1152	3.2E7
179	1124	3.1E7
180	1133	3.2E7

TABLE II

TYPICAL MEASUREMENT OF THE PARTICLE SIZE DISTRIBUTION (FOR RUN # 31)

TSI DIFFERENTIAL MOBILITY PARTICLE SIZER
RUN # 31-RATIO12.3 WITH R.T.=5 SEC

SAMPLE # 1 — AEROSOL FLOW RATE: .3 LPM — MEAS. MODE: 2
DATE: 11-22-1987 — MAXIMUM DIA. MEASURED: .631 UM — START: 23:20:55
MINIMUM DIA. MEASURED: .017 UM — END: 23:35:23

MOBILITY CHANNEL#	MOBILITY MIDPOINT (CM^2/(VS))	DIAMETER MIDPOINT (UM)	CNC CONCENTRATION (PART/CC)	NUMBER CONCENTRATION (PART/CC)
1	2.07E-2	.01	0	0
2	1.69E-2	.011	0	0
3	1.39E-2	.012	0	0
4	1.13E-2	.014	0	0
5	9.30E-3	.015	0	0
6	7.61E-3	.017	4.958	125.84
7	6.23E-3	.018	6.448	139.04
8	5.09E-3	.021	7.938	149.68
9	4.17E-3	.023	10.32	166.75
10	3.41E-3	.025	12.702	179.73
11	2.79E-3	.028	16.675	206.38
12	2.28E-3	.031	20.648	227.45
13	1.86E-3	.035	26.815	273.06
14	1.52E-3	.038	32.983	309.06
15	1.25E-3	.043	39.113	341.8
16	1.02E-3	.048	45.243	373.43
17	8.37E-4	.053	50.173	395.55
18	6.85E-4	.059	55.102	418.7
19	5.60E-4	.066	54.429	401.44
20	4.58E-4	.074	53.757	398.01
21	3.75E-4	.083	47.906	356.59
22	3.07E-4	.093	42.055	318.48
23	2.51E-4	.104	32.89	251.29
24	2.05E-4	.117	23.725	183.59
25	1.68E-4	.132	16.416	130.66
26	1.37E-4	.15	9.108	73.86
27	1.12E-4	.17	5.561	47
28	9.21E-5	.193	2.014	17.38
29	7.53E-5	.221	1.09	9.8
30	6.16E-5	.253	.167	1.53
31	5.04E-5	.291	8.33E-2	.79
32	4.12E-5	.337	0	0
33	3.37E-5	.391	0	0
34	2.76E-5	.457	0	0
35	2.26E-5	.535	6.66E-3	8 E-2
36	1.85E-5	.631	1.33E-2	.17
37	1.51E-5	.746	0	0
38	1.23E-5	.886	0	0
39	1.01E-5	1.056	0	0
		TOTALS:	618.338	5497.139

TABLE III

TYPICAL MEASUREMENT OF THE CUMULATIVE PARTICLE SIZE DISTRIBUTION
(FOR RUN # 31)

TSI DIFFERENTIAL MOBILITY PARTICLE SIZER
RUN # 31-RATIO12.3 WITH R.T.=5 SEC

SAMPLE # 1 — AEROSOL FLOW RATE: .3 LPM — MEAS. MODE: 2
DATE: 11-22-1987 — MAXIMUM DIA. MEASURED: .631 UM — START: 23:20:55
MINIMUM DIA. MEASURED: .017 UM — END: 23:35:23

DIA CH#	DIAMETER MIDPOINT (UM)	CONCENTRATION NUMBER (#/CC)	CONCENTRATION SURFACE (UM^2/CC)	CONCENTRATION VOLUME (UM^3/CC)	PERCENTAGE NUMBER CUMULATIVE	PERCENTAGE SURFACE CUMULATIVE	PERCENTAGE VOLUME CUMULATIVE
1	.011	0	0	0	0	0	0
2	.012	0	0	0	0	0	0
3	.014	0	0	0	0	0	0
4	.017	0	0	0	0	0	0
5	.019	198.653	.228	7.25E-4	3.71	.271	5.11E-2
6	.022	223.89	.343	1.26E-3	7.891	.678	.14
7	.025	252.999	.516	2.19E-3	12.615	1.292	.294
8	.029	296.693	.807	3.95E-3	18.156	2.252	.573
9	.034	360.143	1.307	7.4 E-3	24.881	3.805	1.095
10	.039	424.305	2.053	1.34E-2	32.805	6.246	2.04
11	.045	480.619	3.101	2.34E-2	41.78	9.932	3.69
12	.052	520.834	4.481	3.90E-2	51.506	15.26	6.443
13	.06	537.894	6.171	6.21E-2	61.551	22.598	10.822
14	.07	516.192	7.897	9.18E-2	71.191	31.987	17.293
15	.081	468.602	9.559	.128	79.942	43.354	26.339
16	.093	392.011	10.665	.165	87.262	56.035	37.992
17	.107	281.929	10.228	.183	92.527	68.196	50.897
18	.124	189.956	9.189	.19	96.074	79.123	64.288
19	.143	112.252	7.242	.173	98.171	87.733	76.473
20	.165	61.295	5.273	.145	99.315	94.003	86.719
21	.191	23.673	2.716	8.64E-2	99.757	97.233	92.813
22	.221	10.52	1.609	5.91E-2	99.954	99.145	96.984
23	.255	1.542	.315	1.33E-2	99.983	99.519	97.925
24	.294	.743	.202	9.91E-3	99.996	99.761	98.624
25	.34	0	0	0	99.996	99.761	98.624
26	.392	0	0	0	99.996	99.761	98.624
27	.453	0	0	0	99.996	99.761	98.624
28	.523	6.28E-2	5.40E-2	4.71E-3	99.998	99.825	98.956
29	.604	.128	.147	1.48E-2	100	100	100
20	.698	0	0	0	0	0	0
21	.806	0	0	0	0	0	0
22	.931	0	0	0	0	0	0
TOTALS:		5354.938	84.102	1.419			
FOR MEASURED DATA ONLY							
GEO. MEAN:		5.39E-2	9.07E-2	.113			
SPREAD FACTOR:		1.706	1.61	1.592			

CHAPTER V

EXPERIMENTAL RESULTS AND DISCUSSION

This chapter will present and discuss the experimental results of the reaction between ammonia and nitrogen dioxide at different reaction conditions and the predictions of the theoretical model.

The main objective of this work is to understand the mechanism by which the ammonium nitrate aerosols form and grow. A systematic series of experiments was conducted in order to study the gas-phase reaction of NO_2 with NH_3 in a laminar flow aerosol reactor at atmospheric pressure. The independent parameters in this study included the initial reactant concentrations, the residence time, the reaction temperature, and the reaction time. The dependent parameters included the particle critical size, the particle size distribution, the induction time, the rate of approach to steady state, the total number density, the total surface area, and the total volume of particles.

This work used a mathematical model based on the reaction kinetics and homogeneous nucleation theory was used to predict and explain the experimental results. The classical nucleation theory was used as a basis for this study. The particle growth mechanism was explained by studying the variation of the total number concentration and total volume with time and the evolution of the experimental particle size distribution. The main formation and growth processes considered were homogeneous nucleation, diffusion-controlled growth, surface reaction-

controlled growth, volume reaction-controlled growth, monomer condensation and particle coagulation.

This study conducted a total of 68 experiments. The conditions of each experiment are shown in Table IV. Equimolar and non-equimolar reactant concentrations at atmospheric pressure and temperatures of 4.4 to 21.0 °C (40-70 °F) were considered. The reactant concentrations after mixing were in the range of 0.5-14 ppm with residence times in the range of 3-30 s. These reaction conditions were selected to simulate the equilibrium of the NO_2-NH_3-NH_4NO_3 system in the atmosphere and some industrial operations.

In this study, the change in the total number concentration of ammonium nitrate aerosols with time was measured by the CNC, while the particle size distributions at different reaction conditions were measured by the DMPS. The size distribution measurements were also integrated by the DMPS software to estimate the total number, total surface area, and total volume of the ammonium nitrate particles.

A complete documentation of all the raw experimental data is kept with Dr. M. Seapan in the School of Chemical Engineering at the Oklahoma State University. The results of experiments 1 through 25 are not presented or discussed in this chapter due to the uncertainty in the gas concentrations in cylinders used in these runs (which were in the range of 105-110 ppm). The uncertainty came from the use of these cylinders later than the guaranteed time period of the gas mixture concentrations stated by the manufacturer.

The total number concentrations versus time measured by the CNC were used to determine the induction for each experiment. A summary of induction times is shown in Table V. The results of the measurements of

TABLE IV

CONDITIONS OF THE EXPERIMENTS

Run #	$[NH_3]$ ppm	$[NO_2]$ ppm	Residence Time sec.	Temp. °C	Reaction Zone cm	Reynolds Number
1	1.81	1.83	20.64	22.0	61.3	158
2	2.42	2.68	19.10	22.0	60.7	169
3	2.06	6.93	15.83	22.0	58.9	198
4	2.06	6.93	14.15	22.8	52.7	198
5	2.06	6.93	11.61	22.8	43.2	198
6	5.50	18.50	10.72	22.2	58.9	200
7	8.80	34.00	10.72	22.2	43.2	200
8	12.00	58.00	10.72	22.2	43.2	200
9	12.00	58.00	10.72	22.2	43.2	200
10	1.76	7.20	15.95	26.7	57.1	190
11	0.00	0.00	15.95	27.8	59.7	-----
12	0.00	0.00	15.95	26.7	59.7	-----
13	2.09	7.03	15.87	26.7	58.2	195
14	12.09	7.03	24.92	26.7	91.4	195
15	2.22	7.13	25.18	26.7	87.4	184
16	3.83	12.91	8.19	26.7	40.1	260
17	1.10	1.56	11.54	24.4	33.3	153
18	0.39	0.47	9.40	24.4	58.4	331
19	0.71	0.98	9.93	23.3	49.5	266
20	1.83	1.95	10.30	24.4	43.2	223
21	4.92	5.42	14.41	23.3	49.5	183
22	5.03	5.39	10.45	23.3	36.1	184
23-A	3.38	3.76	10.56	23.3	38.4	194
23-B	3.18	3.67	10.32	23.9	38.4	198
24	0.52	0.64	9.83	23.3	57.7	312
25	1.80	2.18	10.13	22.2	43.2	227
26	5.77	4.88	10.16	20.0	21.6	113
27	11.28	9.87	9.93	23.3	27.1	145
28	2.84	2.49	9.99	21.1	27.1	144
29	1.13	0.99	9.95	21.1	27.0	145
30	11.44	10.01	10.07	20.0	27.1	143
31	13.50	2.95	4.86	22.2	18.0	198
32	13.65	3.19	5.01	20.0	18.0	192
33	13.65	3.19	5.01	20.0	18.0	192
34	5.69	5.02	5.01	20.0	18.9	201
35	5.69	5.02	5.01	20.0	18.9	201
36	1.13	11.35	4.99	18.9	33.8	361
37	1.13	11.35	4.99	18.9	33.8	361
38	5.69	5.01	3.00	24.4	21.1	374
39	5.72	5.03	3.02	23.9	21.1	372
40	5.72	5.00	5.03	21.1	27.1	286
41	5.72	5.00	6.15	21.1	33.0	286
42	5.72	5.00	8.04	21.1	43.2	286

TABLE IV (Continued)

Run #	$[NH_3]$ ppm	$[NO_2]$ ppm	Residence Time sec.	Temp. °C	Reaction Zone cm	Reynolds Number
43	5.72	5.00	9.93	21.1	53.3	286
44	5.72	5.00	2.60	21.1	14.0	286
45	0.57	5.00	5.03	20.0	27.1	286
46	0.50	7.94	4.39	20.0	27.1	328
47	1.13	5.01	5.00	20.0	27.1	288
48	5.65	4.96	10.33	15.6	21.6	111
49	11.28	9.87	9.93	14.4	27.1	145
50	2.96	2.31	10.43	13.9	27.1	138
51	0.96	1.18	9.90	13.3	27.1	145
52	0.59	0.52	10.20	10.0	41.9	219
53	1.14	0.99	10.00	10.0	27.1	144
54	8.15	7.59	30.64	21.1	59.7	104
55	8.15	7.59	24.12	21.1	47.0	104
56	8.15	7.59	17.60	21.1	34.3	104
57	8.15	7.59	11.08	21.1	21.6	104
58	0.48	0.77	9.79	4.4	27.1	147
59	0.97	1.00	10.10	4.4	27.1	143
60	0.47	0.76	9.66	4.4	27.1	149
61	0.47	0.76	14.51	4.4	40.6	149
62	0.47	0.76	21.32	4.4	59.7	149
63	0.47	0.76	9.66	10.0	27.1	149
64	0.28	0.57	3.22	10.0	8.9	147
65	0.28	0.57	21.64	10.0	59.7	147
66	7.49	7.45	-----	21.1	27.1	-----
67	7.49	7.45	-----	21.1	27.1	-----
68	7.49	7.45	_____	21.1	27.1	-----

$[NH_3]$ and $[NO_2]$ are the concentrations of NH_3 and NO_2 after mixing inside the reactor.

Runs 66 to 68 were done to test for the impurities deposited in the EC.

In runs (1-10) the diameter of the impactor nozzle was 0.0508 cm.

In runs (11-68) the diameter of the impactor nozzle was 0.0457 cm.

TABLE V

INDUCTION TIME AND CRITICAL PARTICLE DIAMETER

ESTIMATED FROM EXPERIMENTAL RESULTS

Run #	$[NH_3]$ ppm	$[NO_2]$ ppm	Residence Time sec.	Temperature °C	Induction Time sec.	Critical Size µm
28	2.84	2.49	9.99	21.1	120	0.022
32	13.65	3.19	5.01	20.0	30	0.019
33	13.65	3.19	5.01	20.0	---	0.019
34	5.69	5.02	5.01	20.0	30	0.022
35	5.69	5.02	5.01	20.0	---	0.022
36	1.13	11.35	4.99	20.0	30	0.025
37	1.13	11.35	4.99	20.0	30	0.025
39	5.72	5.03	3.02	23.9	28	0.019
41	5.72	5.00	6.15	21.1	23	0.022
42	5.72	5.00	8.04	21.1	---	0.034
43	5.72	5.00	9.93	21.1	---	0.052
44	5.72	5.00	2.60	21.1	---	0.034
47	1.13	5.01	5.00	20.0	60	0.034
49	11.28	9.87	9.93	14.4	21	0.019
50	2.96	2.31	10.43	13.9	30	0.025
51	0.96	1.18	9.90	13.3	30	0.034
53	1.14	0.99	10.00	10.0	30	0.025
54	8.15	7.59	30.64	21.1	120	0.019
55	8.15	7.59	24.12	21.1	---	0.022
56	8.15	7.59	17.60	21.1	---	0.025
57	8.15	7.59	11.08	21.1	---	0.022
58	0.48	0.77	9.79	4.4	210	0.022
59	0.97	1.00	10.10	4.4	30	0.019
60	0.47	0.76	9.66	4.4	150	0.022
63	0.47	0.76	9.66	10.0	360	0.022

TABLE VI

TOTAL NUMBER CONCENTRATION OF PARTICLES AT T ≃ 20.0 °C[a]

Run #	Concentration NH_3 ppm	Concentration NO_2 ppm	R.T.[d] sec	Total # Density of AN[b] Experimental #/ml.	Total # Density of AN[b] Predicted #/ml.	Experimental Error C.V.[c]
45	0.50	5.00	5.00	0.00	0.00	----
46	0.50	8.00	4.40	0.00	0.00	----
29	1.00	1.00	10.00	0.08	0.00	----
47	1.00	5.00	5.00	20.03	16.31	0.41
36, 37	1.00	11.00	5.00	22.23	15.01	0.24
28	2.50	2.50	10.00	43.94	13.40	0.36
43	5.70	5.00	10.00	381.00	173.90	0.90
40	5.70	5.00	5.00	87.49	54.60	0.12
38	5.70	5.00	3.00	42.61	37.57	0.20
44	5.70	5.00	2.60	18.00	15.00	0.15
41	5.70	5.00	6.00	36.65	30.54	0.12
42	5.70	5.00	8.00	36.33	33.03	0.20
57	8.00	7.60	11.10	54.38	36.00	0.13
56	8.00	7.60	17.60	63.97	49.21	0.20
55	8.00	7.60	24.12	78.31	65.26	0.24
54	8.00	7.60	30.64	146.27	97.51	0.46
27, 30	10.00	10.00	10.00	628.52	349.18	0.55
31,32,33	13.65	3.00	5.00	385.07	319.00	0.21

a- The temperature ranges from 19 to 23 °C, as listed in Table IV.
b- AN stands for ammonium nitrate.
c- C.V. stands for coefficient of variation.
d- Residence Time.

TABLE VII

TOTAL NUMBER CONCENTRATION OF PARTICLES AT T = 15.5 °C[a]

Run #	Concentration NH_3 ppm	Concentration NO_2 ppm	R.T.[d] sec	Total # Density of AN[b] Experimental #/ml.	Total # Density of AN[b] Predicted #/ml.	Experimental Error C.V.[c]
51	1.00	1.00	10.00	15.02	8.29	0.04
40	3.00	2.50	10.00	19.39	13.85	0.10
48	5.50	5.00	10.00	121.43	102.20	0.23
49	11.00	10.00	10.00	220.38	76.95	1.09

a- The temperature ranges from 13 to 15.5 °C.
b- AN stands for ammonium nitrate.
c- C.V. stands for coefficient of variation.
d- Residence Time.

TABLE VIII

TOTAL NUMBER CONCENTRATION OF PARTICLES AT T = 10.0 °C.

Run #	Concentration NH_3 ppm	Concentration NO_2 ppm	R.T.[c] sec	Total # Density of AN[a] Experimental #/ml.	Total # Density of AN[a] Predicted #/ml.	Experimental Error C.V.[b]
63	0.50	0.80	10.00	26.46	10.68	0.28
64	0.30	0.60	3.00	21.25	15.18	0.15
65	0.30	0.60	21.64	17.45	14.54	0.12
52	0.60	0.50	10.00	26.59	17.73	0.22
53	1.00	1.00	10.00	29.12	17.13	0.30

a- AN stands for ammonium nitrate.
b- C.V. stands for coefficient of variation.
c- Residence Time.

TABLE IX

TOTAL NUMBER CONCENTRATION OF PARTICLES AT T = 4.4 °C

Run #	Concentration NH_3 ppm	Concentration NO_2 ppm	R.T.[c] sec	Total # Density of AN[a] Experimental #/ml.	Total # Density of AN[a] Predicted #/ml.	Experimental Error C.V.[b]
58, 60	0.50	0.80	10.00	39.16	21.89	0.03
61	0.50	0.80	14.50	48.77	32.00	0.10
62	0.50	0.80	21.32	49.38	29.05	0.09
59	1.00	1.00	10.00	99.35	47.74	0.21

a- AN stands for ammonium nitrate.
b- C.V. stands for coefficient of variation.
c- Residence Time.

TABLE X

TOTAL SURFACE AREA OF PARTICLES AT T = 20.0 °C[a]

Run #	Concentration NH_3 ppm	Concentration NO_2 ppm	Residence Time sec	Total Surface Area of AN[b] Exp. $\mu m^2/ml.$	Total Surface Area of AN[b] Predict. $\mu m^2/ml.$	Experimental Error C.V.[c]
45	0.50	5.00	5.00	0.00	0.00	----
46	0.50	8.00	4.40	0.00	0.00	----
29	1.00	1.00	10.00	----	0.00	----
47	1.00	5.00	5.00	4.12	9.40	0.35
36, 37	1.00	11.00	5.00	4.55	8.77	0.29
28	2.50	2.50	10.00	5.41	1.41	0.75
43	5.70	5.00	10.00	10.81	35.60	0.50
40	5.70	5.00	5.00	27.33	37.50	0.03
38	5.70	5.00	3.00	12.03	27.67	0.25
44	5.70	5.00	2.60	5.04	7.05	0.32
41	5.70	5.00	6.00	15.72	20.44	0.40
42	5.70	5.00	8.00	15.85	19.81	0.25
57	8.00	7.60	11.10	7.71	12.34	0.11
56	8.00	7.60	17.60	9.53	17.15	0.08
55	8.00	7.60	24.12	10.86	22.81	0.12
54	8.00	7.60	30.64	23.32	53.64	0.18
27, 30	10.00	10.00	10.00	157.20	317.54	0.89
31,32,33	13.65	3.00	5.00	94.78	191.70	0.13

a- The temperature ranges from 19 to 23 °C.
b- AN stands for ammonium nitrate.
c- C.V. stands for coefficient of variation.

TABLE XI

TOTAL SURFACE AREA OF PARTICLES AT T = 15.5 °C[a]

Run #	Concentration NH_3 ppm	Concentration NO_2 ppm	Residence Time sec	Total Surface Area of AN[b] Exp. $\mu m^2/ml.$	Total Surface Area of AN[b] Predict. $\mu m^2/ml.$	Experimental Error C.V.[c]
51	1.00	1.00	10.00	2.30	3.22	0.03
50	3.00	2.50	10.00	3.23	4.52	0.08
48	5.50	5.00	10.00	30.54	75.03	0.31
49	11.00	10.00	10.00	14.51	11.52	0.95

a- The temperature ranges from 13 to 15.5 °C.
b- AN stands for ammonium nitrate.
c- C.V. stands for coefficient of variation.

TABLE XII

TOTAL SURFACE AREA OF PARTICLES AT T = 10.0 °C

Run #	Concentration NH_3 ppm	Concentration NO_2 ppm	Residence Time sec	Total Surface Area of AN[a] Exp. $\mu m^2/ml.$	Total Surface Area of AN[a] Predict. $\mu m^2/ml.$	Experimental Error C.V.[b]
63	0.50	0.80	10.00	2.69	1.17	0.35
64	0.30	0.60	3.00	2.12	2.00	0.22
65	0.30	0.60	21.64	2.01	1.72	0.45
52	0.60	0.50	10.00	2.76	3.59	0.38
53	1.00	1.00	10.00	3.66	6.89	0.19

a- AN stands for ammonium nitrate.
b- C.V. stands for coefficient of variation.

TABLE XIII

TOTAL SURFACE AREA OF PARTICLES AT T = 4.4 °C

Run #	Concentration NH_3 ppm	Concentration NO_2 ppm	Residence Time sec	Total Surface Area of AN[a] Exp. $\mu m^2/ml.$	Total Surface Area of AN[a] Predict. $\mu m^2/ml.$	Experimental Error C.V.[b]
58, 60	0.50	0.80	10.00	4.55	4.16	0.06
61	0.50	0.80	14.50	4.99	4.56	0.10
62	0.50	0.80	21.32	4.54	4.21	0.12
59	1.00	1.00	10.00	12.53	13.18	0.19

a- AN stands for ammonium nitrate.
b- C.V. stands for coefficient of variation.

TABLE XIV

TOTAL VOLUME OF NITRATE PARTICLES AT T = 20.0 °C[a]

Run #	Concentration NH_3 ppm	Concentration NO_2 ppm	Residence Time sec	Total Volume of AN[b] Exp. $\mu m^3/ml.$	Total Volume of AN[b] Predict. $\mu m^3/ml.$	Experimental Error C.V.[c]
45	0.50	5.00	5.00	0.00	0.00	----
46	0.50	8.00	4.40	0.00	0.00	----
29	1.00	1.00	10.00	----	0.00	----
47	1.00	5.00	5.00	0.26	0.97	0.35
36, 37	1.00	11.00	5.00	0.30	0.92	0.40
28	2.50	2.50	10.00	0.32	0.05	1.13
43	5.70	5.00	10.00	0.83	3.91	0.76
40	5.70	5.00	5.00	1.97	3.52	0.02
38	5.70	5.00	3.00	0.82	2.85	0.28
44	5.70	5.00	2.60	0.34	0.63	0.25
41	5.70	5.00	6.00	1.20	3.00	0.43
42	5.70	5.00	8.00	1.21	2.40	0.12
57	8.00	7.60	11.10	0.39	0.61	0.35
56	8.00	7.60	17.60	0.49	0.81	0.02
55	8.00	7.60	24.12	0.52	0.88	0.06
54	8.00	7.60	30.64	1.24	2.43	0.13
27, 30	10.00	10.00	10.00	10.03	25.08	0.98
31,32,33	13.65	3.00	5.00	6.04	18.57	0.11

a- The temperature ranges from 19 to 23 °C.
b- AN stands for ammonium nitrate.
c- C.V. stands for coefficient of variation.

TABLE XV

TOTAL VOLUME OF NITRATE PARTICLES AT T = 15.5 °C[a]

Run #	Concentration NH_3 ppm	Concentration NO_2 ppm	Residence Time sec	Total Volume of AN[b] Exp. $\mu m^3/ml.$	Total Volume of AN[b] Predict. $\mu m^3/ml.$	Experimental Error C.V.[c]
51	1.00	1.00	10.00	0.12	0.23	0.08
50	3.00	2.50	10.00	0.19	0.25	0.10
48	5.50	5.00	10.00	2.02	7.72	0.34
49	11.00	10.00	10.00	0.54	0.58	0.85

a- The temperature ranges from 13 to 15.5 °C.
b- AN stands for ammonium nitrate.
c- C.V. stands for coefficient of variation.

TABLE XVI

TOTAL VOLUME OF NITRATE PARTICLES AT T = 10.0 °C[a]

Run #	Concentration NH_3 ppm	Concentration NO_2 ppm	Residence Time sec	Total Volume of AN[a] Exp. $\mu m^3/ml.$	Total Volume of AN[a] Predict. $\mu m^3/ml.$	Experimental Error C.V.[b]
63	0.50	0.80	10.00	0.13	0.11	0.38
64	0.30	0.60	3.00	0.10	0.10	0.08
65	0.30	0.60	21.64	0.11	0.23	0.25
52	0.60	0.50	10.00	0.13	0.14	0.11
53	1.00	1.00	10.00	0.19	0.27	0.30

a- AN stands for ammonium nitrate.
b- C.V. stands for coefficient of variation.

TABLE XVII

TOTAL VOLUME OF NITRATE PARTICLES AT T = 4.4 °C[a]

Run #	Concentration NH_3 ppm	Concentration NO_2 ppm	Residence Time sec	Total Volume of AN[a] Exp. $\mu m^3/ml.$	Total Volume of AN[a] Predict. $\mu m^3/ml.$	Experimental Error C.V.[b]
58, 60	0.50	0.80	10.00	0.23	0.26	0.13
61	0.50	0.80	14.50	0.23	0.26	0.13
62	0.50	0.80	21.32	0.19	0.23	0.11
59	1.00	1.00	10.00	0.61	0.91	0.16

a- AN stands for ammonium nitrate.
b- C.V. stands for coefficient of variation.

TABLE XVIII

DEVELOPMENT OF TOTAL NUMBER AND TOTAL VOLUME WITH REACTION TIME

	RUN 63		RUN 60		RUN 47		RUN 39	
Sample	Total # ml^{-1}	Total Volume $\mu m^3/ml$	Total # ml^{-1}	Total Volume $\mu m^3/ml$	Total # ml^{-1}	Total Volume $\mu m^3/ml$	Total # ml^{-1}	Total Volume $\mu m^3/ml$
1	8.75	0.055	34.99	0.169	14.74	0.151	52.37	1.07
2	21.41	0.069	36.94	0.225	15.70	0.292	40.145	0.76
3	30.91	0.123	36.85	0.206	29.65	0.338	35.29	0.62
4.	33.10	0.125	----	----	----	----	----	----
5.	24.82	0.129	----	----	----	----	----	----
6.	29.36	0.174	----	----	----	----	----	----
7.	33.64	0.258	----	----	----	----	----	----
8.	29.31	0.157	----	----	----	----	----	----

TABLE XIX

COMPARISON BETWEEN DMPS AND CNC MEASUREMENTS OF THE TOTAL NUMBER CONCENTRATION

Run #	$[NH_3]$ ppm	$[NO_2]$ ppm	Residence Time sec.	Temperature °C	Reynolds Number	Total Number Concentration Measurements by CNC (A)	DMPS (B)	(A)/(B)
26	5.77	4.88	10.16	20.0	113	820	683	1.20
28	2.84	2.49	9.99	21.1	144	56	55	1.00
31	13.50	2.95	4.86	22.2	197	2109	5497	0.38
32	13.65	3.19	5.01	20.0	191	889	446	1.90
33	13.65	3.19	5.01	20.0	191	792	331	2.40
34	5.69	5.02	5.01	20.0	201	2094	97	22.00
35	5.69	5.02	5.01	20.0	201	1970	82	24.00
36	1.13	11.35	4.99	18.9	361	440	18	24.00
37	1.13	11.35	4.99	18.9	361	440	26	17.00
38	5.69	5.01	3.00	24.4	373	2000	122	16.00
39	5.72	5.03	3.02	23.9	372	2027	53	38.00
40	5.72	5.00	5.03	21.1	286	2300	44	52.00
47	1.13	5.01	5.00	20.0	288	14	15	1.00
48	5.65	4.96	10.33	15.6	111	142	142	1.00
50	2.96	2.31	10.43	13.9	138	1700	20	85.00
51	0.96	1.18	9.90	13.3	145	140	15	9.30
52	0.59	0.52	10.20	10.0	218	27	27	1.00
53	1.14	0.99	10.00	10.0	144	200	29	6.90
54	8.15	7.59	30.64	21.1	103	150	146	1.10
58	0.48	0.77	9.79	4.4	147	600	50	12.00
59	0.97	1.00	10.10	4.4	142	2000	115	17.00
60	0.47	0.76	9.66	4.4	149	600	40	15.00

DMPS as the total number concentration, total surface area, and total volume of particles are shown in Tables VI through XVII. These distributions were also used to estimate the critical particle diameter as mentioned in Section 4.2 of Chapter IV and are shown in Table V.

The experimental results are simulated using a model based on the reaction kinetics and the classical nucleation theory. Table XVIII shows the development of the total number and total volume of particles with reaction time. These data are used to examine the significance of the condensation and coagulation processes. Table XIX shows a comparison between the total number concentration measurement of the DMPS and the CNC alone. Before analyzing and discussing the results of this project, development of the mathematical model and the computational procedure will be described.

5.1 Mathematical Model

The theoretical model used in this study is based on the classical nucleation theory and the kinetics of the NO_2-NH_3 reaction described by Mearns and Ofosu-Asiedu, 1984b. This model considered the reaction mechanism suggested by Falk, 1955 and revised by Mearns and Ofosu-Asiedu, 1984a,b. At the beginning of the calculations, the model is used to estimate the reaction rate constants, k_a and k_b, at the experimental temperature. The rate equations of both Falk, 1955 and Mearns and Ofosu-Asiedu, 1984a were tested. The k-values of Falk, 1955 were shown to fit the data better than those of Ofosu-Asiedu, 1984a.

The critical particle diameter, estimated from the experimental measurements, is used to calculate the critical or initial supersaturation ratio of ammonium nitrate (S^i). This initial supersaturation

ratio is used to check for the formation of solid ammonium nitrate as discussed below. The formation and growth of NH_4NO_3 resulting from the NO_2-NH_3 reaction can be represented by four stages. Figure 4 shows these stages schematically. Based on these steps, the next section describes the computational procedure of the model.

5.1.1 Steps of the Model

General assumptions: Flow regime in the reactor is laminar. The Reynolds numbers for different runs are calculated and listed in Table IV, which shows the Reynolds numbers varying between approximately 100 and 380. The flow in the reactor is assumed to be uniform, resembling a plug flow reactor. The gases entering into the reactor have uniform velocity distribution because of the two perforated mixing plates just before the central gas delivery nozzle. The radial velocity profile is expected to develop along the tube if the tube is long. The pipe length necessary for development of a laminar velocity distribution may be calculated from the following equation:

$$\frac{X_t}{D} = 0.05\ N_{Re}$$

This equation indicates that a length of 35 cm and 133 cm would be required for Reynolds numbers of 100 and 380 respectively. Thus, the assumption of a uniform velocity profile is not unreasonable.

It is furthermore assumed that the radial variation of concentrations at any axial position is uniform. This assumption is justified by the slow reaction rate compared with the rapid diffusion of reactants in the air. Thus, the reaction system resembles a mixed flame system.

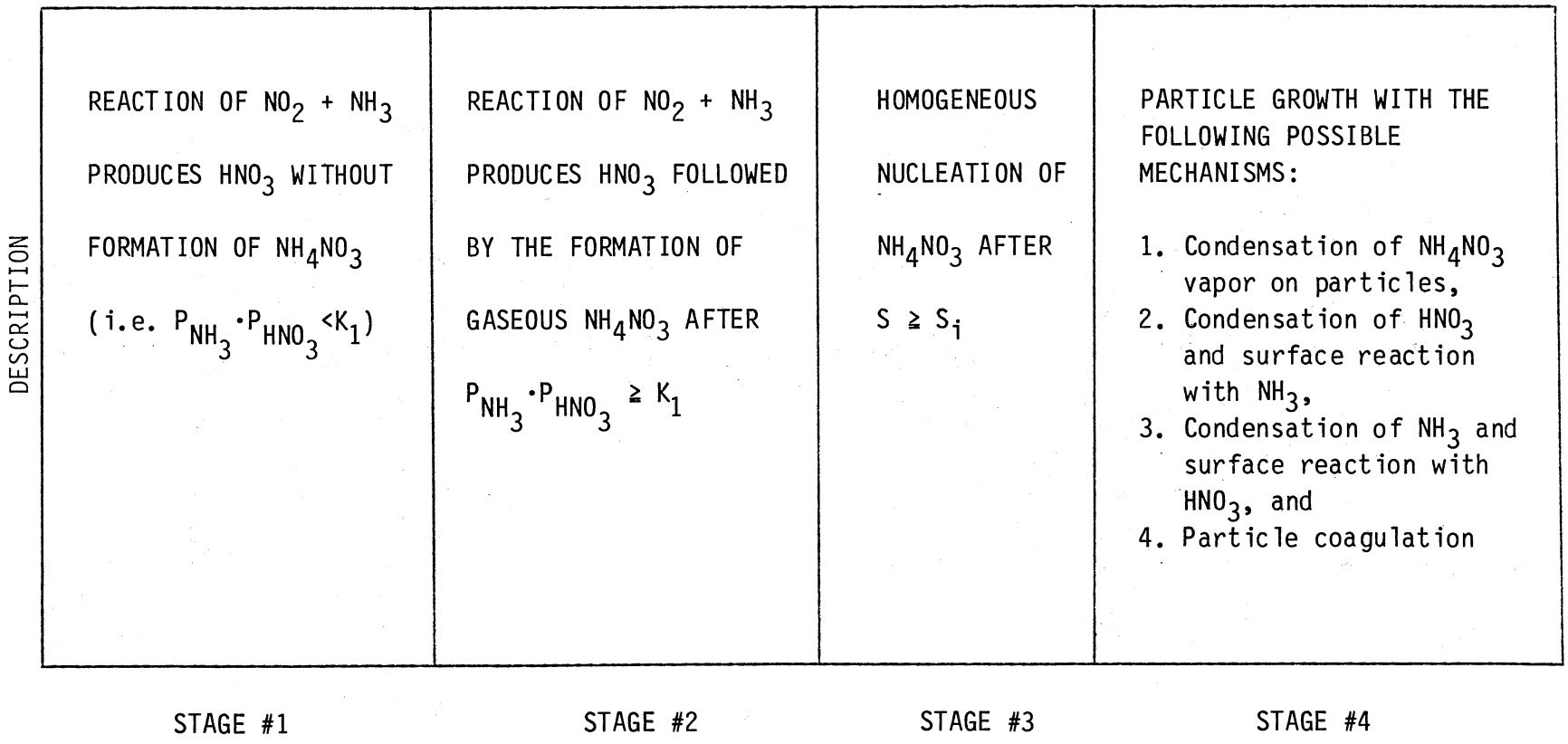

Figure 4. Schematic Diagram of the Four Stages of the Theoretical Model

Overall, the reactor is envisioned as a plug flow system. The reactants, upon entrance into the reactor mix rapidly and as the reactant gases flow down the reactor the reaction of NO_2 and NH_3 slowly proceeds. The reactor from the mixing plane to the detection point can be divided into four sections or stages as shown in Figure 4. As one moves from stage one to four, a new physiochemical process is added to the system.

Stage 1. At the beginning of the reaction, NO_2 reacts with NH_3 to produce HNO_3 without forming any NH_4NO_3 as long as $P_{NH_3} \cdot P_{HNO_3} < K_1$. In this case the reaction rate expression given by equation [16] is used to calculate the partial pressures of NO_2, NH_3, H_2O, and HNO_3. The method used to solve the differential equation is discussed in Section 5.1.2. The product $(P_{NH_3} \cdot P_{HNO_3})$ is compared to the value of the equilibrium constant K_1. When this product exceeds K_1, ammonium nitrate starts to form designating the beginning of stage 2.

Stage 2. In the second stage, while NO_2 and NH_3 continue to react, concentration of HNO_3 reaches a level such that NH_3 reacts with HNO_3 to produce gaseous NH_4NO_3. At this stage, the reaction rate expression described by equation [18] is used. The solution of the differential equation of this stage is discussed in Section 5.1.2. This rate expression is used to calculate the partial pressures of NO_2, NH_3, H_2O, and NH_4NO_3 as time progresses. A supersaturation ratio (S) is calculated by dividing the calculated partial pressure of ammonium nitrate by the vapor pressure of the pure solid ammonium nitrate. The new (or updated) supersaturation ratio is compared to the initial supersaturation (S^i), which is calculated from the experimental critical particle diameter. When the new supersaturation ratio equals or exceeds

the initially estimated one (i.e. $S \geq S^i$), the stage 3 starts.

Stage 3. The time from the beginning of the reaction until the beginning of this stage is recorded as the induction time. At this stage the supersaturation ratio of ammonium nitrate is high enough to allow the homogeneous nucleation of ammonium nitrate (i.e. the formation of stable nuclei). The classical nucleation theory is used to calculate (g^*) which is the number of vapor molecules in an embryo or nucleus of a critical size. The total number concentration of ammonium nitrate particles is, then, calculated by dividing the total number of molecules of ammonium nitrate by g^*.

Stage 4. This stage represents the particle growth by one or more of the possible growth mechanisms. The possible growth mechanisms include: condensation of NH_4NO_3 on the surface of nucleated particles; condensation of HNO_3 and surface reaction with NH_3; condensation of NH_3 and surface reaction with HNO_3; and particle coagulation. This stage starts when nucleation ceases and total number concentration of particle reaches a maximum value.

Three different tests were incorporated in this study to examine the mechanism of the particle growth. These three tests are the calculation of the condensation rates of NO_2, NH_3, HNO_3 and NH_4NO_3, species using equation [32] to see the significance of each rate, the use of a size distribution function based on the condensation equation to fit the measured size distribution, and the use of the approach of the evolution of the size distributions, reported by Seinfeld, 1986, as shown in Figures 1a and 1b in Chapter III.

It was found that ammonium nitrate aerosols form by homogeneous nucleation and grow by the condensation of ammonium nitrate vapor on the

freshly nucleated particles. Correction for condensation, in the computational procedure, is accounted for by first calculating the rate of condensation of ammonium nitrate vapors and then calculating the number of condensing molecules. The partial pressure and the supersaturation ratio of ammonium nitrate are then corrected by subtracting the condensed molecules from the total number of molecules in the gas phase.

The steps of the computational procedure are represented in a flow chart as shown in Figure 5.

5.1.2 Solution of the Differential Equations

Before discussing the solution of the differential equations, the derivation of the reaction rate equations shown in equations [16] and [18] is presented. Consider the reaction mechanism, reported by Mearns and Ofosu-Asiedu, 1984a and represented by the following reactions:

$$2NO_2 \underset{k_2}{\overset{k_1}{\rightleftharpoons}} N_2O_4 \qquad \text{fast} \qquad [10]$$

$$N_2O_4 + NH_3 \xrightarrow{k_3} HNO_3 + NH_2{\cdot}NO \qquad \text{slow} \qquad [11]$$

$$NH_2{\cdot}NO \xrightarrow{k_4} N_2 + H_2O \qquad \text{fast} \qquad [5]$$

$$N_2O_4 + H_2O \xrightarrow{k_5} HNO_3 + HNO_2 \qquad \text{slow} \qquad [13]$$

$$HNO_2 + NH_3 \underset{k_7}{\overset{k_6}{\rightleftharpoons}} NH_4NO_2 \qquad \text{fast} \qquad [14]$$

$$HNO_3 + NH_3 \underset{k_9}{\overset{k_8}{\rightleftharpoons}} NH_4NO_3 \qquad \text{fast} \qquad [4]$$

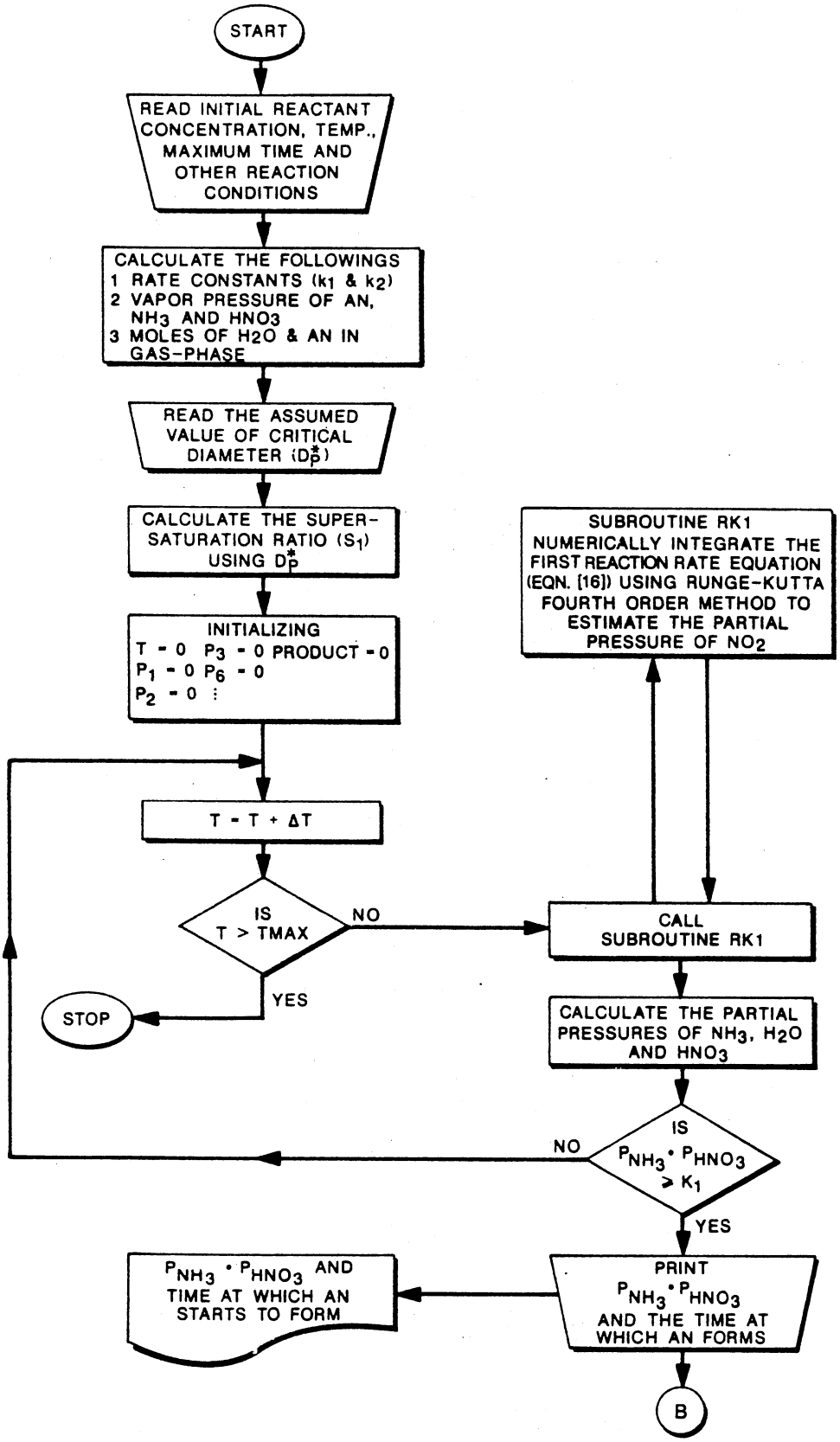

Figure 5. Flow Chart of the Computational Procedure

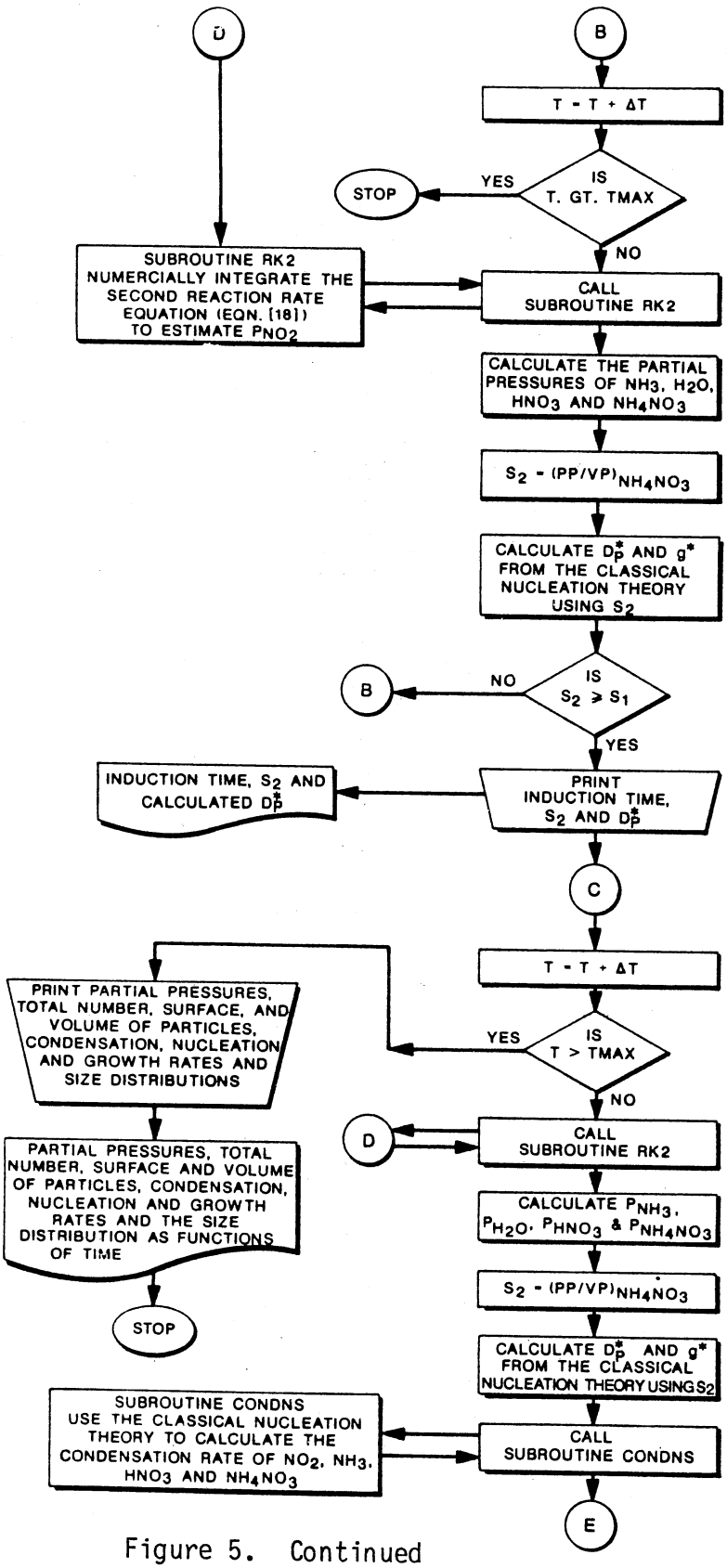

Figure 5. Continued

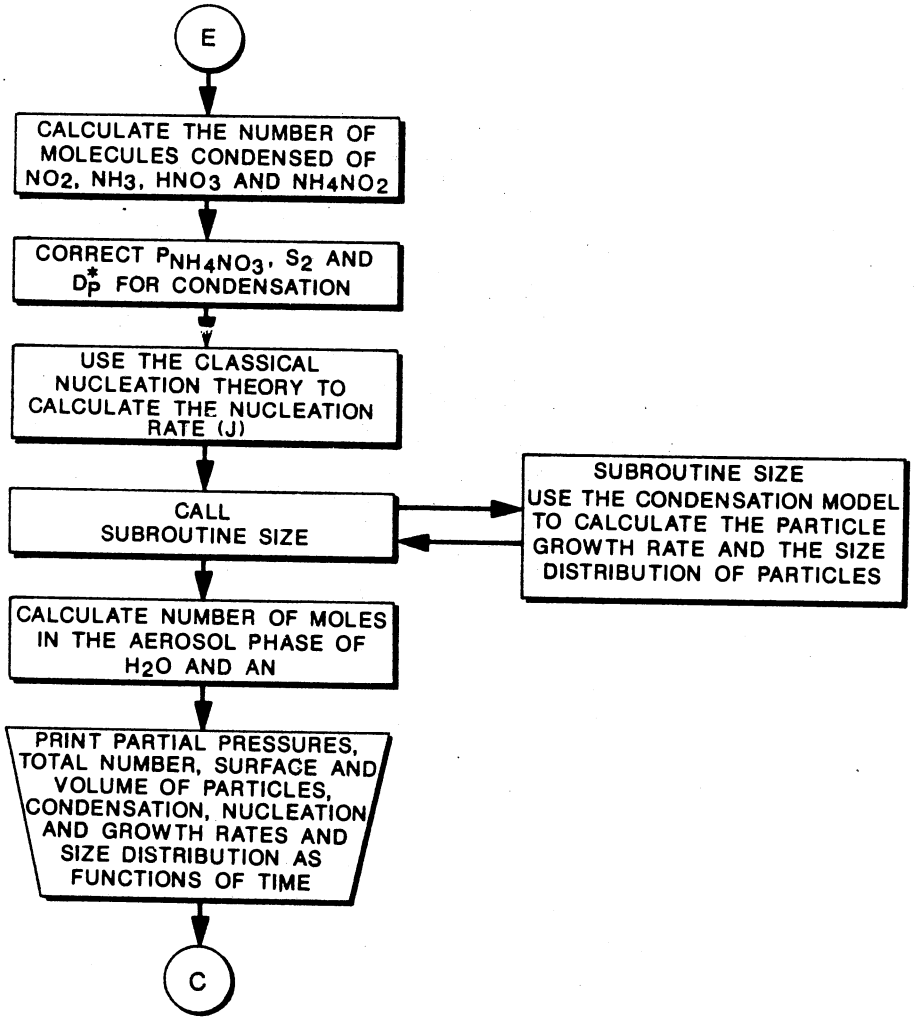

Figure 5. Continued

Reactions [4], [10] and [14] are fast and are limited by their thermodynamic equilibria. Reaction [5] is an irreversible and fast reaction, while reactions [11] and [13] are the rate controlling steps. The net rate of NO_2 consumption is equal to the net N_2O_4 consumption through equations [11] and [13]. That is:

$$-2\frac{dP_{NO_2}}{dt} = -\left(\frac{dP_{N_2O_4}}{dt}\right)_{\text{net by [11] and [13]}}$$

$$= k_3 P_{N_2O_4} P_{NH_3} + k_5 P_{N_2O_4} P_{H_2O}$$

at equilibrium of reaction [10]

$$K = \frac{k_1}{k_2} = \frac{P_{N_2O_4}}{(P_{NO_2})^2}$$

or

$$P_{N_2O_4} = KP_{NO_2}^2$$

Therefore,

$$-2\frac{dP_{NO_2}}{dt} = k_3 K P_{NO_2}^2 P_{NH_3} + k_5 K P_{NO_2}^2 P_{H_2O}$$

which is the same as equation [16], with $k_a = k_3K$ and $k_b = k_5K$, where K is the equilibrium constant of reaction [10].

The equilibrium constant of reaction [10] was calculated from the Gibbs free energies of the reactant and product and found to be 6.8.

The equilibrium concentration of N_2O_4 at ambient temperature and atmospheric pressure was calculated from the equilibrium constant of reaction [10] and found to be negligible compared to the concentration of NO_2. For example, for an NO_2 concentration of 30 ppm in air, the calculated equilibrium concentration of N_2O_4 was only 6.12 ppb. This indicates that in the reactant gas entering into the reactor, only 0.02% of NO_2 is in the form of N_2O_4.

The following steps are followed to solve the differential equations:

A. Stage 1:

Using the following notation for equation [12],

$$\underset{\text{(species 1)}}{2NO_2} + \underset{\text{(species 2)}}{NH_3} \longrightarrow \underset{\text{(species 3)}}{HNO_3} + \underset{\text{(species 4)}}{H_2O} + \underset{\text{(species 5)}}{N_2} \qquad [12]$$

Equation [16] can be written as:

$$-\frac{dP_1}{dt} = k_a P_2 P_1^2 + k_b P_4 P_1^2 \ , \quad \text{or}$$

$$-\frac{dP_1}{dt} = P_1^2(k_a P_2 + k_b P_4) \qquad [43]$$

Since $n_1 = n_1^o - n_1^r$ or $n_1^r = n_1^o - n_1$

and $n_2 = n_2^o - n_2^r$

where

n_i = number of moles of species i at any time

n_i^o = initial moles of species i at any time

n_i^r = reacted moles of species i at any time

From stoichiometry:

$$n_1^r = 2n_2^r \quad \text{or} \quad n_2^r = \tfrac{1}{2}\, n_1^r$$

Therefore,

$$n_2 = n_2^o - \tfrac{1}{2}\, n_1^r = n_2^o - \tfrac{1}{2}\, n_1^o + \tfrac{1}{2}\, n_1$$

since

$$n_i/V = P_i/RT = C_i$$

then,

$$C_2 = C_2^o - \tfrac{1}{2}\, C_1^o + \tfrac{1}{2}\, C_1$$

$$\frac{P_2}{RT} = \frac{P_2^o}{RT} - \tfrac{1}{2}\, \frac{P_1^o}{RT} + \tfrac{1}{2}\, \frac{P_1}{RT}$$

$$\therefore \quad P_2 = P_2^o - \tfrac{1}{2}\, P_1^o + \tfrac{1}{2}\, P_1$$

Similarly, we can find: $P_3 = \tfrac{1}{2}\, P_1^o - \tfrac{1}{2}\, P_1$, and

$$P_4 = \tfrac{1}{2}\, P_1^o - \tfrac{1}{2}\, P_1$$

Substitute for P_2 and P_4 in equation [43] to get a differential equation with one unknown:

$$\frac{-dP_1}{dt} = P_1^2 \left\{k_a P_2^o - \tfrac{1}{2}\, k_a P_1^o + \tfrac{1}{2}\, k_a P_1 + \tfrac{1}{2}\, k_b P_1^o - \tfrac{1}{2}\, k_b P_1\right\}$$

$$= P_1^2 \{k_a P_2^o - \tfrac{1}{2} k_a P_1^o + \tfrac{1}{2} k_b P_1^o + \tfrac{1}{2}(k_a - k_b) P_1\}$$

Let: $\alpha_1 = k_a P_2^o - \tfrac{1}{2} k_a P_1^o + \tfrac{1}{2} k_b P_1^o$, and

$$\beta_1 = \tfrac{1}{2} (k_a - k_b)$$

$$\therefore \frac{-dP_1}{dt} = P_1^2\{\alpha_1 + \beta_1 P_1\} = \alpha_1 P_1^2 + \beta_1 P_1^3 = f(P_1) \qquad [44]$$

or $$\frac{dP_1}{P_1^2(\alpha_1 + \beta_1 P_1)} = - dt$$

This equation can be analytically solved to yield

$$t = - \frac{1}{\alpha_1 P_1^o} + \frac{\beta_1}{\alpha_1} \ln \frac{\alpha_1 + \beta_1 P_1^o}{P_1^o} + \frac{1}{\alpha_1 P_1} - \frac{\beta_1}{\alpha_1} \ln \frac{\alpha_1 + \beta_1 P_1}{P_1}$$

or

$$t = \frac{1}{\alpha_1}\left(\frac{1}{P_1} - \frac{1}{P_1^o}\right) + \frac{\beta_1}{\alpha_1^2} \ln \left[\frac{P_1}{P_1^o} \frac{\alpha_1 + \beta_1 P_1^o}{\alpha_1 + \beta_1 P_1}\right] \qquad [45]$$

B. Stage 2:

Recall equation [1]

$$\underset{\text{(species 1)}}{2NO_2} + \underset{\text{(species 2)}}{2NH_3} \rightleftharpoons \underset{\text{(species 3)}}{NH_4NO_3} + \underset{\text{(species 4)}}{H_2O} + \underset{\text{(species 5)}}{N_2} \qquad [1]$$

The rate equation of stage 2 has the same form as the rate equation for stage 1, except that the consumption terms for ammonia, P_2, are different.

Equation [18] can be written as

$$\frac{-dP_1}{dt} = P_1^2 (k_a P_2 + k_b P_4)$$

In this case: $n_2^r = n_1^r$ or $P_2 = P_2^o - P_1^o + P_1$

and $P_4 = \frac{1}{2} P_1^o - \frac{1}{2} P_1$

$$\therefore \frac{-dP_1}{dt} = P_1^2\{k_a P_2^o - k_a P_1^o + k_a P_1 + \frac{1}{2} k_b P_1^o - \frac{1}{2} k_b P_1\}$$

$$= P_1^2\{k_a P_2^o - k_a P_1^o + \frac{1}{2} k_b P_1^o + (k_a - \frac{1}{2} k_b) P_1\}$$

$$\frac{-dP_1}{dt} = P_1^2\{\alpha_2 + \beta_2 P_1\} = \alpha_2 P_1^2 + \beta_2 P_1^3 = f(P_1) \qquad [46]$$

where $\alpha_2 = k_a P_2^o - k_a P_1^o + \frac{1}{2} k_b P_1^o = k_a P_2^2 - (k_1 - \frac{1}{2} k_b) P_1^o$

$$\beta_2 = k_a - \frac{1}{2} k_b$$

and

$$P_6 = P_{NH_4NO_3} = \frac{1}{2} P_1^o - \frac{1}{2} P_1$$

Equation [45] can be analytically solved to give

$$t - t_1 = \frac{1}{\alpha_2}\left(\frac{1}{P_1} - \frac{1}{P_1^o}\right) + \frac{\beta_2}{\alpha_2^2} \ln \left[\frac{P_1}{P_1^o} \frac{\alpha_2 + \beta_2 P_1^o}{\alpha_2 + \beta_2 P_1}\right] \qquad [47]$$

A numerical technique can be used to integrate equations [44] and [46], or the analytical solution can be solved by Newton-Raphson technique. In the model used in this project, equations [44] and [46] were solved

by a fourth order Runge-Kutta technique.

5.2 Discussion of the Results

As discussed in Section 4.2, the size distribution measurements are used to determine the critical particle size for each experiment. This task is done by considering the smallest particle diameter at which the DMPS is able to detect particles. This is usually above the lower detection limit of the DMPS indicating that smaller size particles could not have existed and this size is the critical particle diameter. Table V shows the estimated critical diameters of different reaction conditions. These critical diameters are used in the theoretical model to predict the initial supersaturation ratio (S^i), which is used to check for the formation of solid ammonium nitrate.

5.2.1 Variation of the Total Number Concentration With Time

The variations of the total ammonium nitrate particles with time, measured by the CNC alone and predicted by the model, are represented in Figures 8 through 26. These figures show an induction time followed by a burst in the total number concentration, which assympotically approaches a constant steady state level. The induction time is defined as the time elapsed before any particle starts to form. This behavior of an induction time followed by a burst in the nucleation agrees with the observations of de Pena, et al., 1973; and Olszyna, et al, 1974, for their NH_3-O_3-NH_4NO_3 system. It also agrees with the theoretical findings of the behavior of the aerosols in a laminar flow aerosol reactor (LFAR) of Warren and Seinfeld, 1984; Pratsinis, et al., 1986;

and Kodas and Friedlander, 1988. The induction times are shown in Table V for different reaction conditions, and are graphically shown in Figures 11 and 12 for two experiments, 26 and 28, respectively.

The mathematical model is used to predict the total number concentration of nitrate. These calculations are compared to the experimental data. When all the molecules of ammonium nitrate are assumed to form aerosols via homogeneous nucleation, very high total number concentrations are obtained, as represented by the dashed curves in Figures 8 through 21. However, when the condensation of ammonium nitrate vapor is also considered, the modeling results are improved and much lower concentrations are predicted. The condensation rates of NO_2, NH_3, HNO_3, H_2O and NH_4NO_3 are calculated assuming that all the above mentioned species condense immediately as they reach the surface of the particle (i.e. a condensation factor of unity is assumed). The results are presented in Table XX.

Table XX shows the calculated steady state condensation rates of NO_2, NH_3, HNO_3, H_2O and NH_4NO_3 at different reaction conditions. Two sets of these calculations are shown in Figures 6 and 7, corresponding to experiments 39 and 49 respectively. In general, the calculations show that the condensation rates of NO_2 and NH_3 are initially higher than those of HNO_3, H_2O and NH_4NO_3. The two former rates then assymptotically decreased. The condensation rate of H_2O and NH_4NO_3 start low and increase until they reach a high steady state value. On the other hand, the condensation rates of HNO_3 is smaller and varies at a very small rate. For example, the condensation rates of NO_2, NH_3, HNO_3, H_2O and NH_4NO_3, corresponding to experiment 49, initially are 2.7×10^{17}, 1.0×10^{18}, 9.3×10^{11}, 1.7×10^{17} and 7.9×10^{17} molecule cm^{-2} s^{-1},

TABLE XX

STEADY STATE VALUES OF THE CALCULATED CONDENSATION

RATES OF NO_2, NH_3, HNO_3, H_2O, AND NH_4NO_3

Run #	$[NH_3]$ ppm	$[NO_2]$ ppm	Temperature °C	Condensation Rate, molecule/cm^2/sec, of				
				NO_2	NH_3	HNO_3	H_2O	NH_4NO_3
26	5.77	4.88	20.0	7.5E+15	3.6E+17	5.6E+11	9.2E+16	4.4E+17
28	2.84	2.49	21.1	1.9E+16	1.6E+17	1.4E+12	4.6E+16	2.2E+17
32	13.65	3.19	20.0	5.2E+15	0.0E+00	2.7E+11	5.9E+16	2.8E+17
35	5.69	5.02	20.0	9.9E+15	3.6E+17	5.9E+11	9.5E+16	4.5E+18
37	1.13	11.35	20.0	5.5E+15	0.0E+00	2.4E+12	2.1E+17	1.0E+18
39	5.72	5.03	23.9	6.4E+16	3.7E+17	7.0E+11	1.0E+17	4.2E+17
47	1.13	5.01	20.0	1.0E+16	0.0E+00	2.7E+12	9.5E+16	4.5E+17
48	5.65	4.96	15.6	1.0E+16	2.9E+17	2.5E+11	9.4E+16	4.5E+17
49	11.28	9.87	14.4	2.1E+15	5.6E+17	9.3E+11	1.9E+17	1.0E+18
58	0.48	0.77	4.4	5.4E+17	9.0E+15	1.0E+11	1.0E+17	5.1E+17
60	0.47	0.76	4.4	5.8E+16	8.2E+15	1.1E+11	1.0E+17	4.8E+17

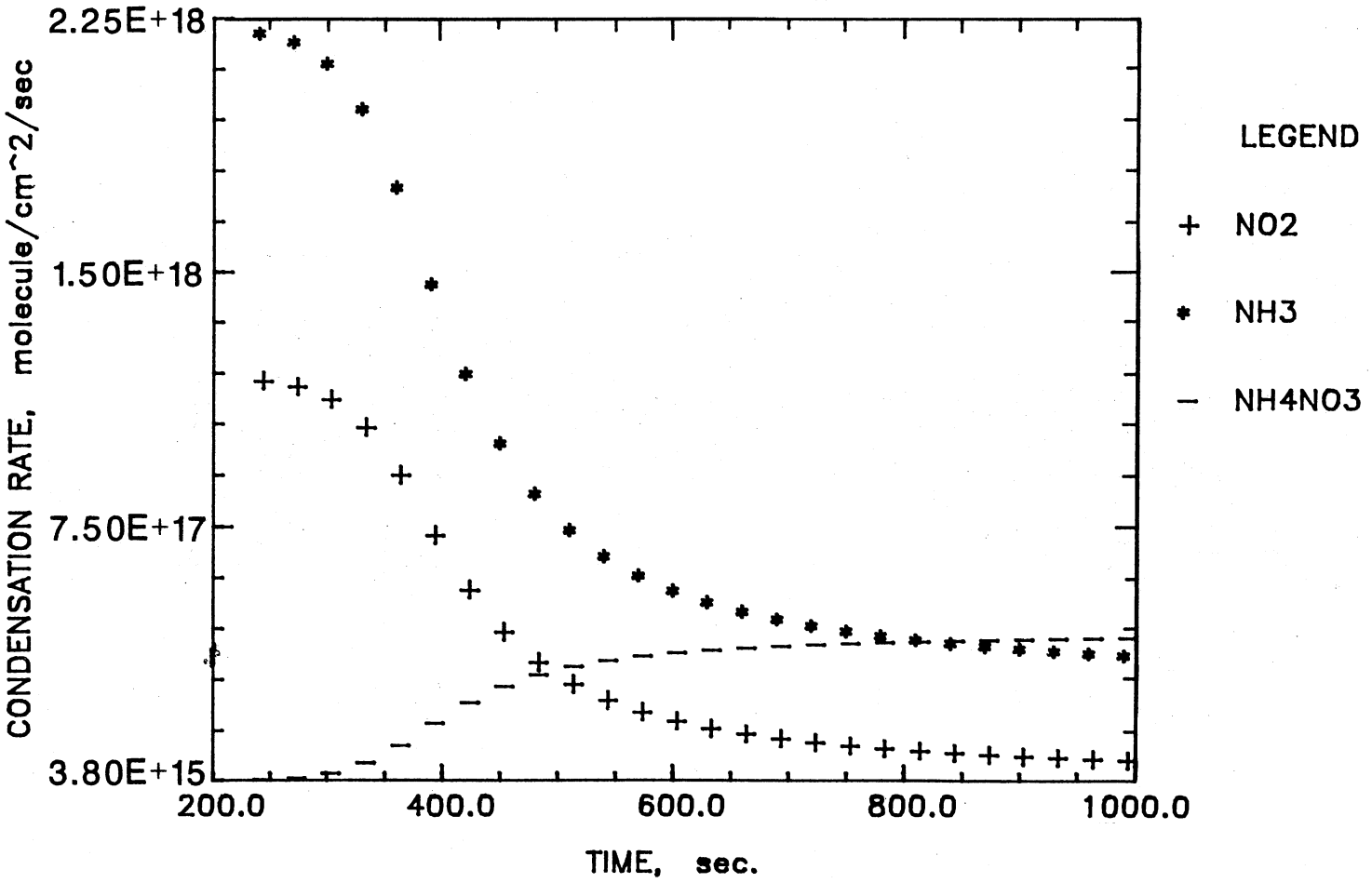

Figure 6. Condensation Rates of Nitrogen Dioxide, Ammonia and Ammonium Nitrate for $[NH_3] = [NO_2] = 5$ ppm, RT. = 3 s and T = 24 °C (Experiment 39)

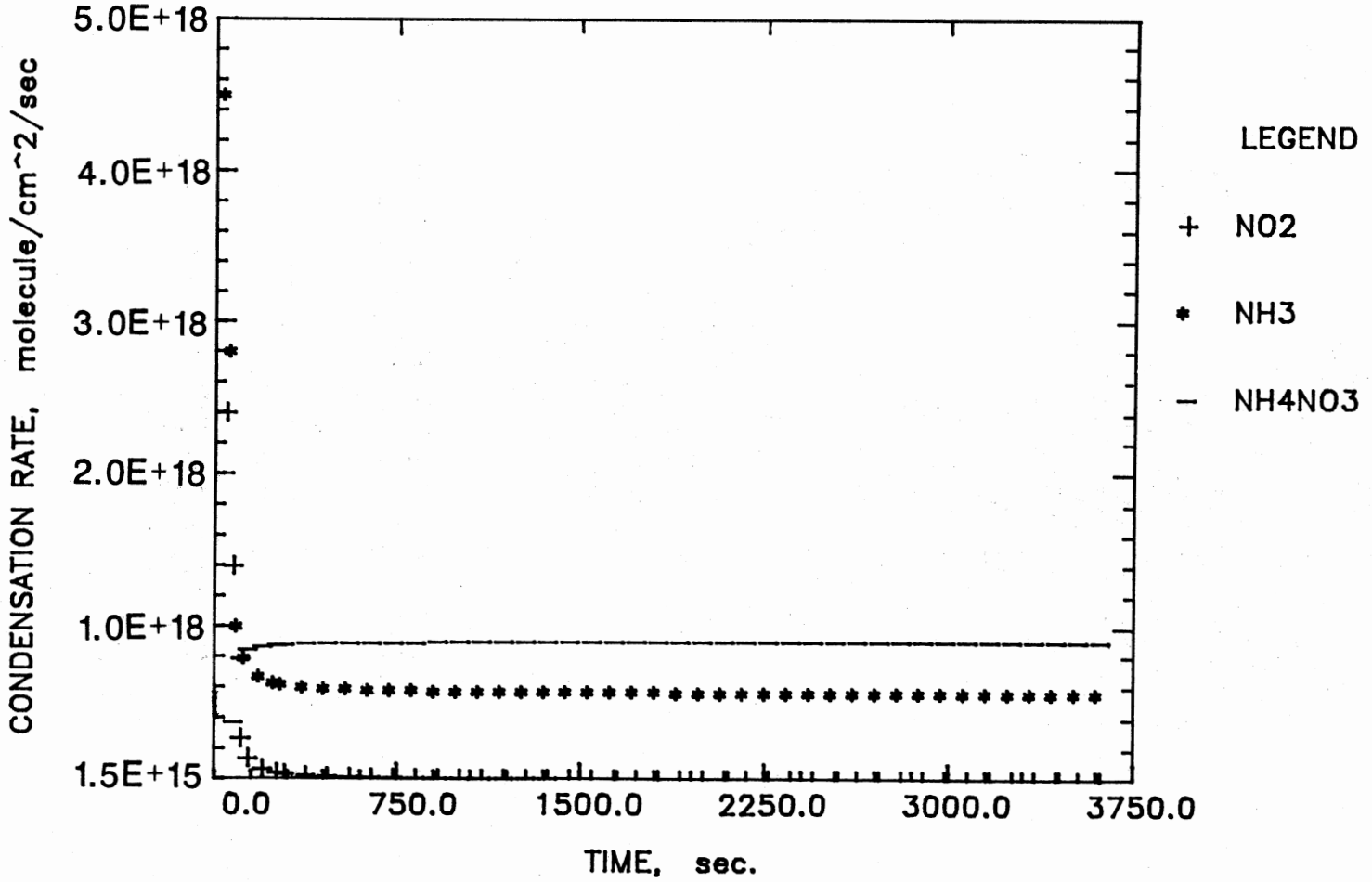

Figure 7. Condensation Rates of Nitrogen Dioxide, Ammonia and Ammonium Nitrate for $[NH_3] = [NO_2] = 10$ ppm, RT. = 3 s and T = 14 °C (Experiment 49)

respectively. The steady state values of the condensation rates of NO_2, NH_3, HNO_3, H_2O and NH_4NO_3 are 2.1×10^{15}, 5.6×10^{17}, 9.27×10^{11}, 1.9×10^{17} and 1.0×10^{18} molecule cm^{-2} s^{-1}, respectively. This shows that it is possible that any of these gases condense on the surface of the particles. However, the condensation of vapor molecules of NH_4NO_3 is the dominant one.

The reaction rate constants (k_a and k_b) reported by Falk (1955) are used in the model which give a better prediction than those reported by Mearns and Ofosu-Asiedu (1984a) as can be seen in Figures 8 and 9. For most of the experiments, when the k-values of Mearns and Ofosu-Asiedu, 1984a are used, the model does not predict any particles, even when only the nucleation is considered, until at a very late reaction time.

Figures 8 to 26 show that as the temperature or the concentration of nitrogen dioxide decreases, the deviation between the experimental measurements and the theoretical calculation increases. For example, at low concentration of NO_2, less than 3 ppm as shown in Figures 19-21 the model predicts lower number concentrations of ammonium nitrate at longer induction times. At very low concentrations of NO_2 (less than or equal to 1 ppm as in the case of Figures 22-26), the calculation predicts no particles, even when only nucleation is considered, while experiments show a significant concentration. This observation agrees with the finding of Mearns and Ofosu-Asiedu, 1984a, in that the time for the onset of the salt formation can be increased by decreasing the partial pressure of NO_2 regardless of the temperature or the residence time.

The conclusion from these results is that the initial super-saturation ratio rapidly increases leading to a burst in the homogeneous nucleation, which then decreases due to the condensation of the monomer

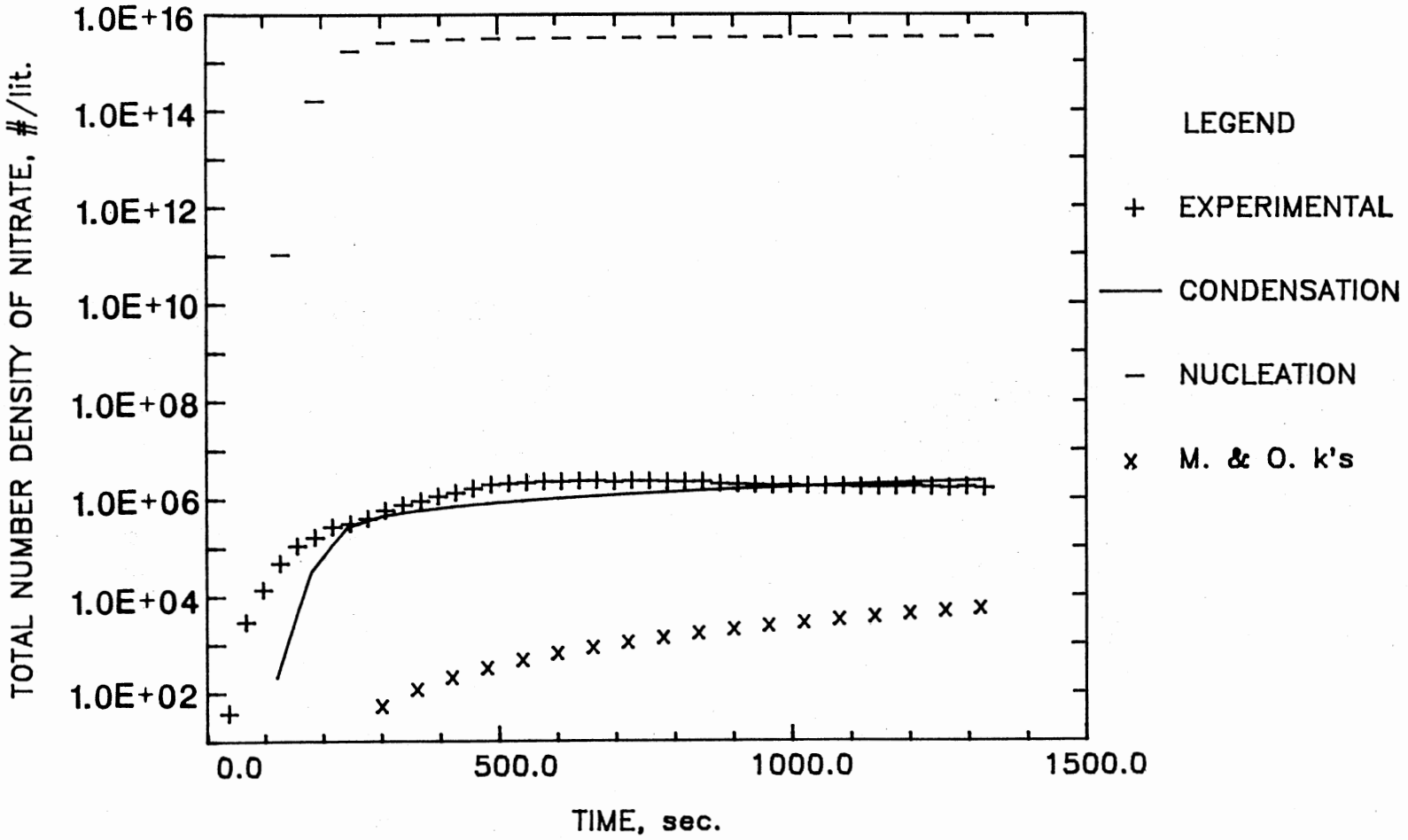

Figure 8. Total Number Concentration of Ammonium Nitrate vs. Reaction Time for $[NH_3] = [NO_2] = 5$ ppm, RT. = 10 s and T = 15.5 °C (Experiment 48) (M & O k's Stands for Mearns and Ofosu-Asiedu, 1984a k-values)

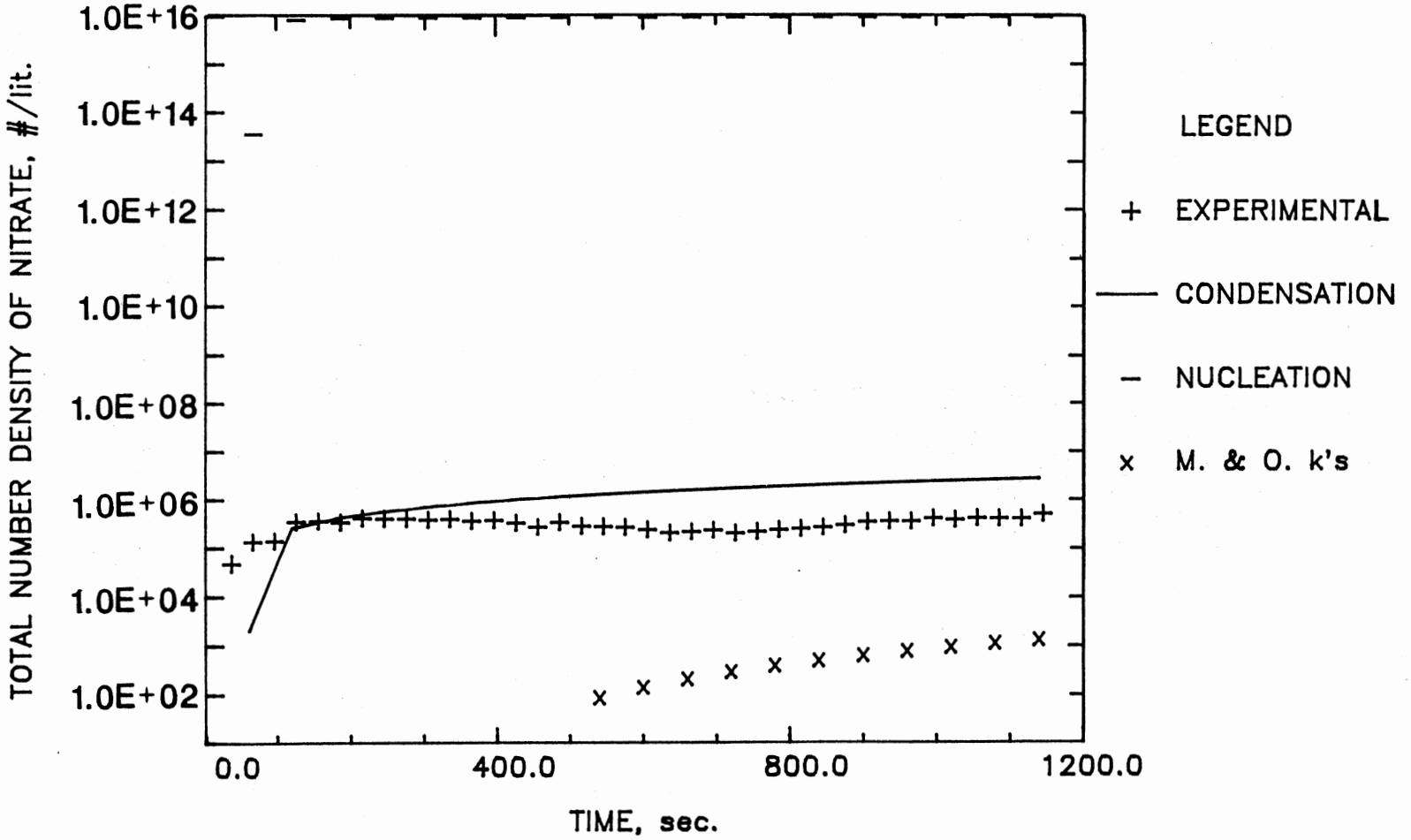

Figure 9. Total Number Concentration of Ammonium Nitrate vs. Reaction Time for $[NH_3]$ = 1 ppm, $[NO_2]$ = 11 ppm, RT. = 5 s and T = 19 °C (Experiment 36) (M & O k's Stands for Mearns and Ofosu-Asiedu, 1984a k-values)

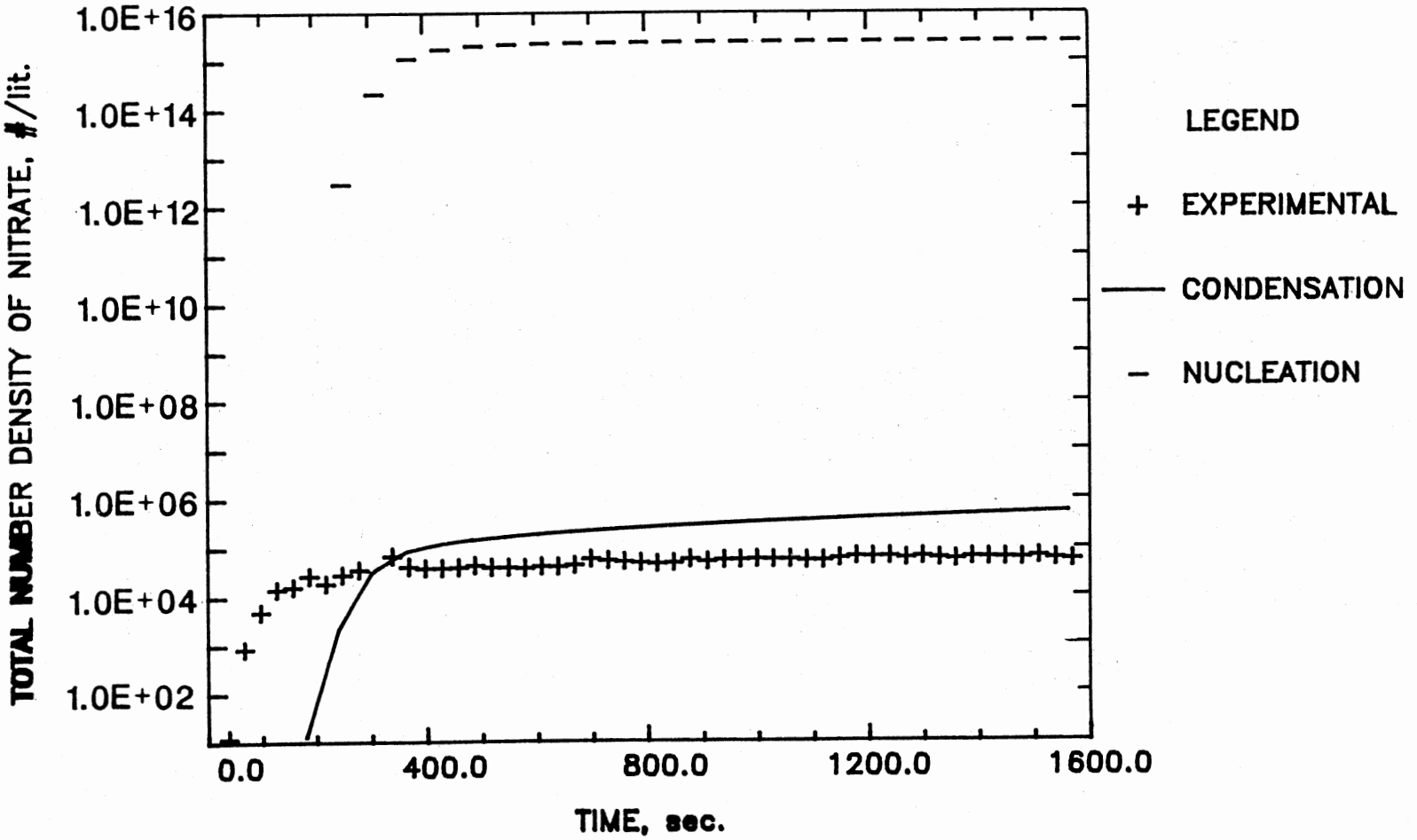

Figure 10. Total Number Concentration of Ammonium Nitrate vs. Reaction Time for $[NH_3]$ = 1 ppm $[NO_2]$ = 5 ppm, RT. = 5 s and T = 20 °C (Experiment 47)

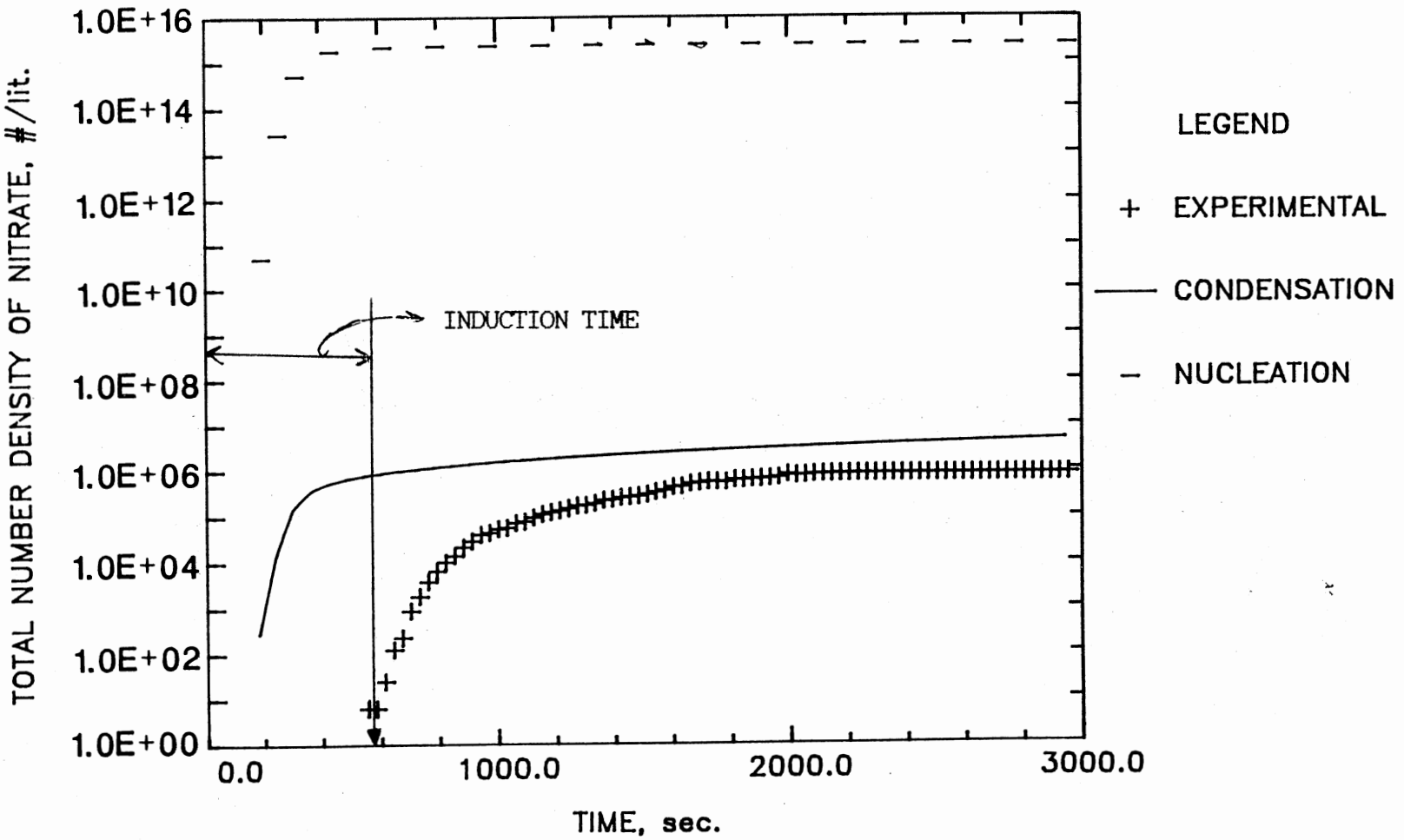

Figure 11. Total Number Concentration of Ammonium Nitrate vs. Reaction Time for $[NH_3] = [NO_2] = 5$ ppm, RT. = 10 s and T = 20 °C (Experiment 26)

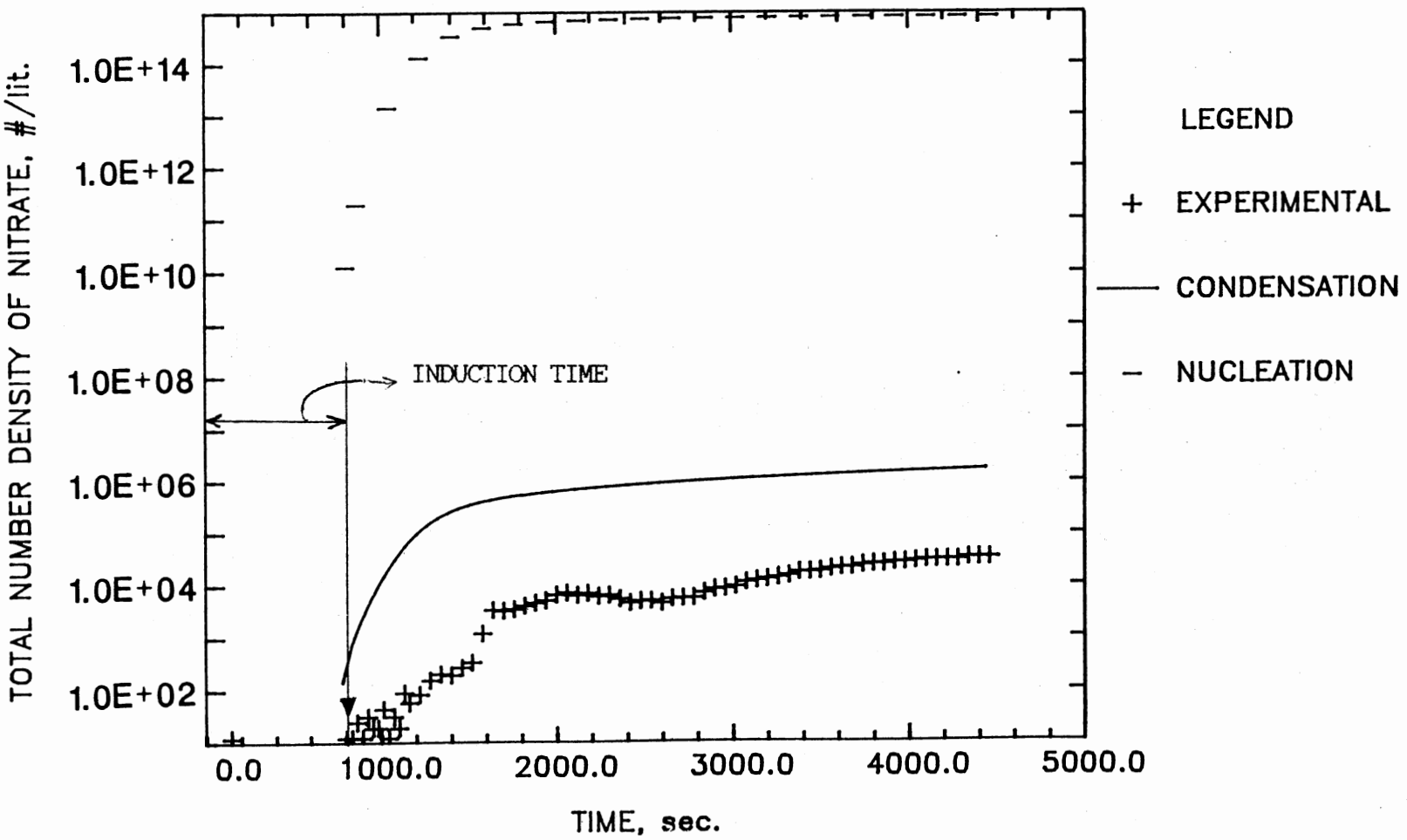

Figure 12. Total Number Concentration of Ammonium Nitrate vs. Reaction Time for $[NH_3] = [NO_2] = 2.5$ ppm, RT. = 10 s and T = 21 °C (Experiment 28)

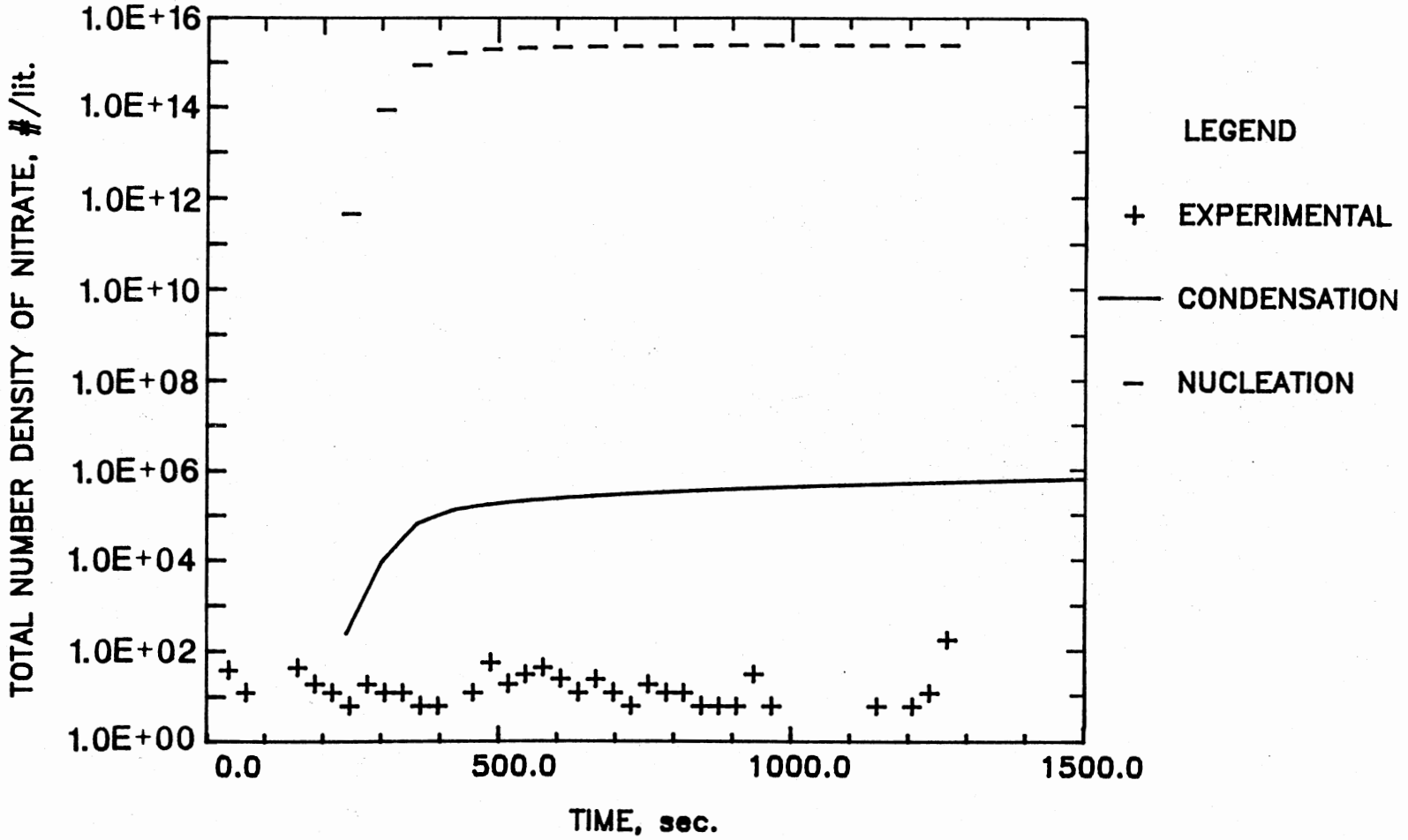

Figure 13. Total Number Concentration of Ammonium Nitrate vs. Reaction Time for $[NH_3]$ = 0.5 ppm $[NO_2]$ = 5 ppm, RT. = 5 s and T = 20 °C (Experiment 45)

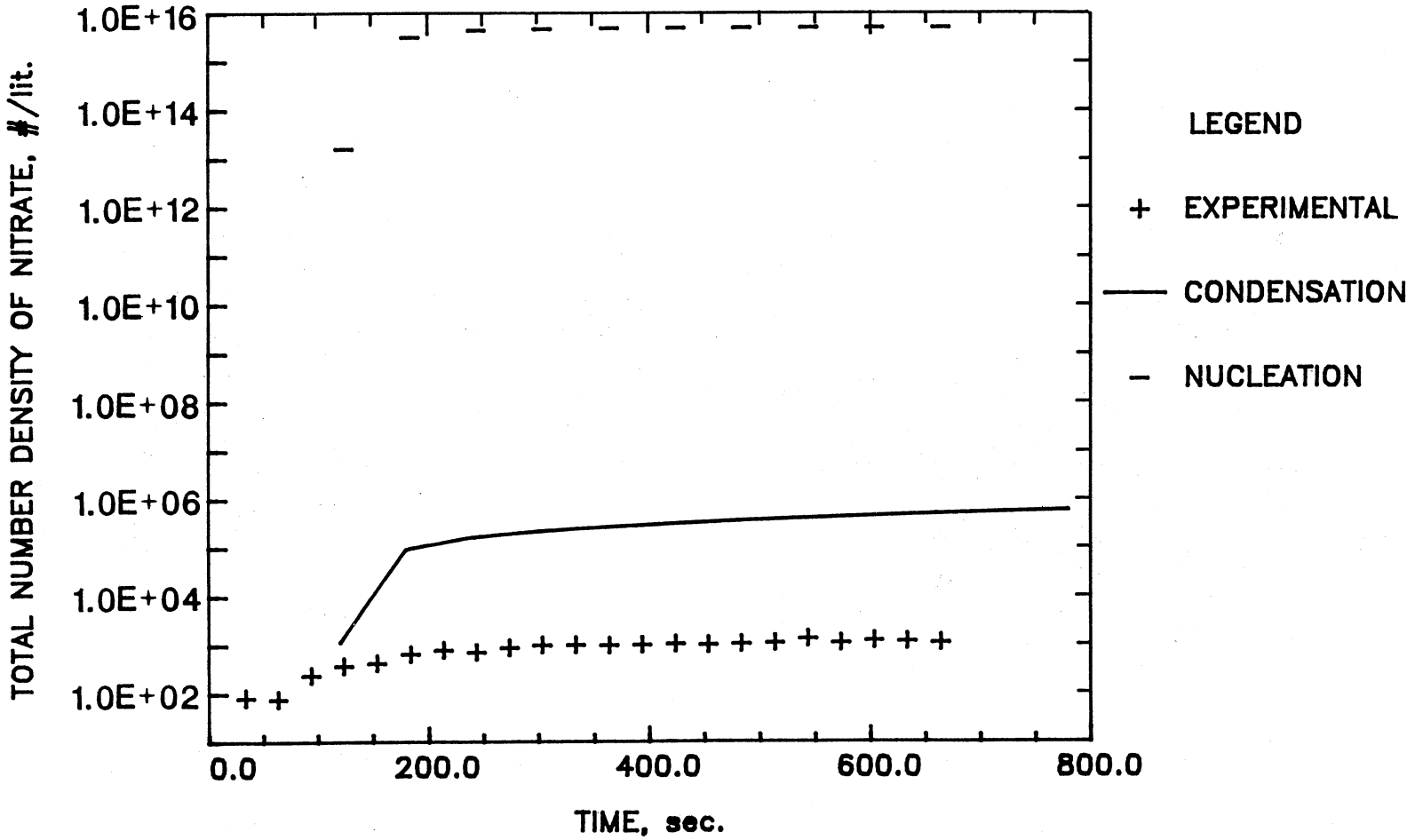

Figure 14. Total Number Concentration of Ammonium Nitrate vs. Reaction Time for $[NH_3]$ = 0.5 ppm $[NO_2]$ = 8 ppm, RT. = 4 s and T = 20 °C (Experiment 46)

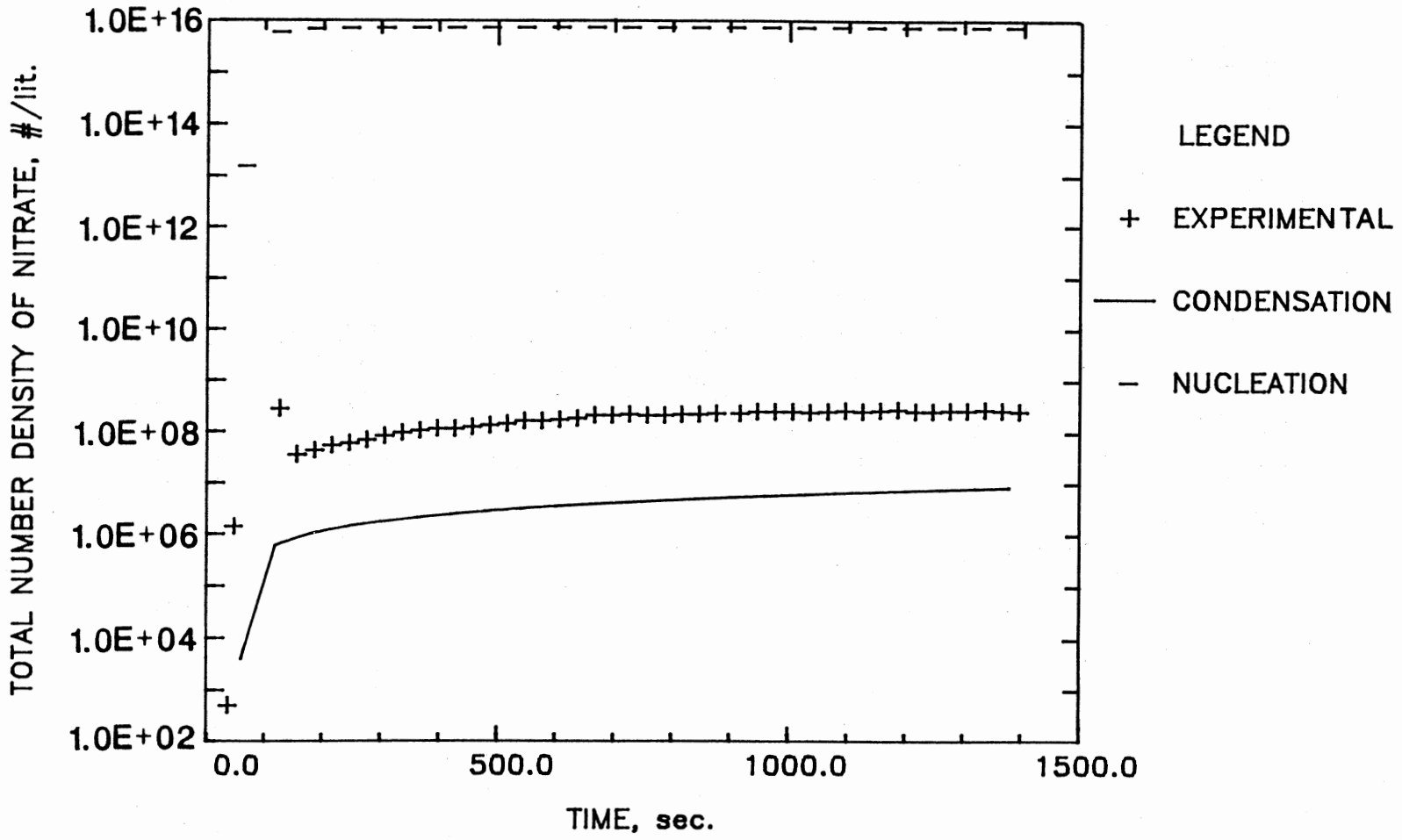

Figure 15. Total Number Concentration of Ammonium Nitrate vs. Reaction Time for $[NH_3] = [NO_2] = 10$ ppm, RT. = 10 s and T = 20 °C (Experiment 30)

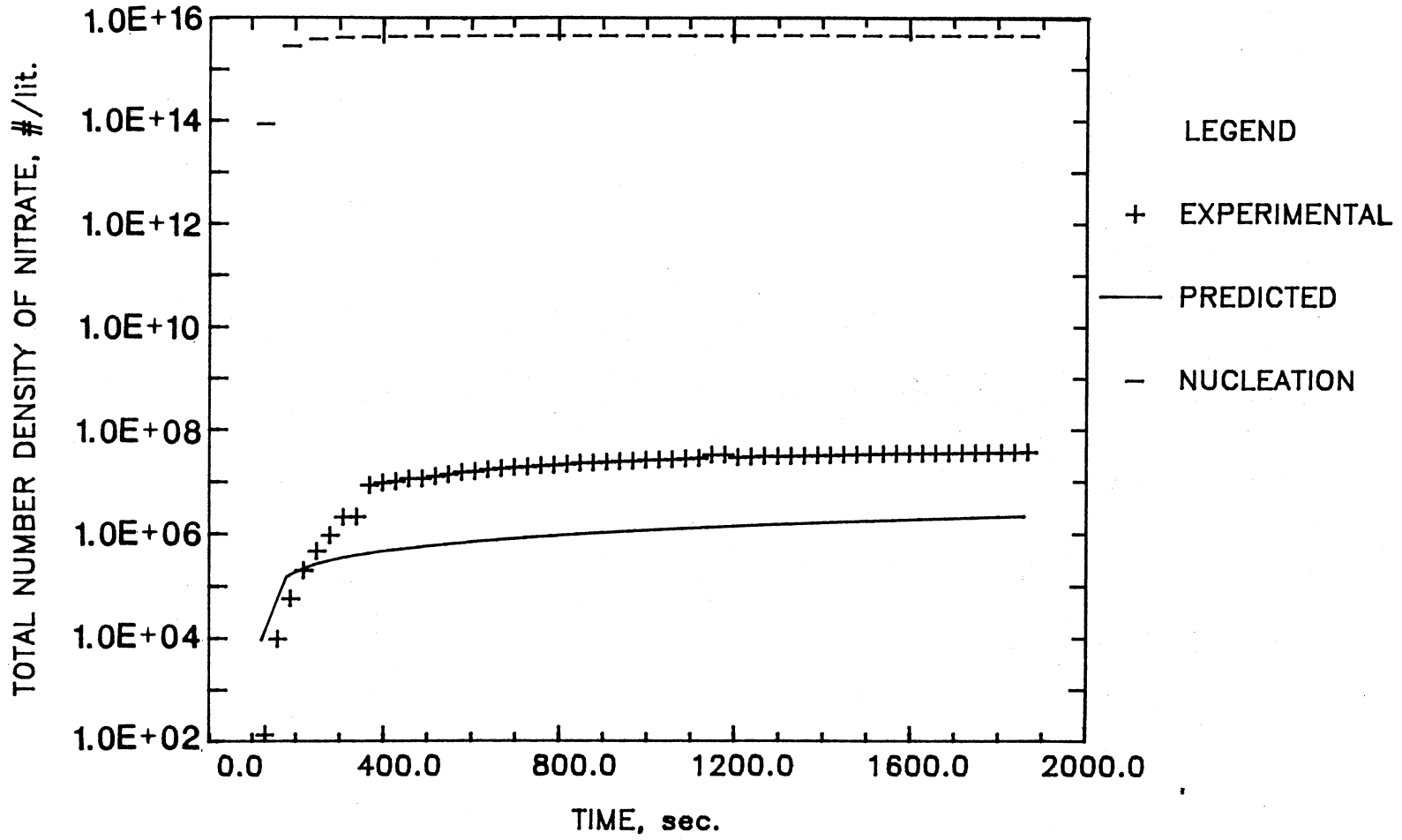

Figure 16. Total Number Concentration of Ammonium Nitrate vs. Reaction Time for $[NH_3] = [NO_2] = 8$ ppm, RT. = 30 s and T = 21 °C (Experiment 54)

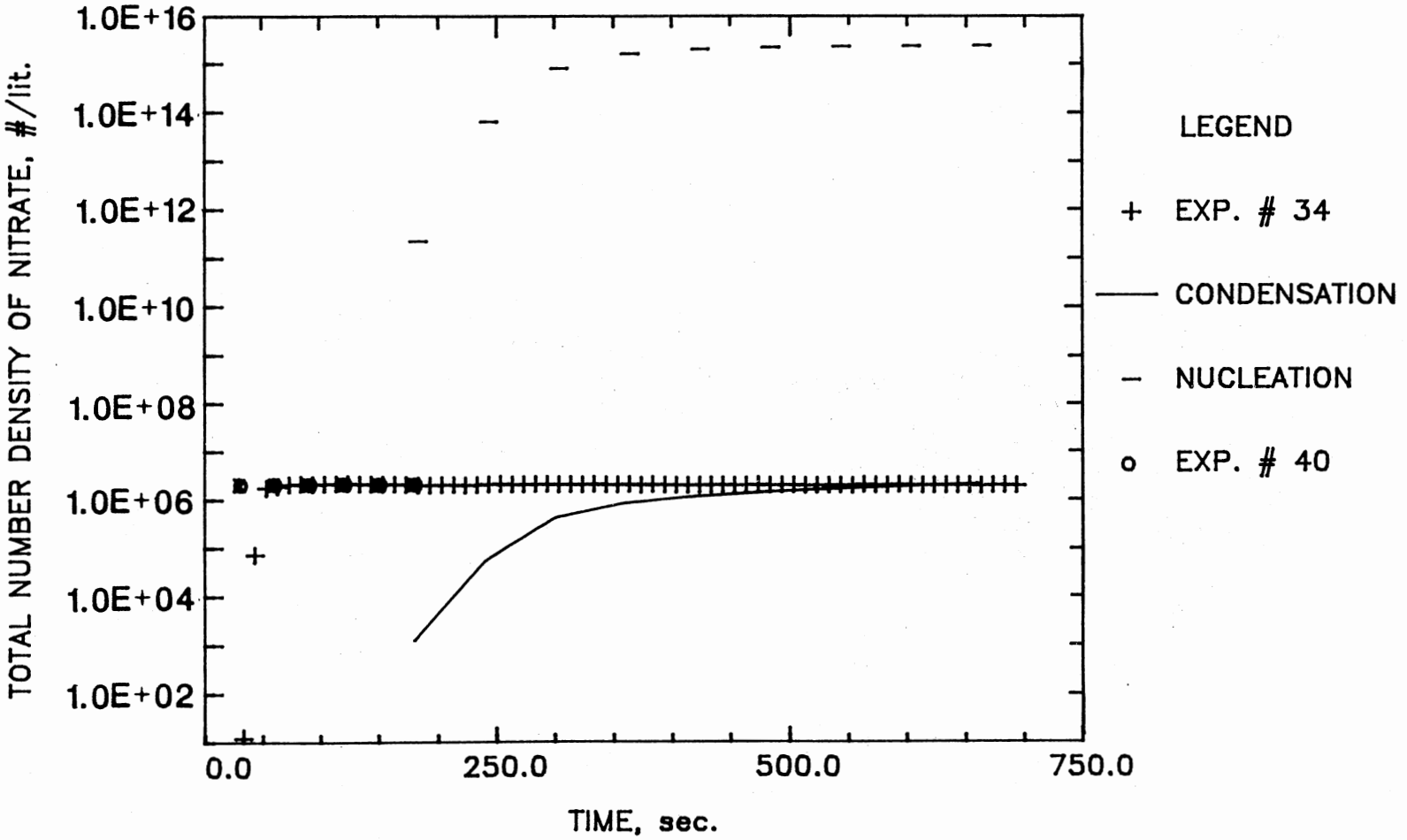

Figure 17. Total Number Concentration of Ammonium Nitrate vs. Reaction Time for $[NH_3] = [NO_2] = 5$ ppm, RT. = 5 s and T = 20 °C (Experiments 34 & 40)

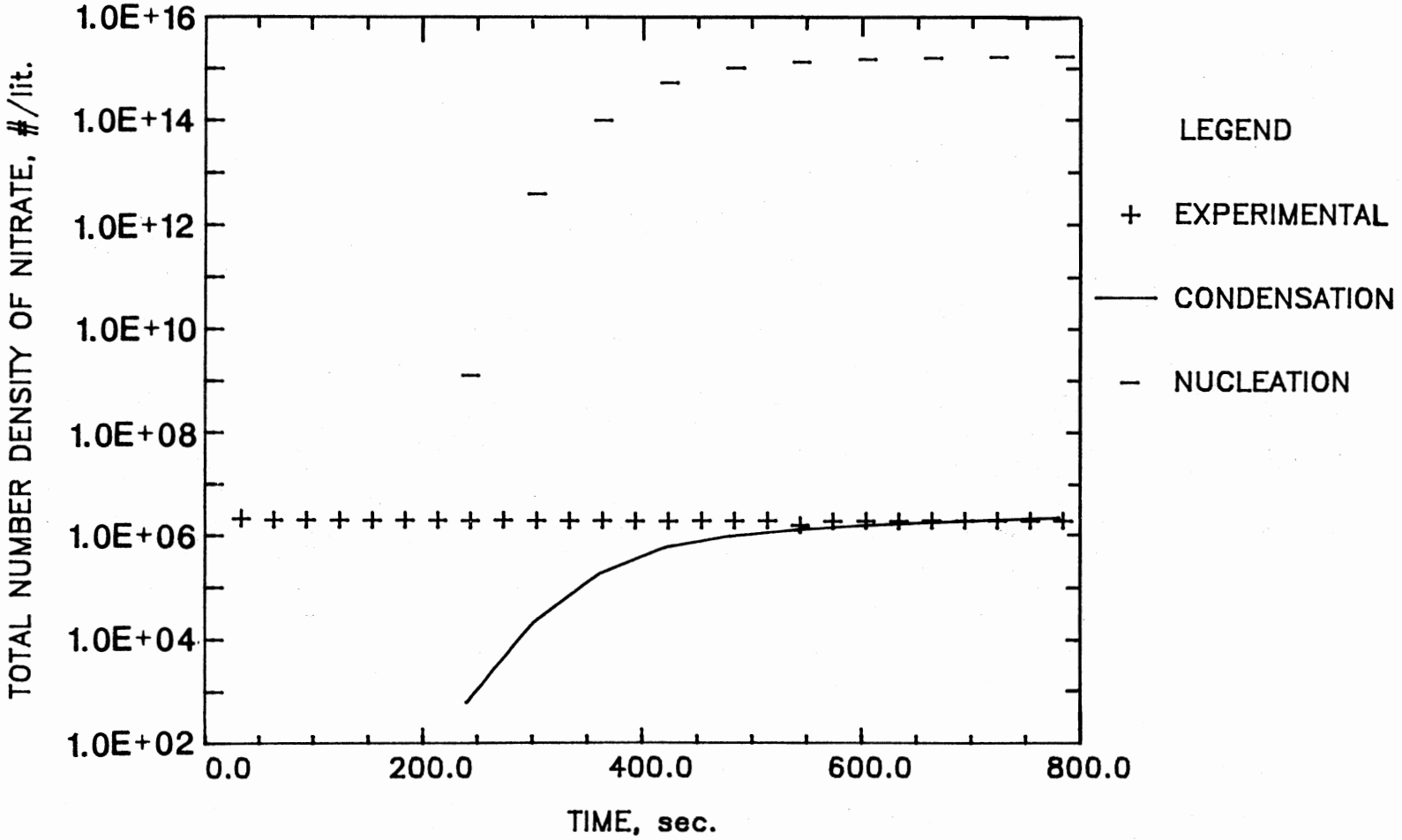

Figure 18. Total Number Concentration of Ammonium Nitrate vs. Reaction Time for $[NH_3] = [NO_2] = 5$ ppm, RT. = 3 s and T = 24 °C (Experiment 38)

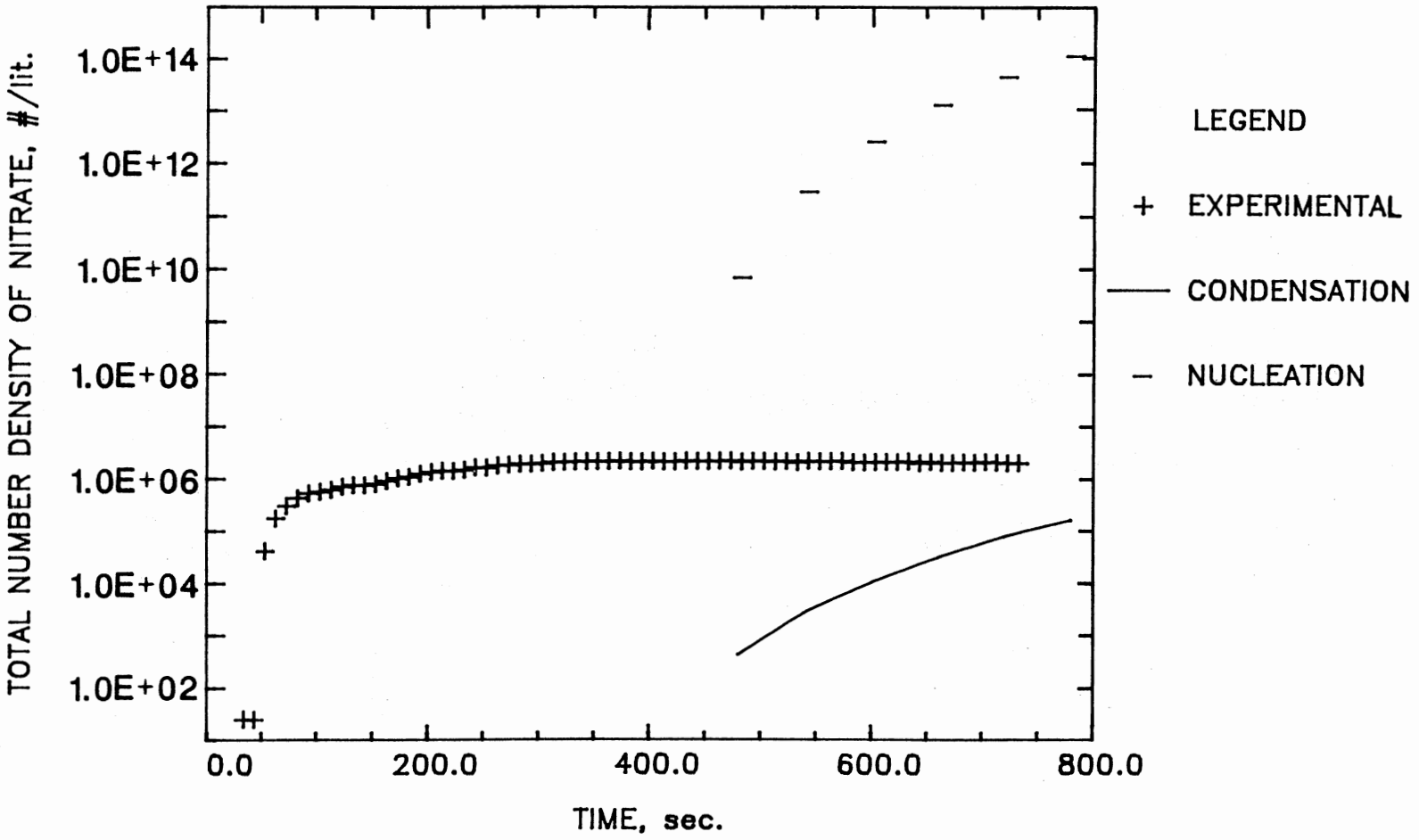

Figure 19. Total Number Concentration of Ammonium Nitrate vs. Reaction Time for $[NH_3]$ = 13.5 ppm $[NO_2]$ = 3 ppm, RT. = 5 s and T = 22 °C (Experiment 31)

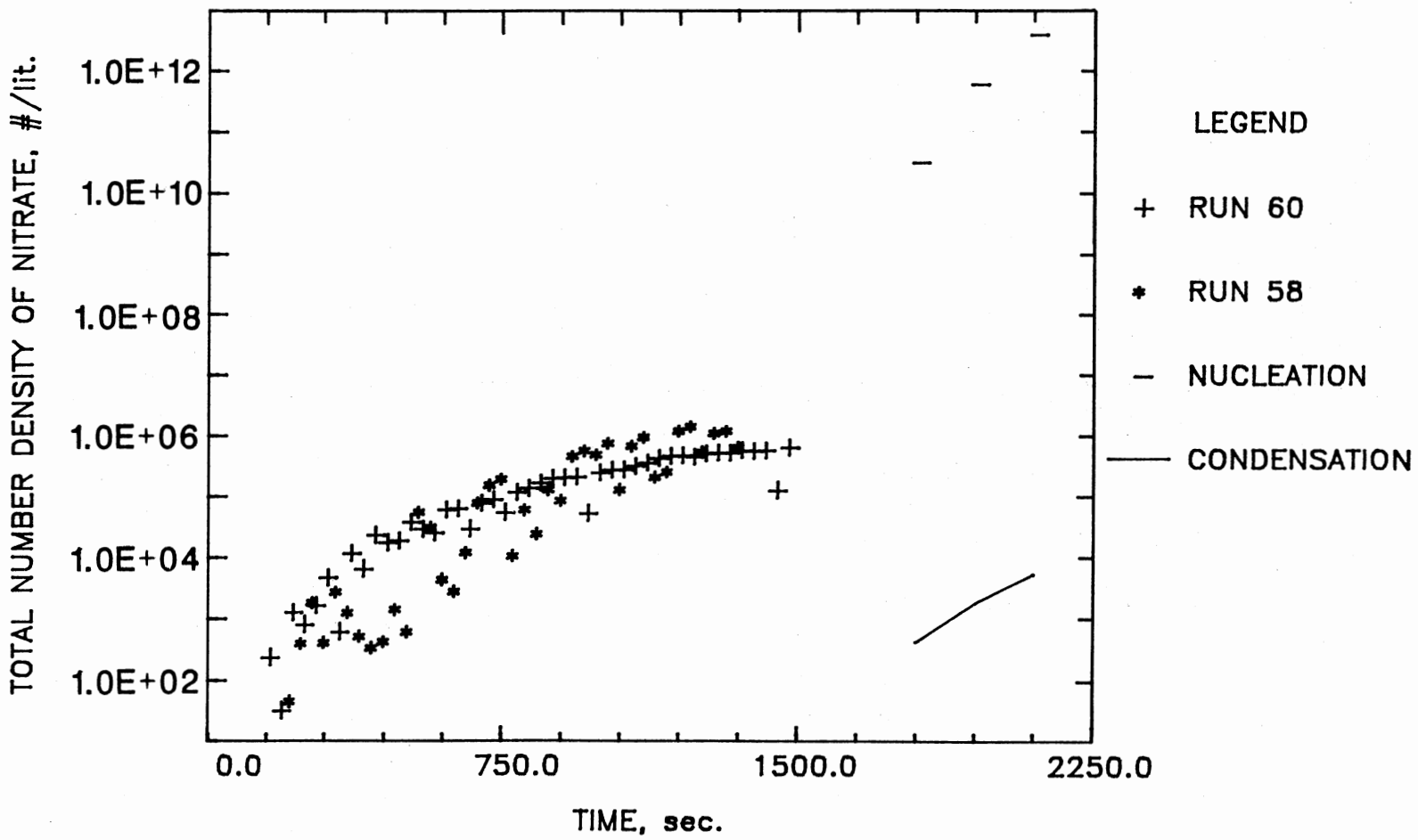

Figure 20. Total Number Concentration of Ammonium Nitrate vs. Reaction Time for $[NH_3] = [NO_2] = 0.5$ ppm, RT. = 10 s and T = 4 °C (Experiments 58 & 60)

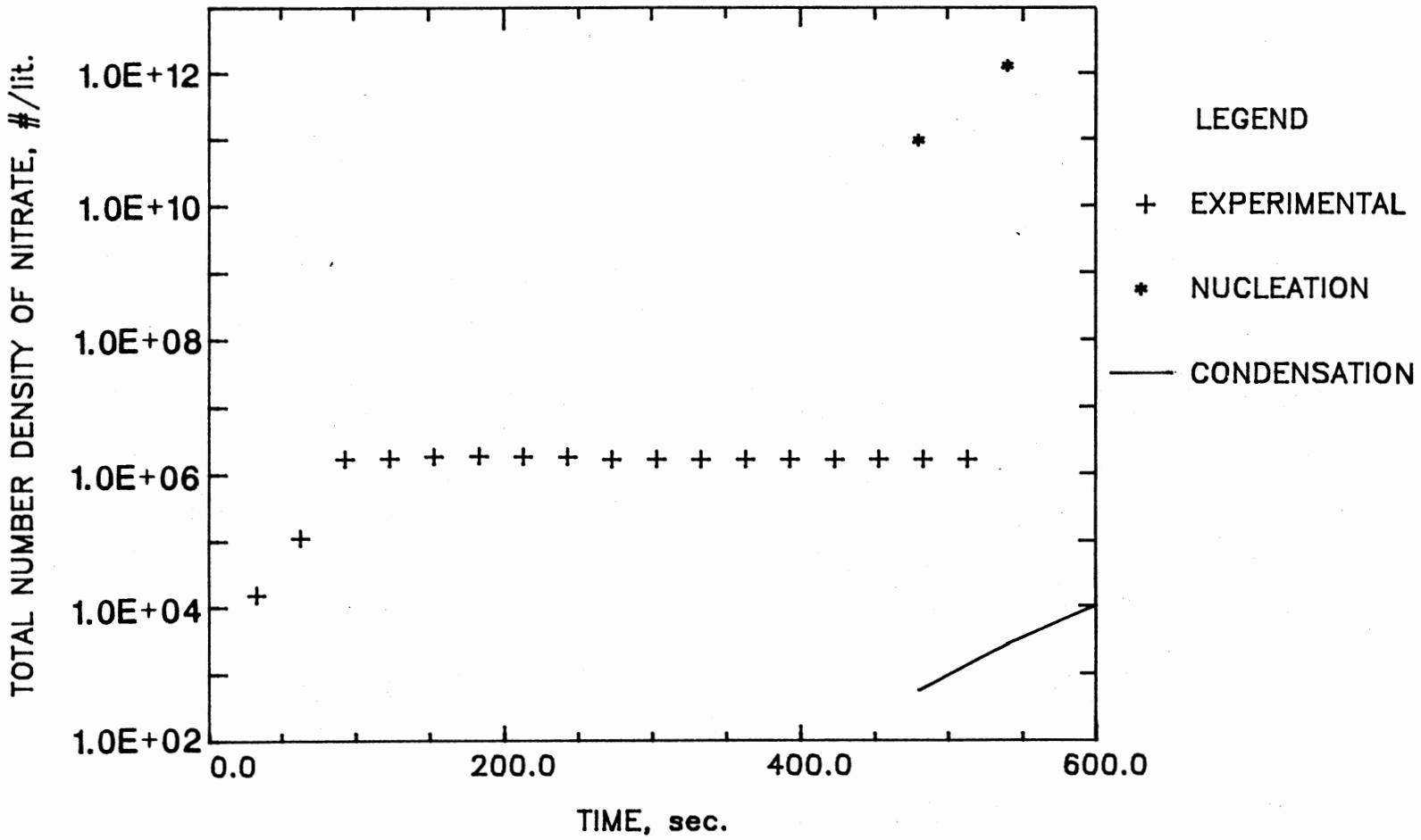

Figure 21. Total Number Concentration of Ammonium Nitrate vs. Reaction Time for $[NH_3]$ = 3 ppm $[NO_2]$ = 2 ppm, RT. = 10 s and T = 14 °C (Experiment 50)

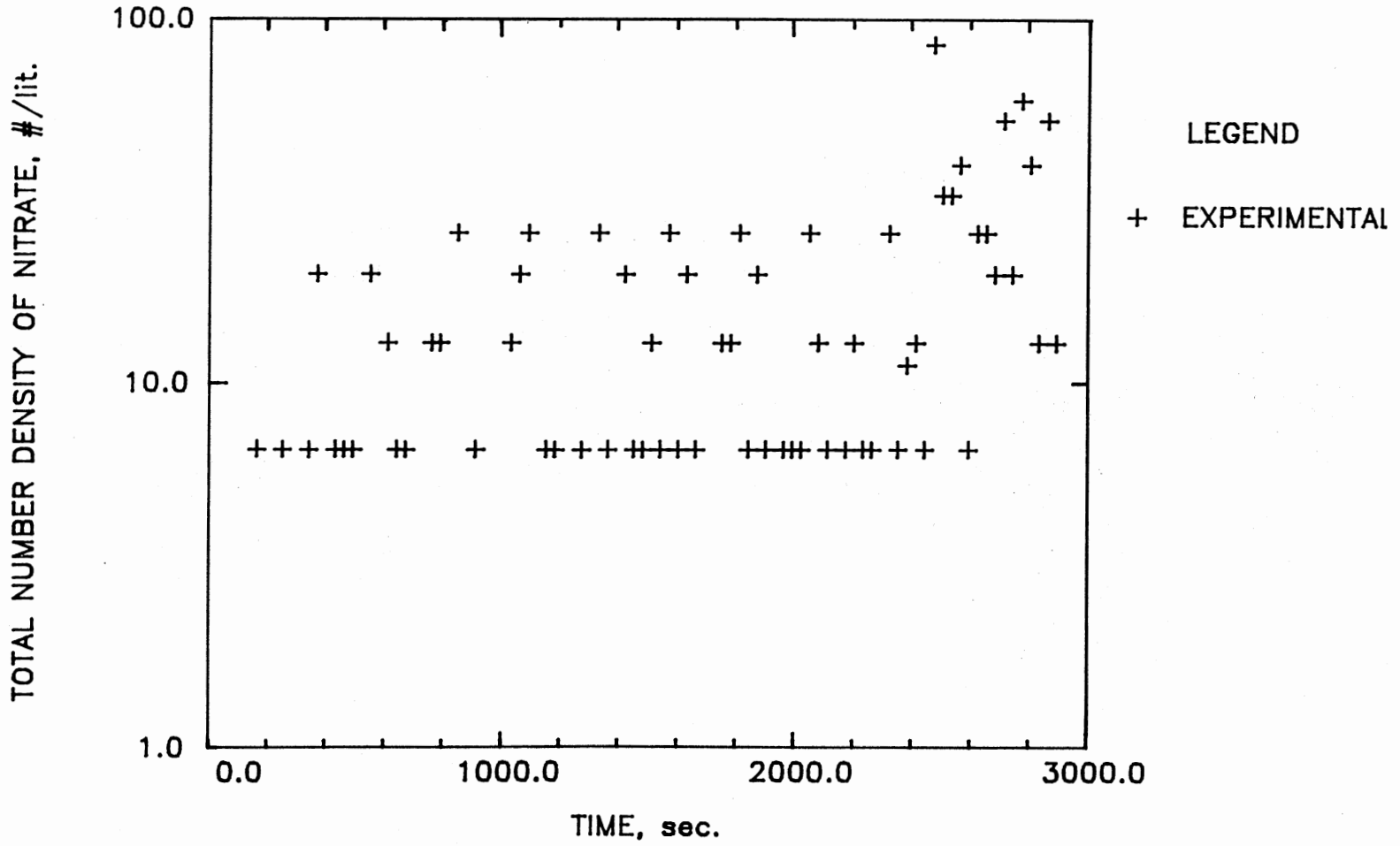

Figure 22. Total Number Concentration of Ammonium Nitrate vs. Reaction Time for $[NH_3] = [NO_2] = 1$ ppm, RT. = 10 s and T = 21 °C (Experiment 29)

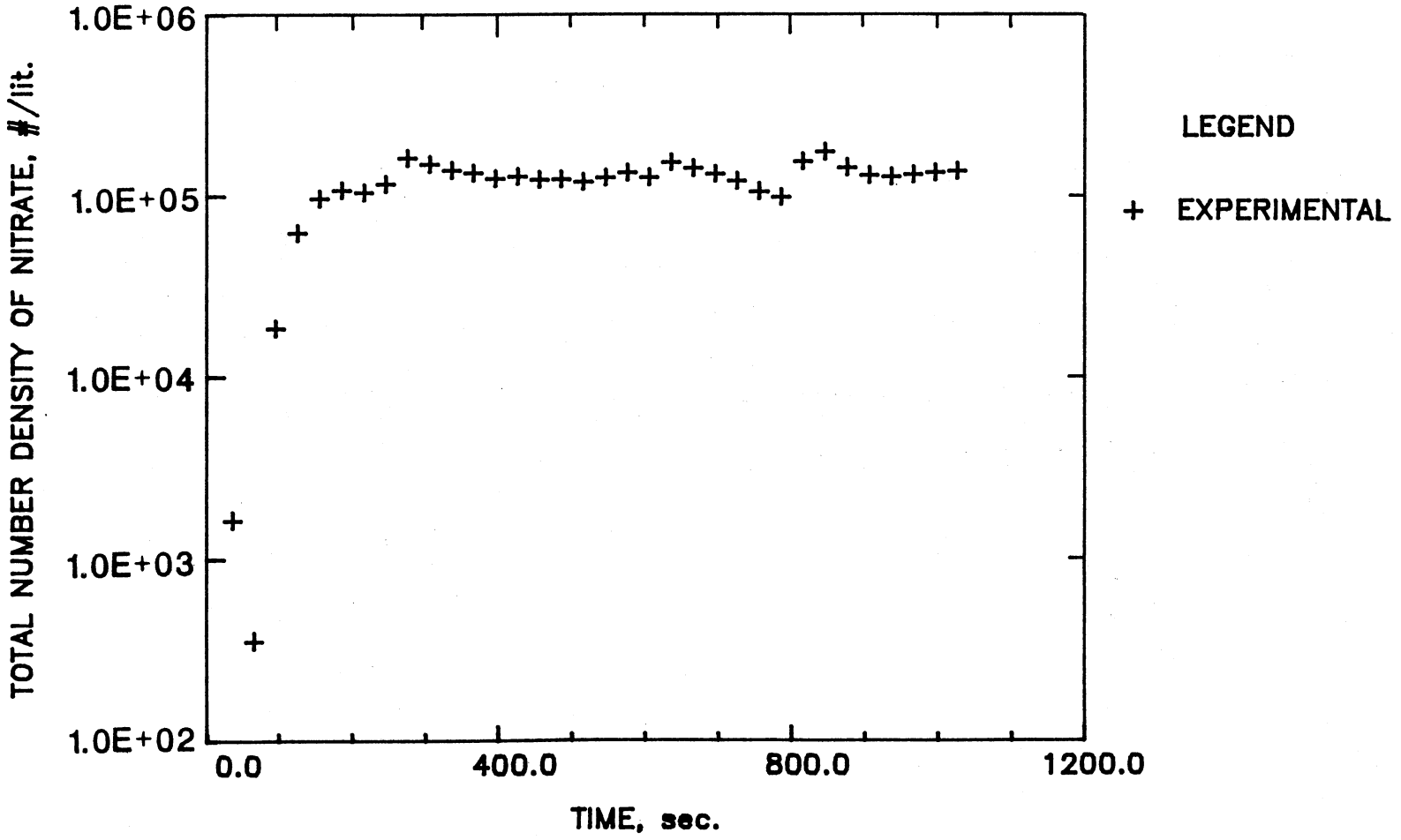

Figure 23. Total Number Concentration of Ammonium Nitrate vs. Reaction Time for $[NH_3] = [NO_2] = 1$ ppm, RT. = 10 s and T = 13 °C (Experiment 51)

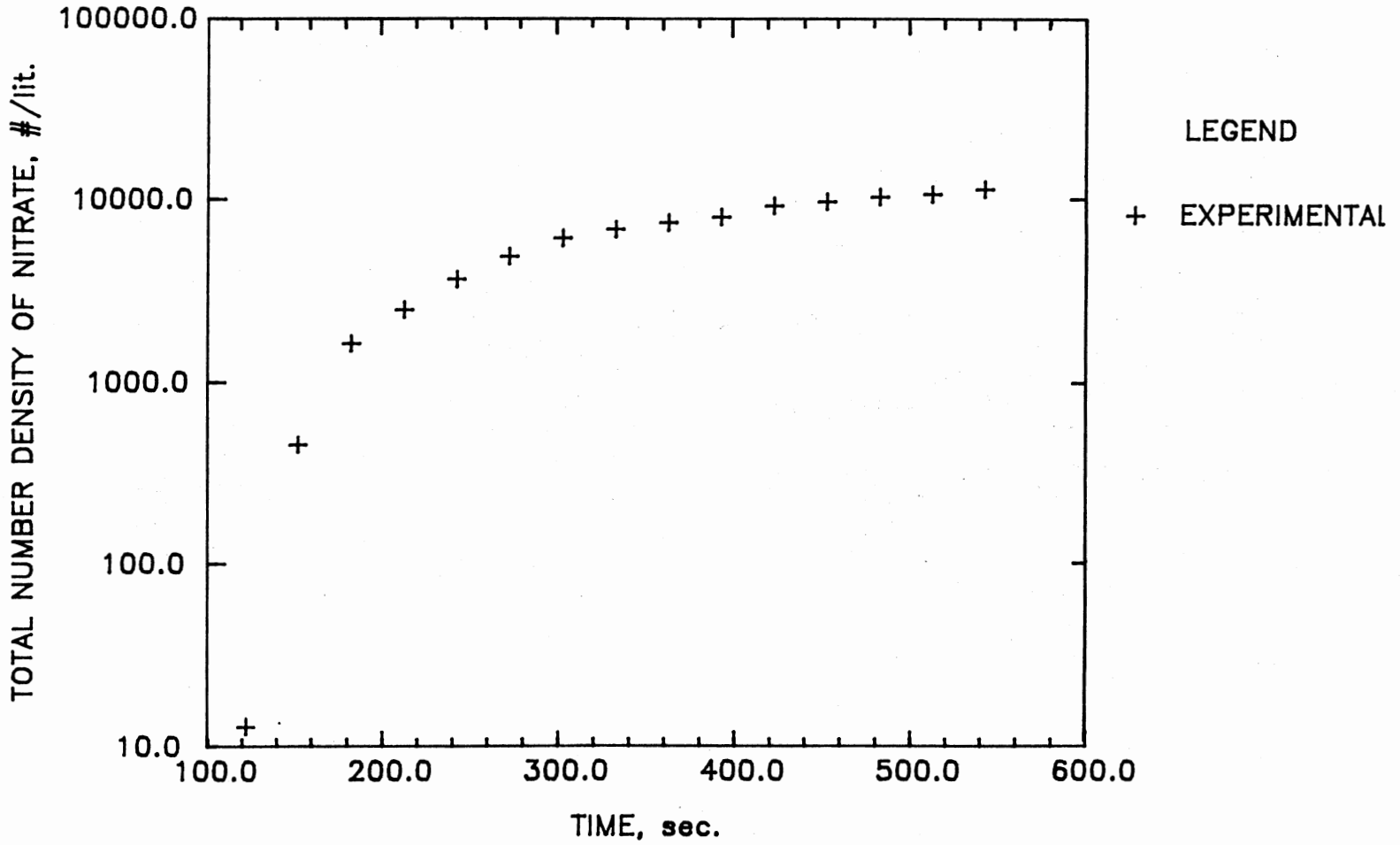

Figure 24. Total Number Concentration of Ammonium Nitrate vs. Reaction Time for $[NH_3] = [NO_2] = 0.5$ ppm, RT. = 10 s and T = 10 °C (Experiment 52)

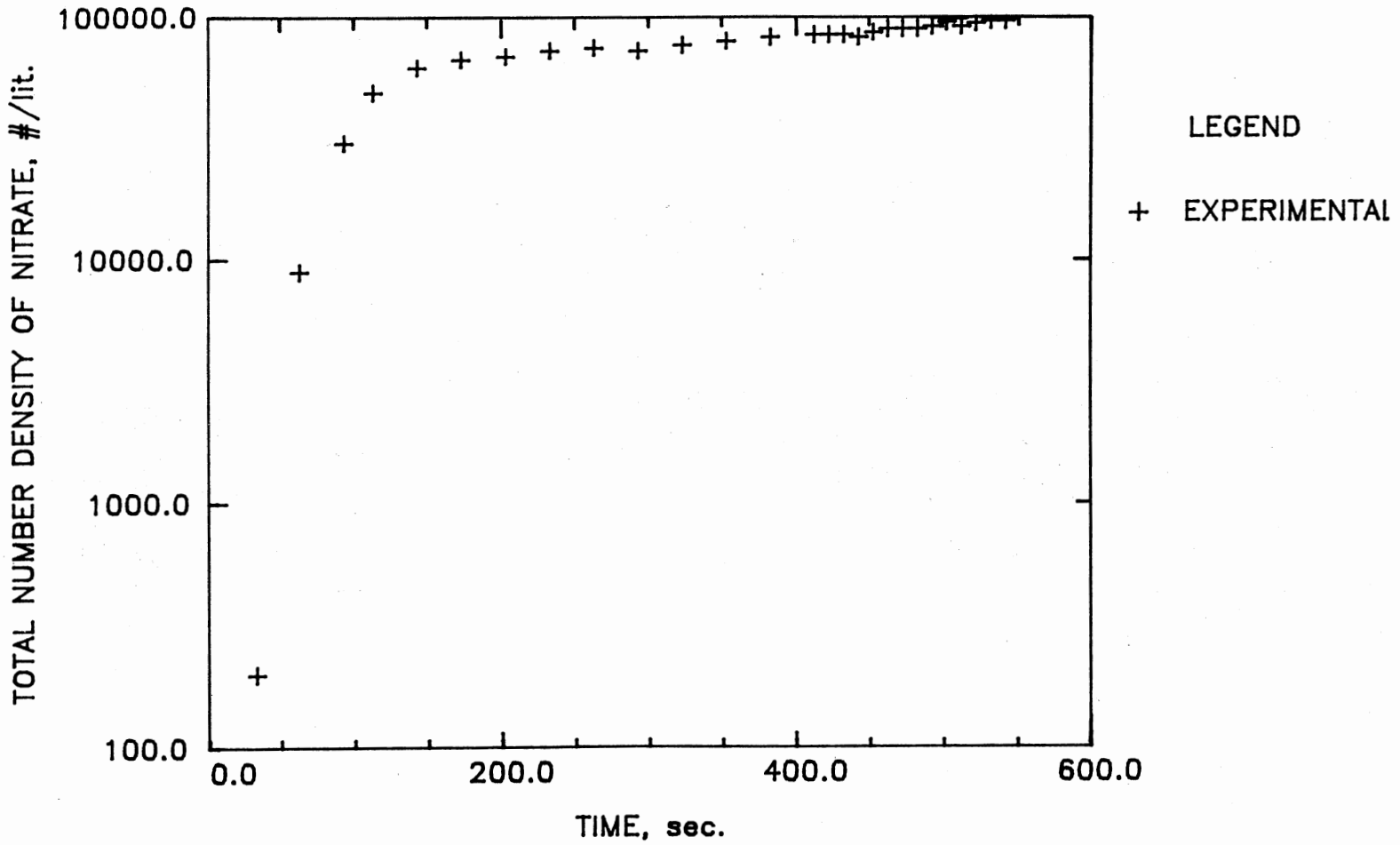

Figure 25. Total Number Concentration of Ammonium Nitrate vs. Reaction Time for $[NH_3] = [NO_2] = 1$ ppm, RT. = 10 s and T = 10 °C (Experiment 53)

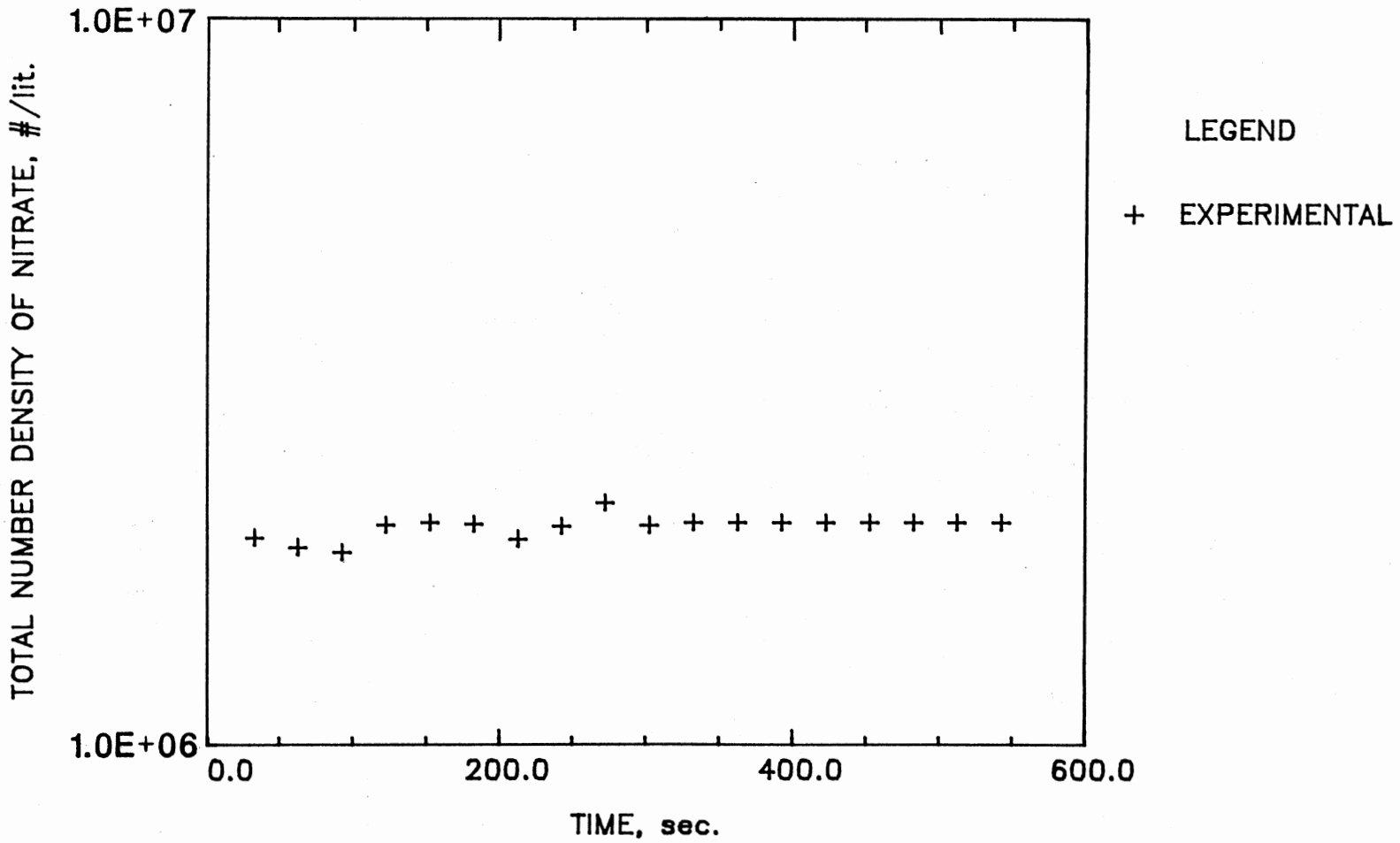

Figure 26. Total Number Concentration of Ammonium Nitrate vs. Reaction Time for $[NH_3] = [NO_2] = 1$ ppm, RT. = 10 s and T = 4 °C (Experiment 59)

vapor on the nucleated particles. The condensed vapor reduces the partial pressure of the monomer in the gas phase and hence the supersaturation ratio, causing the homogeneous nucleation to decrease and the particles to grow.

5.2.2 Total Number Concentrations Measured by the DMPS Versus Those Measured by the CNC

The total number concentration of ammonium nitrate particles, estimated from the DMPS size distribution measurements, are compared to the total number concentration measured by the CNC alone. This comparison, shown in Table XIX at different reaction conditions, shows that for some experiments these two measurements agree and for others they do not. The disagreement between these two measurements, represented as the ratio of the CNC to the DMPS measurements, was as high as 85. A 20% difference between the total number concentrations of CNC and DMPS is quite common (Keady, 1988). However, larger deviations have not been observed in other studies. An attempt was made to identify a trend for large deviations with total number concentration, particle size distribution, reactant concentration and temperature. However, no systematic relation between deviations and the system parameters could be observed. Thus, the deviations are attributed to some unkown random error which might have been due to leaks in the DMPS system. If the deviation in the number concentration resulted from a leak in the DMPS, the size distributions should still be valid for comparative purposes. However, if the deviation was due to preferential removal of certain size particles, then the size distributions would be erroneous. However, a comparison of variations of size distributions

from suspicious runs with those from reliable runs indicates that most probably the reduction in the particle number concentration was due to dilution by leaks rather than perferential particle removal.

Therefore, only the size distributions of the experiments in which the DMPS and the CNC measurements agree with each other are considered in the data analysis. The results of the experiments in which these two measurements do not agree are presented and used as supporting material. No major conclusions regarding the behavior of the ammonium nitrate aerosols are independently drawn from these data. The graphs that include suspicious particle size distribution results include Figures 28, 29, 33, 37, 38, 39, 41, 44, 45 and 46.

5.2.3 Size Distribution

The experimental size distribution measurements shown in Figures 27 to 42 are taken after making sure that the total number of particles has reached its steady state (as shown in Figures 8 - 26). This normally happens 15 to 30 minutes after the beginning of the reaction. The size distribution equation, given by equation [34] and discussed by Seinfeld, 1986, is used to fit the size distribution data. This equation is based on the solution of the condensation equation of the GDE. The parameters used in this equation (such as diffusivity, mean free path, Cunningham correction factor, etc.) are calculated based on the physical properties and reaction conditions. The initial total number, used in equation [34], is predicted from the reaction kinetic model. This equation is fitted to the experimental size distribution by varying the median diameter ($\overline{D}_{pg}$) and the geometric standard deviation (σ_g). The ranges of these fitting parameters, $\overline{D}_{pg}$ and σ_g, are 0.1-0.35 μm and 1.5-2.0,

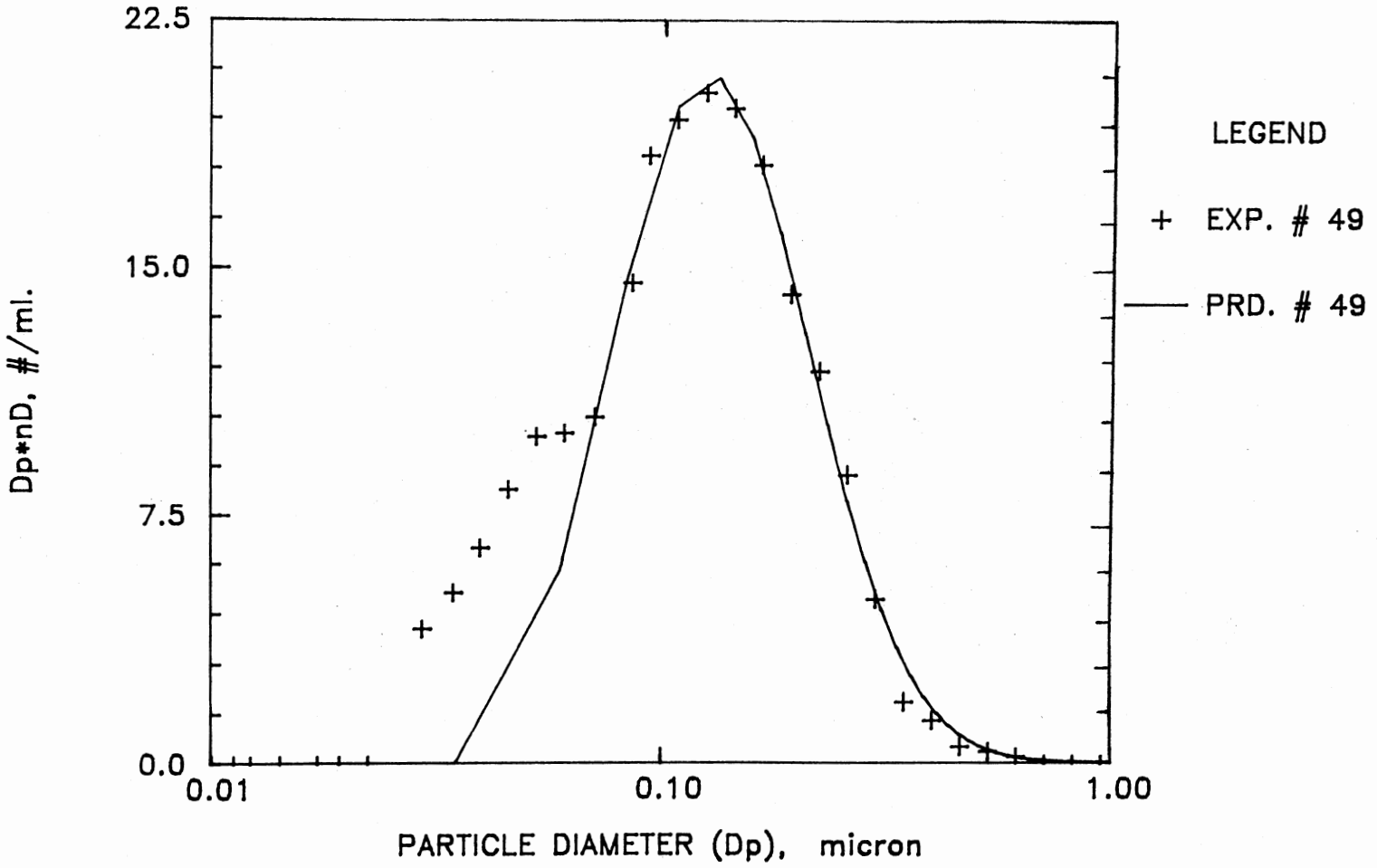

Figure 27. Size Distribution for $[NH_3]$ = $[NO_2]$ = 10 ppm, RT. = 10 s and T = 14 °C (Experiment 49, + Measured; - Condensation Model)

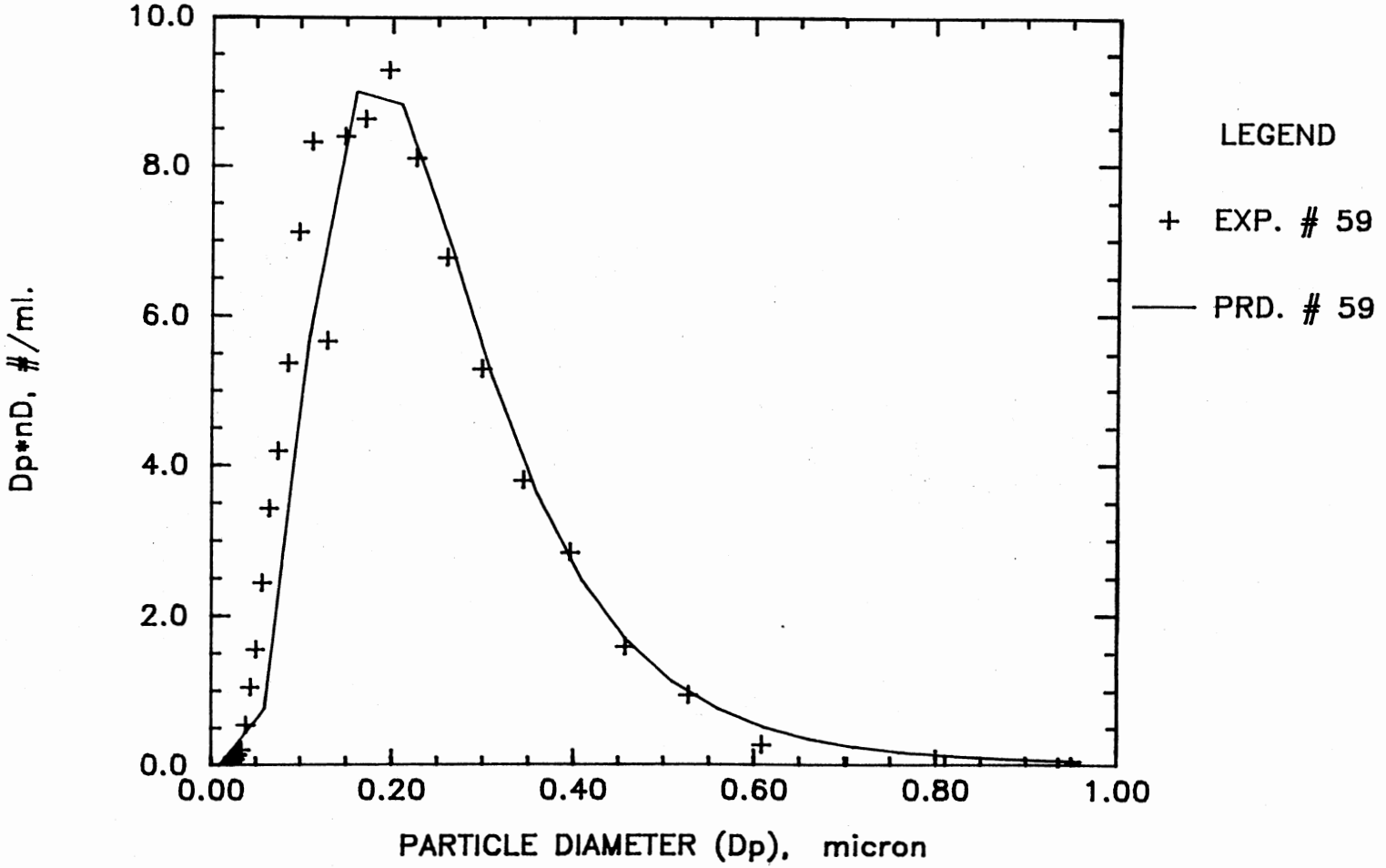

Figure 28. Size Distribution for $[NH_3] = [NO_2] = 1$ ppm, RT. = 10 s and T = 4 °C (Experiment 59, + Measured; - Condensation Model)

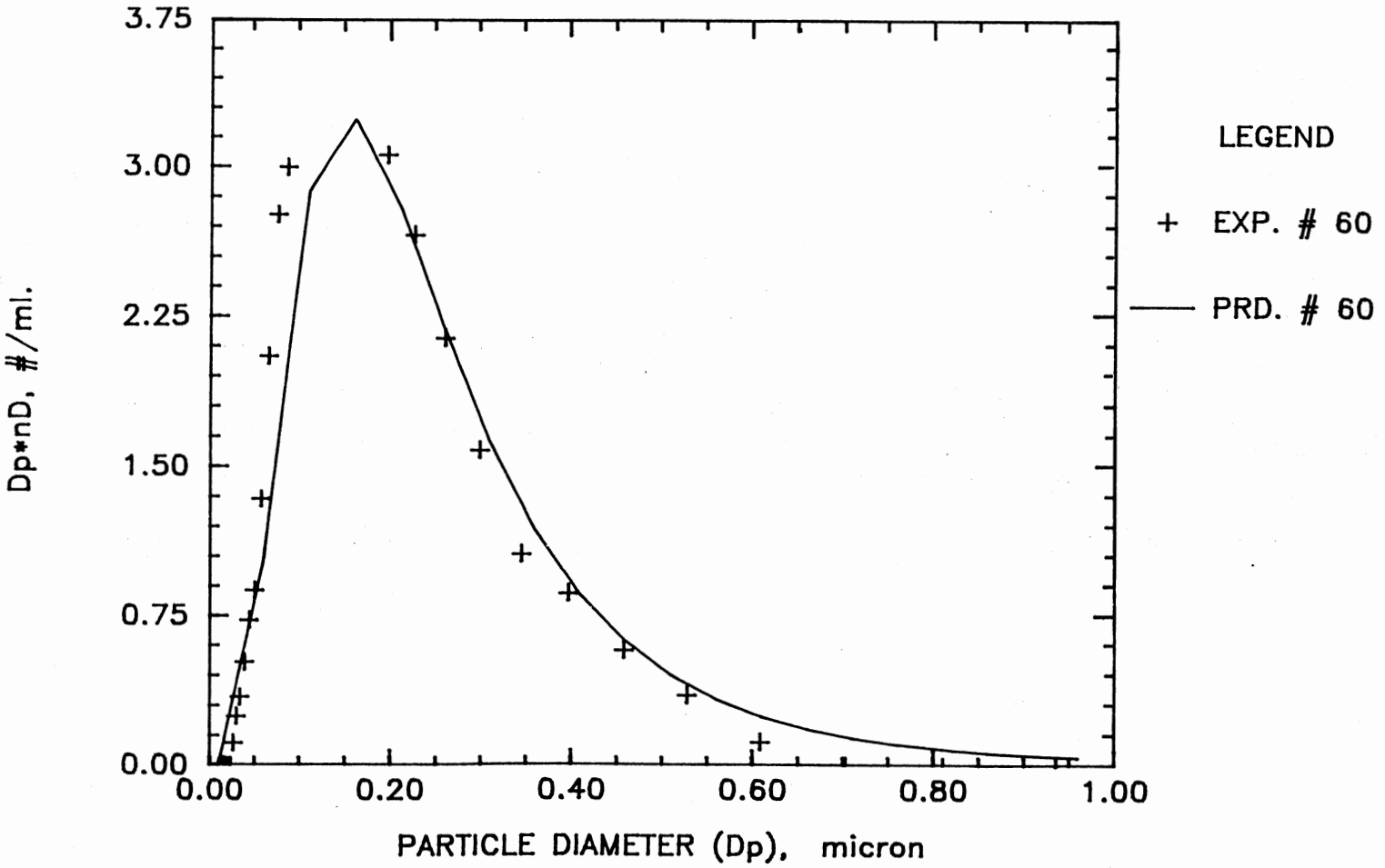

Figure 29. Size Distribution for $[NH_3] = [NO_2] = 0.5$ ppm, RT. = 10 s and T = 4 °C (Experiment 60, + Measured; - Condensation Model)

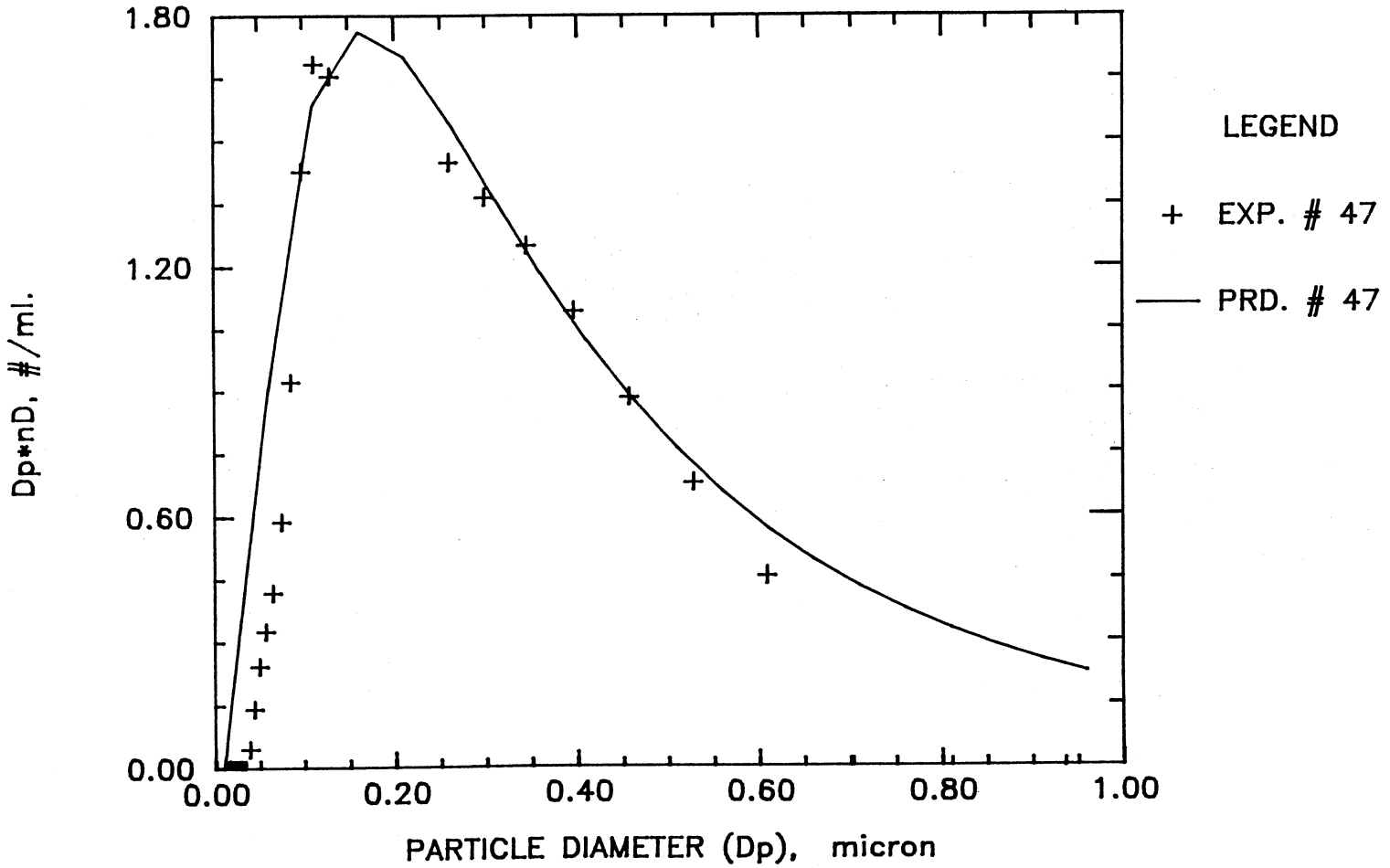

Figure 30. Size Distribution for $[NH_3]$ = 1 ppm, $[NO_2]$ = 5 ppm, RT. = 5 s and T = 20 °C (Experiment 47, + Measured; – Condensation Model)

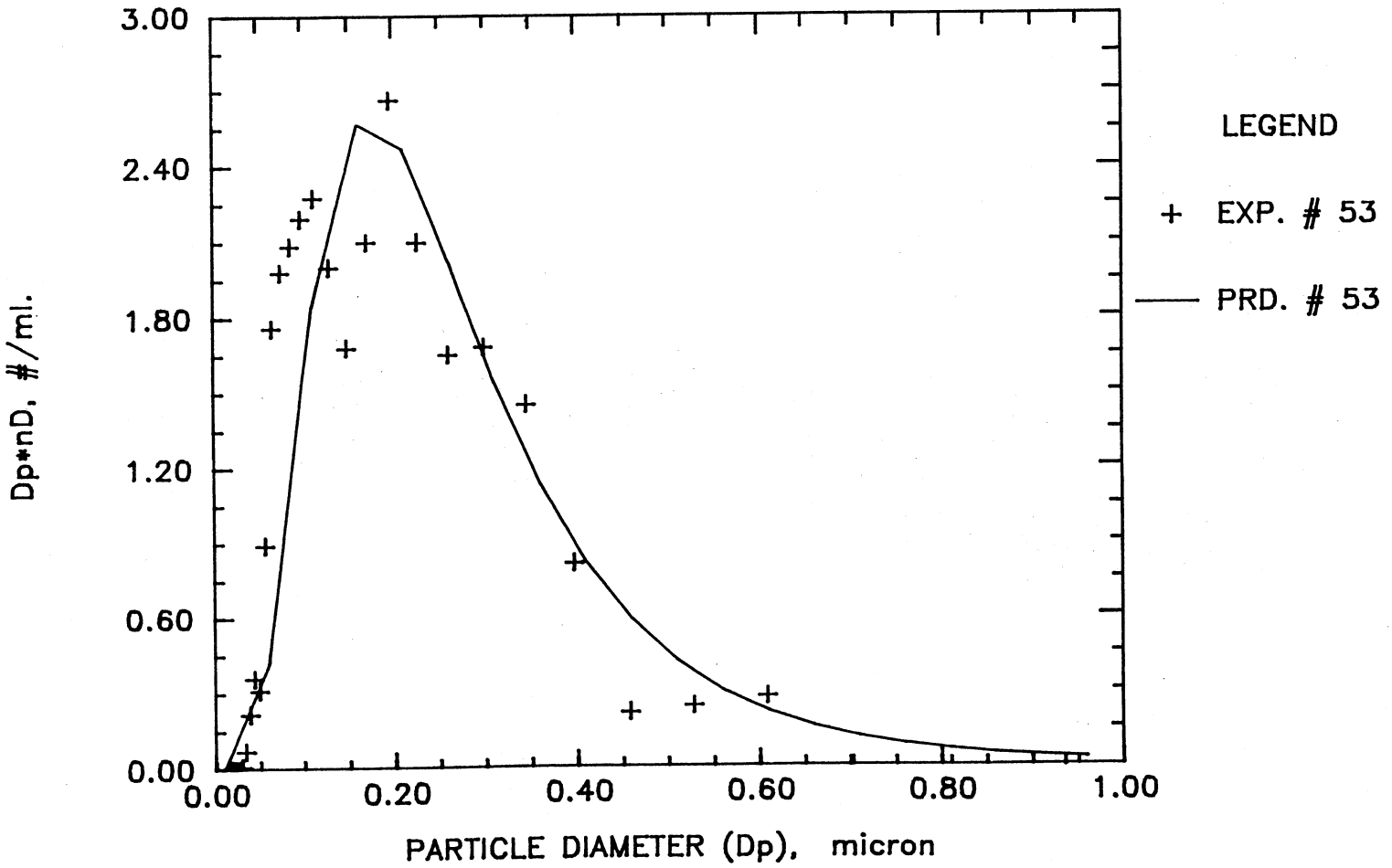

Figure 31. Size Distribution for $[NH_3] = [NO_2] = 1$ ppm, RT. = 10 s and T = 10 °C (Experiment 53, + Measured; - Condensation Model)

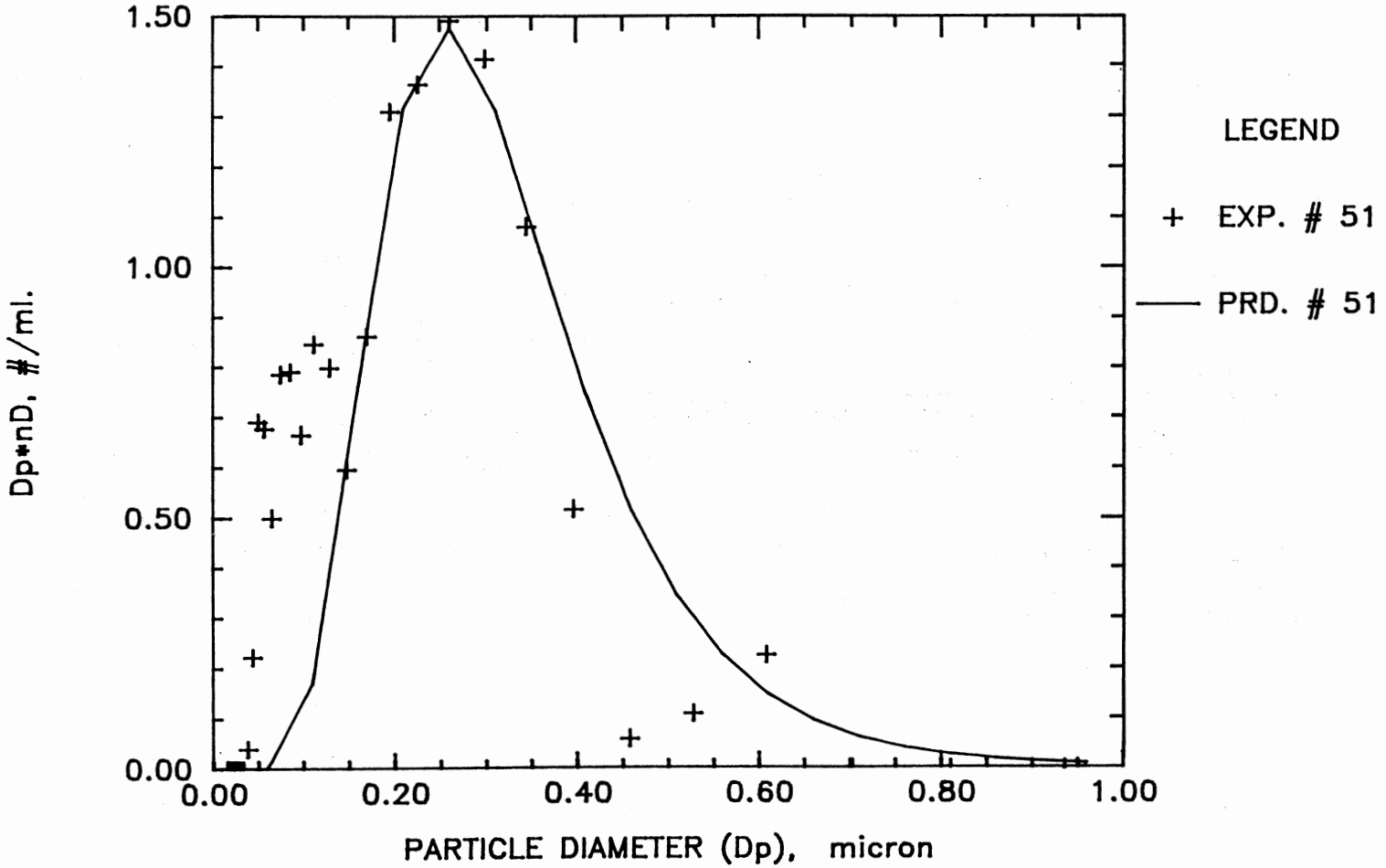

Figure 32. Size Distribution for $[NH_3] = [NO_2] = 1$ ppm, RT. = 10 s and T = 13 °C (Experiment 51, + Measured; - Condensation Model)

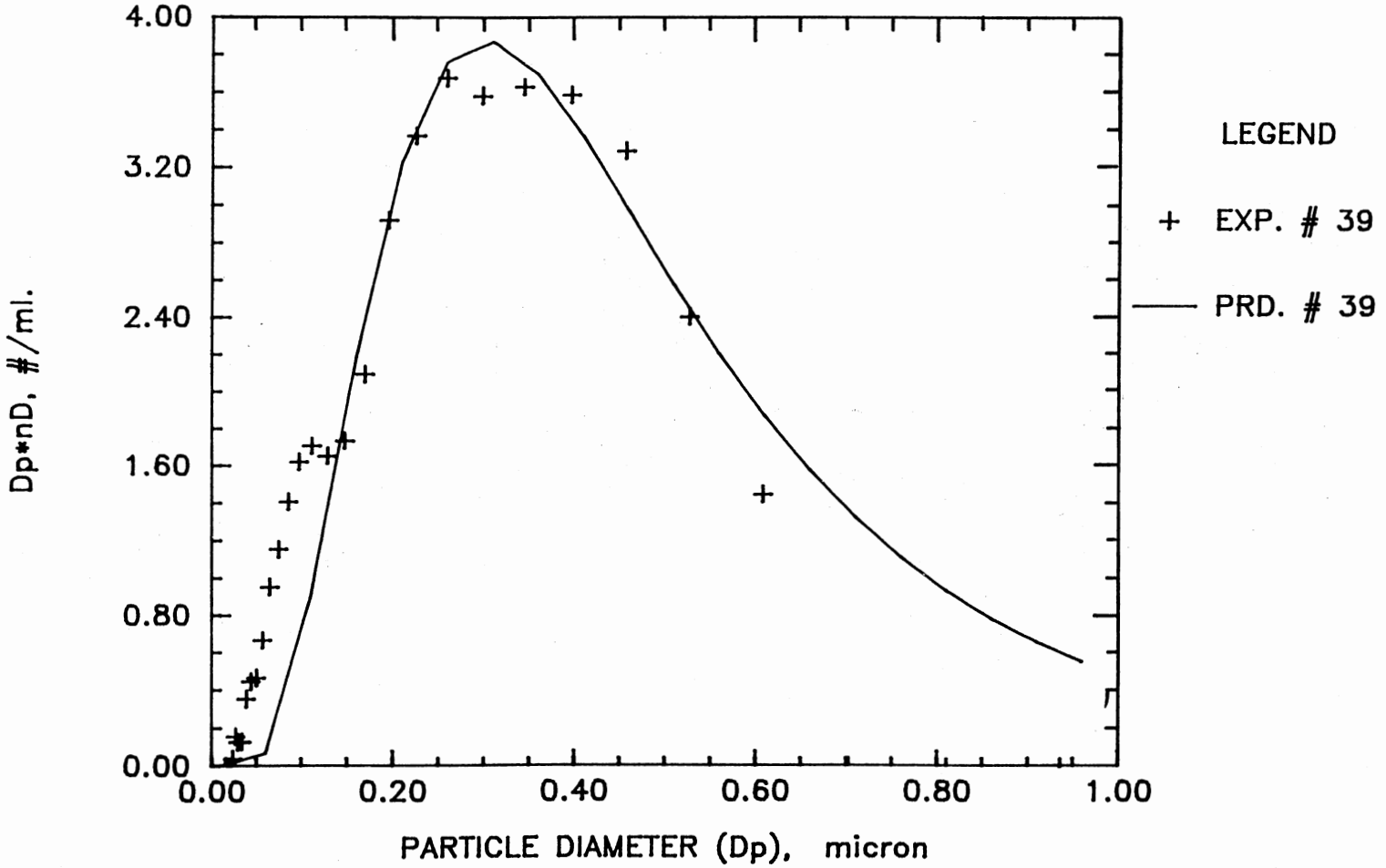

Figure 33. Size Distribution for $[NH_3]$ = $[NO_2]$ = 5 ppm, RT. = 3 s and T = 24 °C (Experiment 39, + Measured; - Condensation Model)

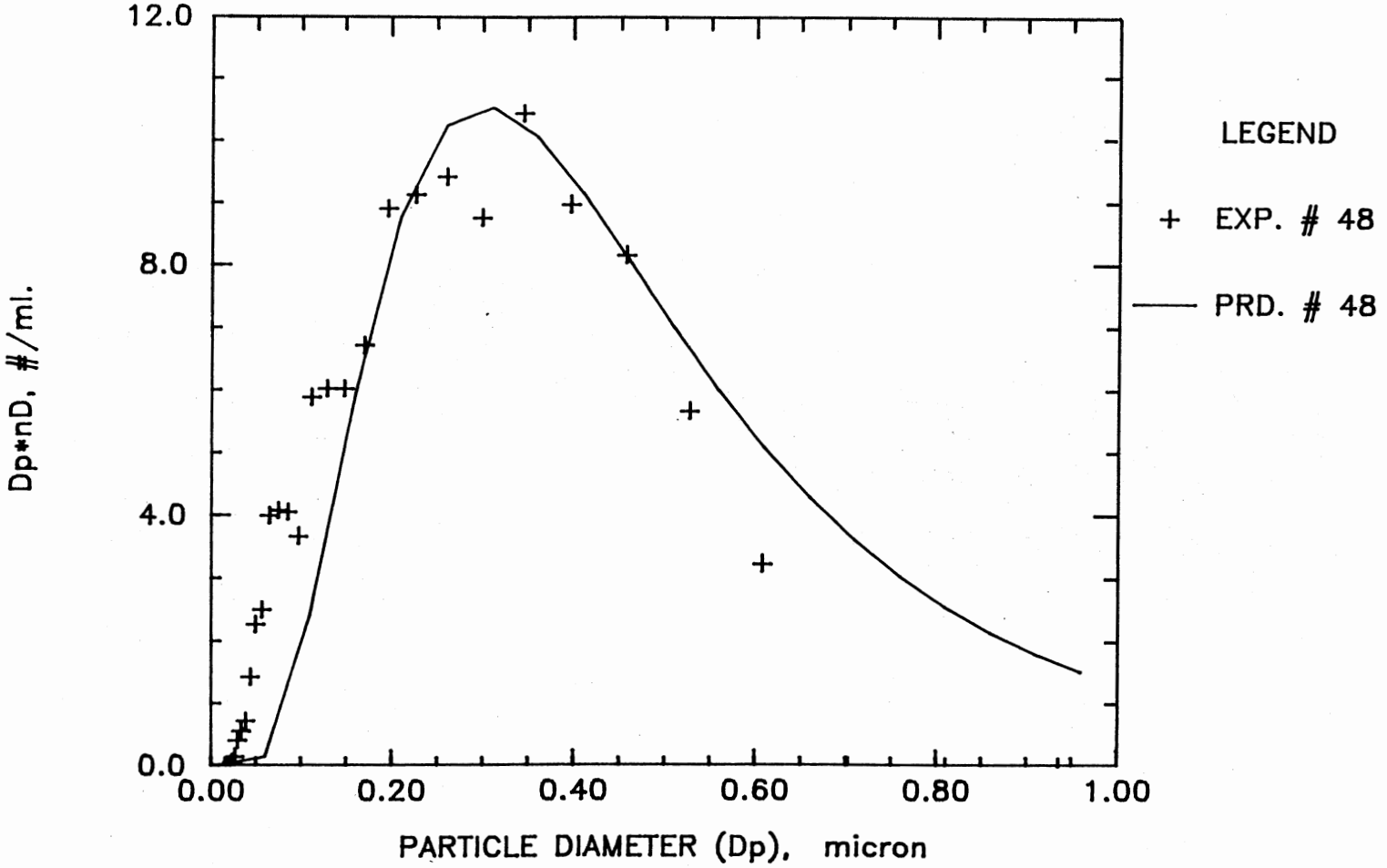

Figure 34. Size Distribution for $[NH_3] = [NO_2] = 5$ ppm, RT. = 10 s and T = 15 °C (Experiment 48, + Measured; - Condensation Model)

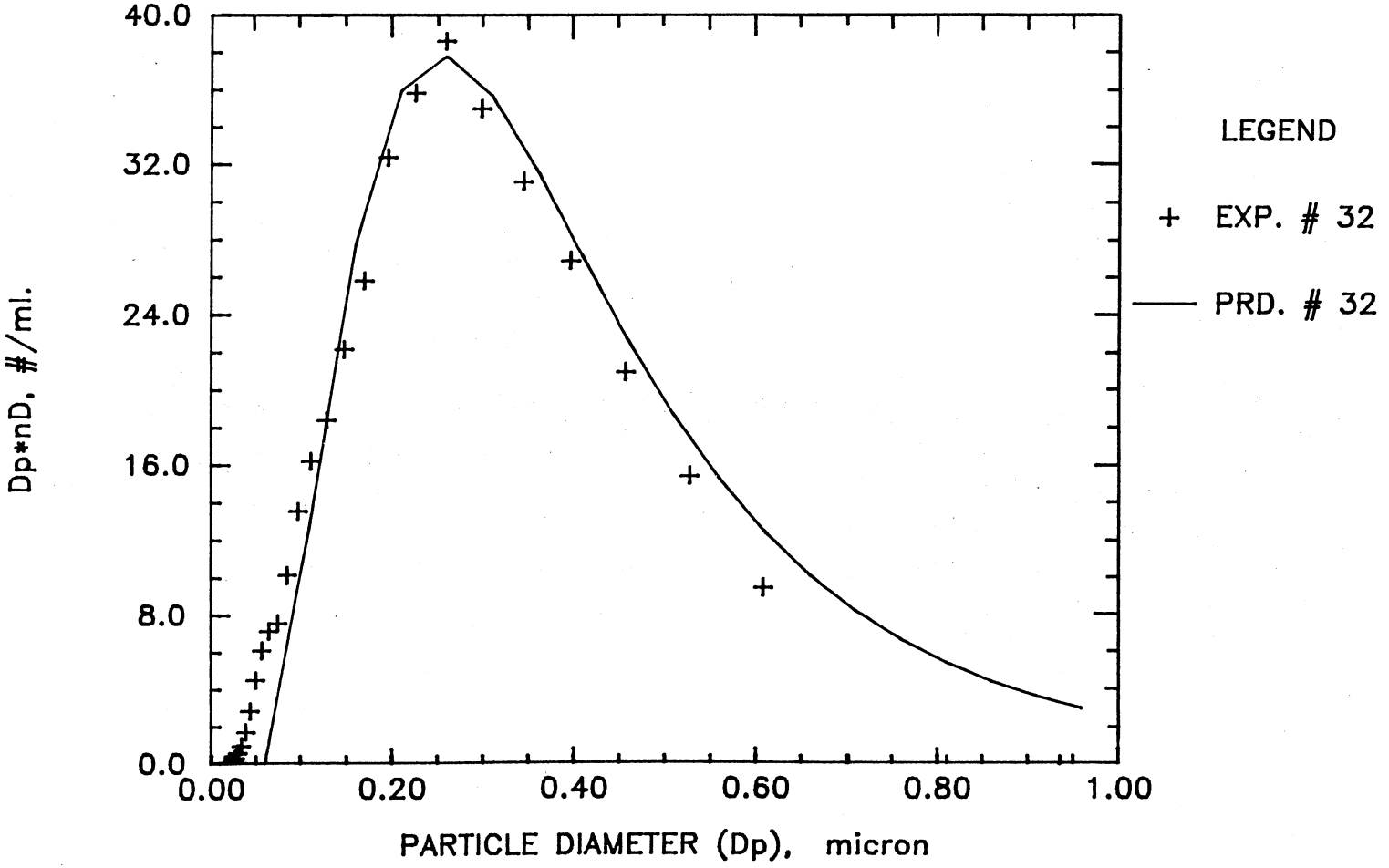

Figure 35. Size Distribution for $[NH_3]$ = 13.5 ppm, $[NO_2]$ = 3 ppm, RT. = 5 s and T = 20 °C (Experiment 32, + Measured; - Condensation Model)

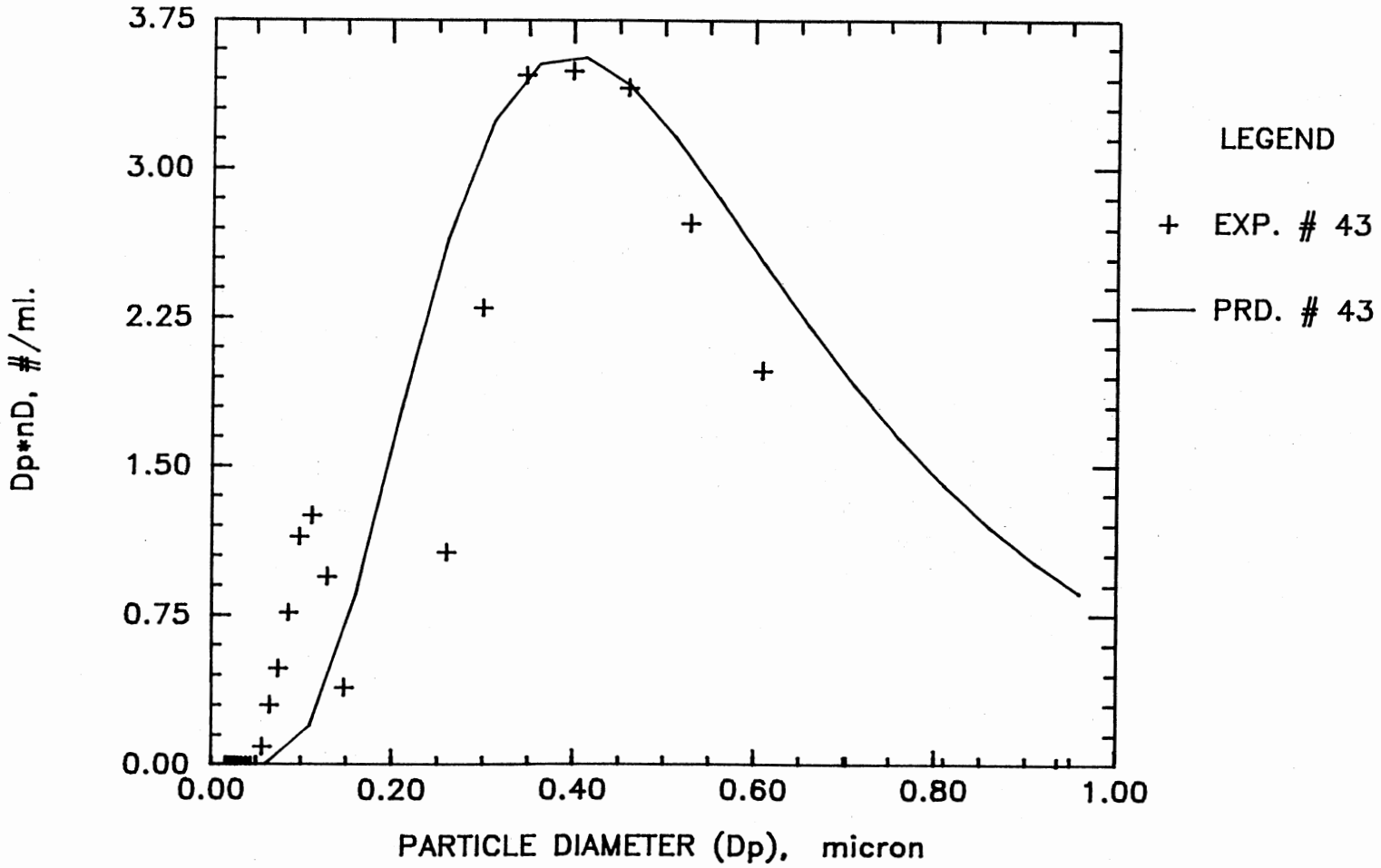

Figure 36. Size Distribution for $[NH_3] = [NO_2] = 5$ ppm, RT. = 10 s and T = 21 °C (Experiment 43, + Measured; - Condensation Model)

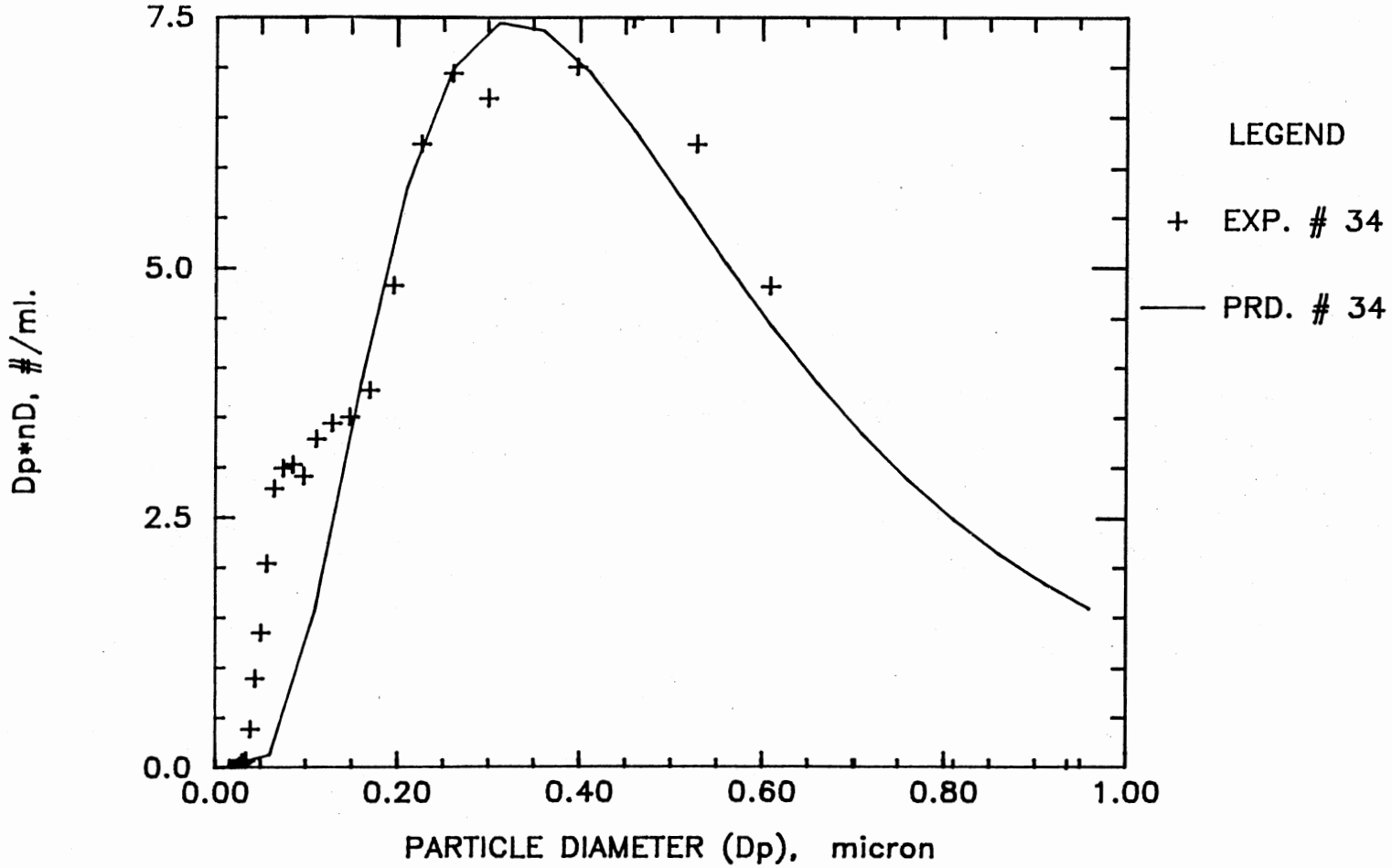

Figure 37. Size Distribution for $[NH_3]$ = $[NO_2]$ = 5 ppm, RT. = 5 s and T = 20 °C (Experiment 34, + Measured; - Condensation Model)

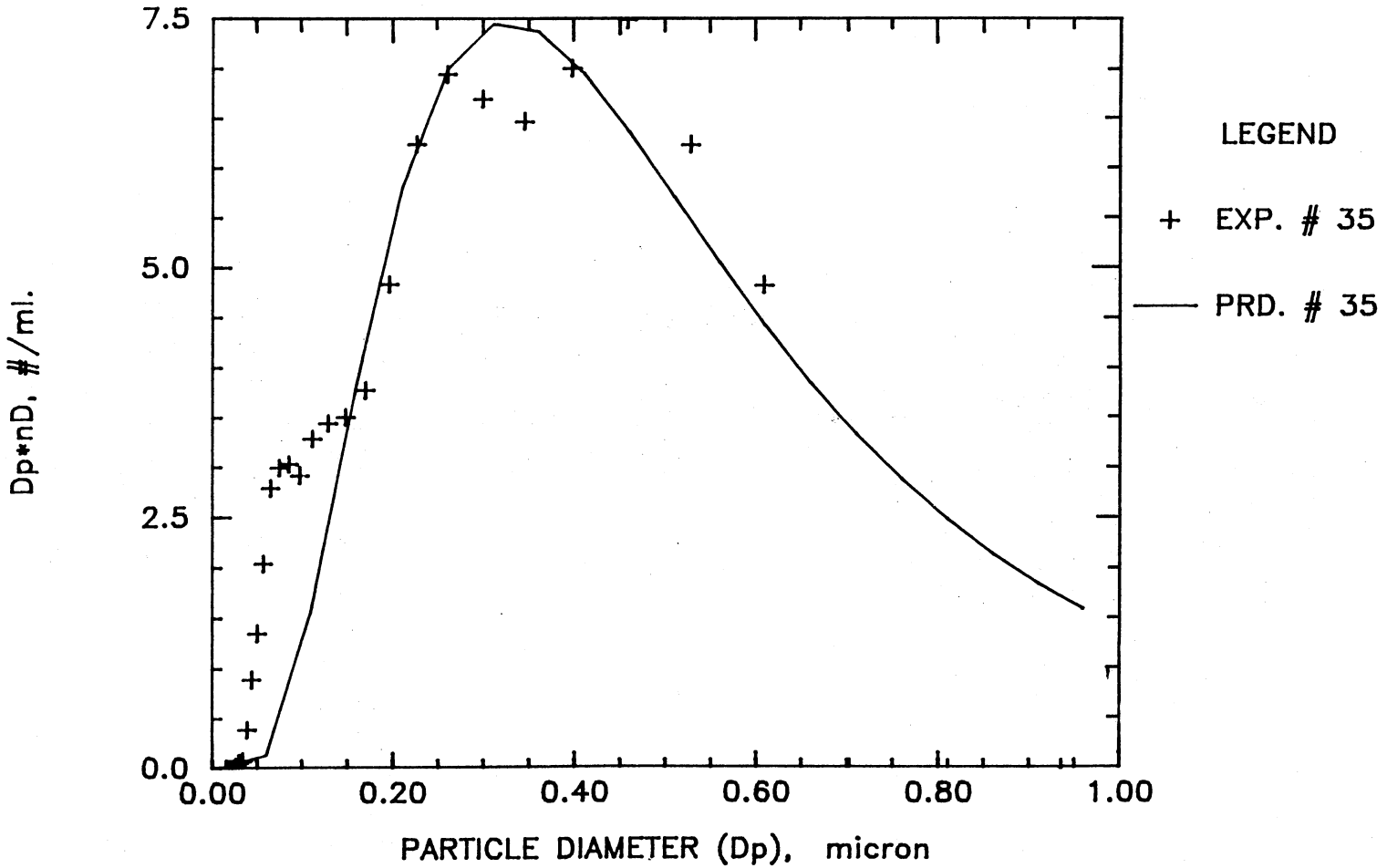

Figure 38. Size Distribution for $[NH_3] = [NO_2] = 5$ ppm, RT. = 5 s and T = 20 °C (Experiment 35, + Measured; - Condensation Model)

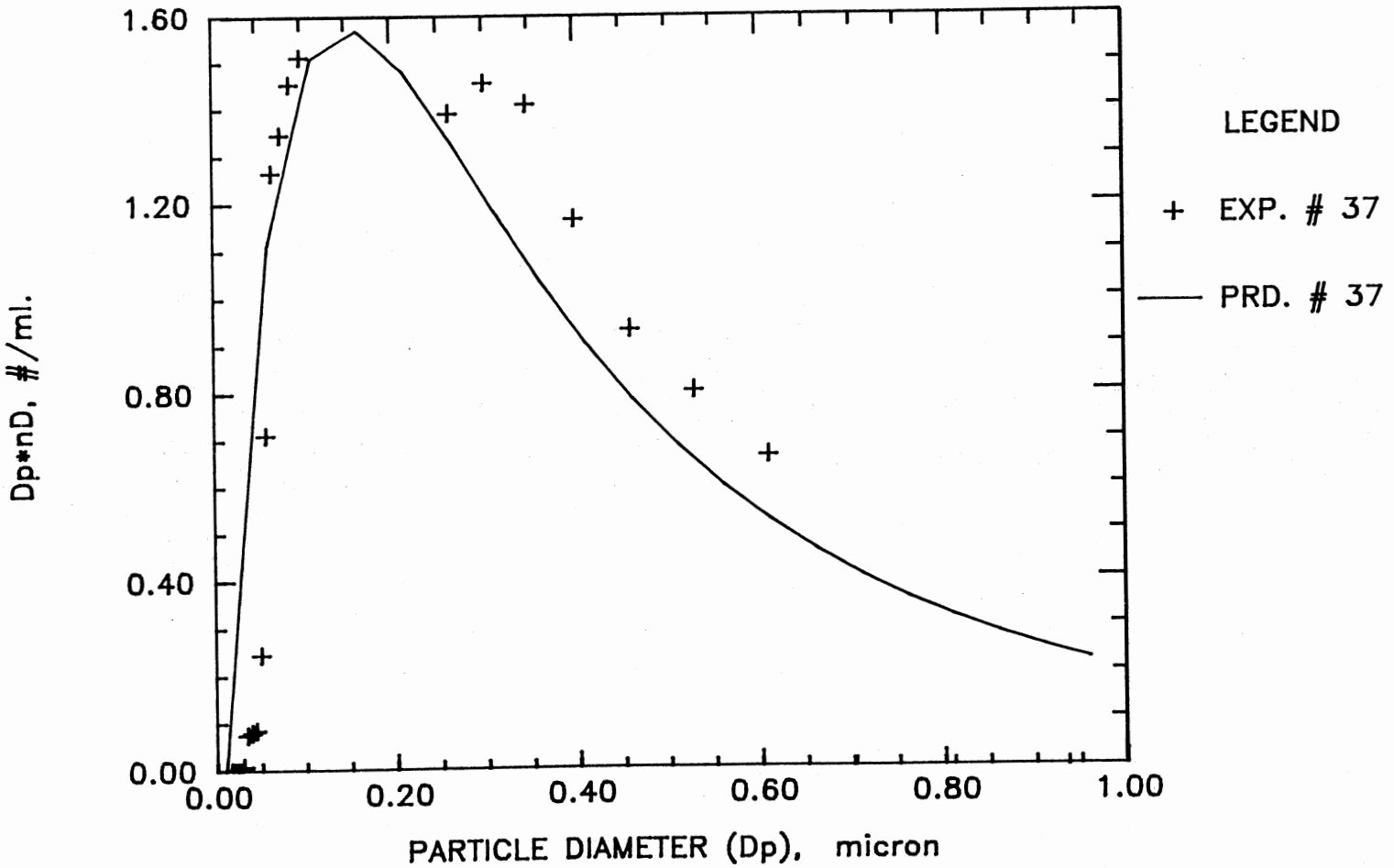

Figure 39. Size Distribution for $[NH_3]$ = 1 ppm, $[NO_2]$ = 11 ppm, RT. = 5 s and T = 19 °C (Experiment 37, + Measured; – Condensation Model)

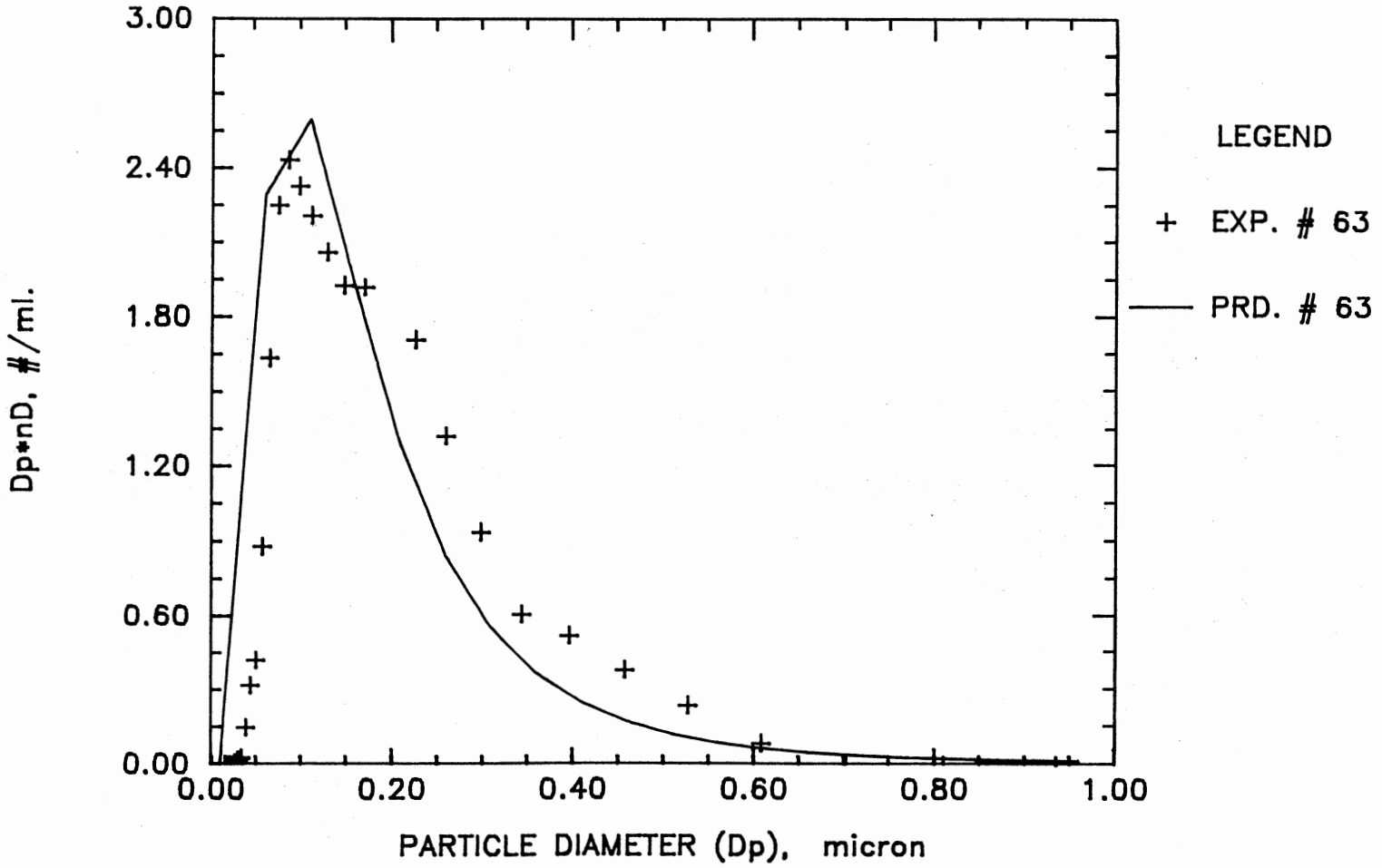

Figure 40. Size Distribution for $[NH_3] = [NO_2] = 0.5$ ppm, RT. = 10 s and T = 10 °C (Experiment 63, + Measured; - Condensation Model)

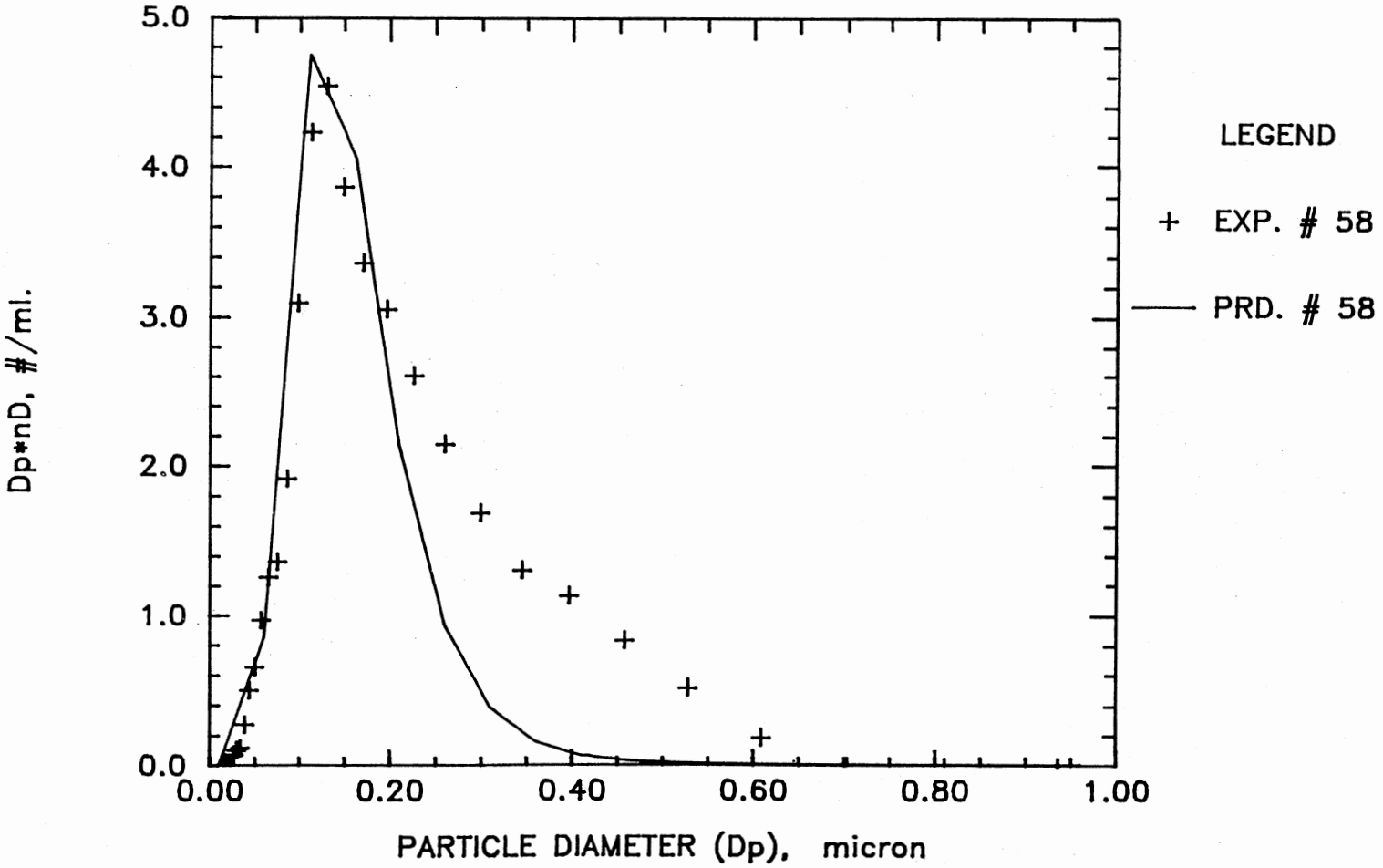

Figure 41. Size Distribution for $[NH_3] = [NO_2] = 0.5$ ppm, RT. = 10 s and T = 4 °C (Experiment 58, + Measured; - Condensation Model)

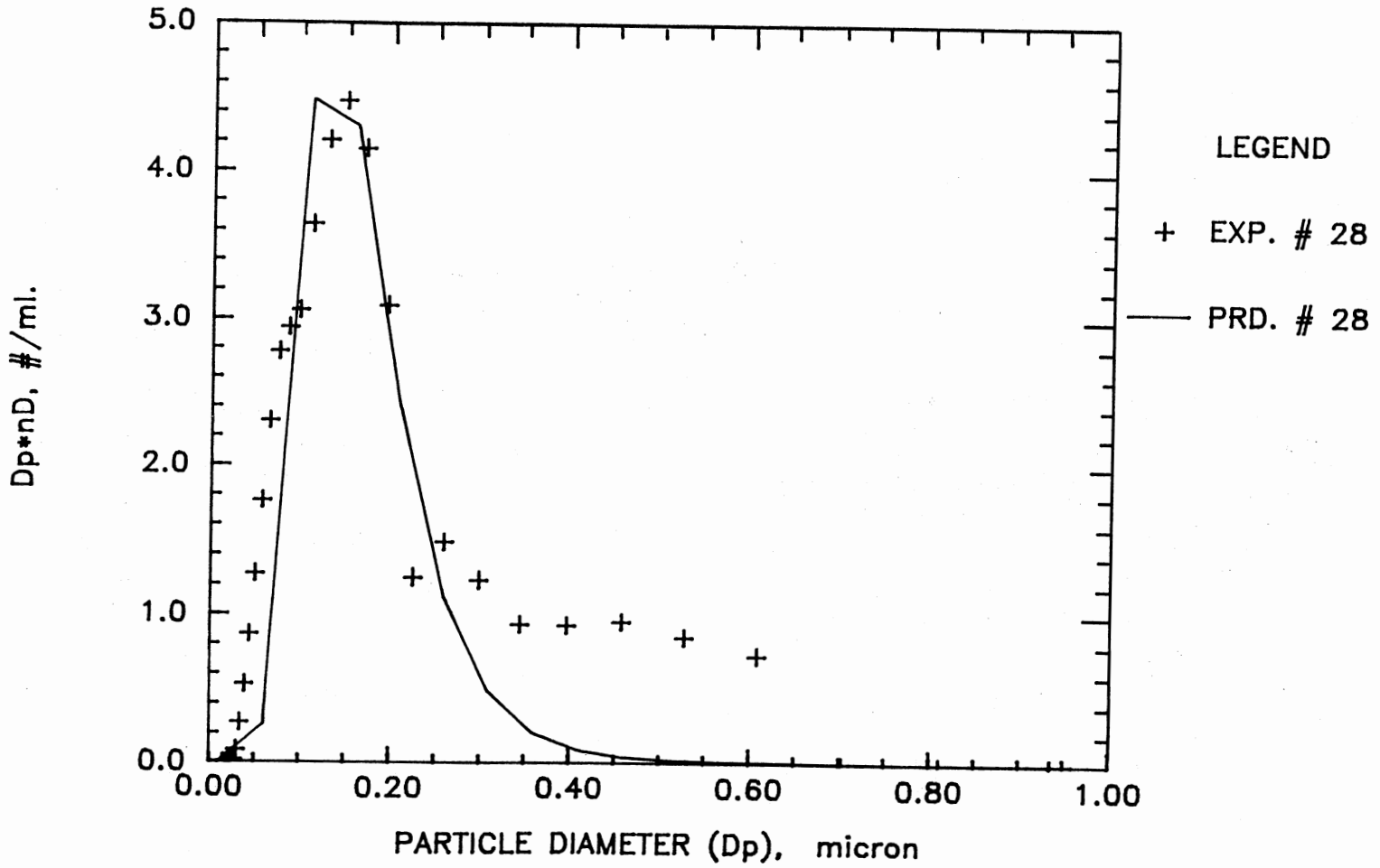

Figure 42. Size Distribution for $[NH_3] = [NO_2] = 2.5$ ppm, RT. = 10 s and T = 21 °C (Experiment 28, + Measured; - Condensation Model)

respectively. The measured size distributions at different conditions show that the minimum particle diameter detected is in the range of 0.018-0.052 μm as can be seen from Table V. Since this range is above the lower detection limit of the DMPS system, these diameters are considered to represent the critical size of ammonium nitrate particles, as discussed in Section 5.2.5.

The theoretical size distribution equation, which incorporates the diffusion growth law, assumes that coagulation is neglected and the only source of new particles is nucleation. In general, the theoretical distributions based on these assumptions, fit the experimental size distributions of particles well as can be seen in Figures 27 through 42. Figure 27 shows a log-normal plot of the experimental size distribution measurement and the theoretical fit. The experimental size distribution in this case is fitted to the least square fit. Similarly, the experimental size distribution shown in Figures 28 through 42 can be fitted to the least square fit and plotted on a log-normal plot. This fact indicates that the particle growth mechanism is a diffusion-controlled growth. This agrees with the conclusion obtained from the results of the history of the total number concentration discussed above that the condensation of the monomer vapor on the newly nucleated particles is the dominant growth process.

The smaller particles of the size distribution measurements, shown in Figures 27 through 42, show two different rates of growth. This appears as a "shoulder" on the left of the theoretical curves. This behavior is explained as a continuation of the nucleation of NH_4NO_3 to form new small particles, accompanying the growth of the existing particles.

In order to reach the objective of explaining the particle growth mechanism, a second approach is used. This approach, as discussed in Chapter III, follow the evolution of the ammonium nitrate size distributions. The mechanism of the particle growth is to be inferred by following the growth rate of the small particles (free regime) and the large particles (continuum regime). The evolution of the size distribution, shown in Figure 43, is measured four successive times in order to examine the mechanism of the particle growth. This figure shows that, as time progresses, the total number of particles increases until it reaches a constant value, while the large particles continue to grow. The general shape of the curves in this graph suggests a diffusion-controlled, a surface reaction-controlled growth mechanism or a combination of both. This indicates that the particle growth is the result of a condensation of monomer molecules on the particle surface, an adsorption of vapor molecules (such as NH_3 or HNO_3) followed by a surface reaction, or a combination of the two processes. Since the calculation of the condensation rates shows that ammonium nitrate has the highest condensation rate, it is concluded that the condensation of ammonium nitrate vapor molecules on the particle surface is the dominant growth process. This also supports our previous observation that by counting for the condensation of NH_4NO_3 molecules a satisfactory fit can be obtained for the total number concentration.

Figures 44 through 46 show that the total number of particles starts to increase and then decrease while large particles stay constant as time progresses. These figures also show that the maximum of the distribution shifts toward the smaller particle size. This unexpected behavior occurs in experiments where the DMPS and the CNC measurement do

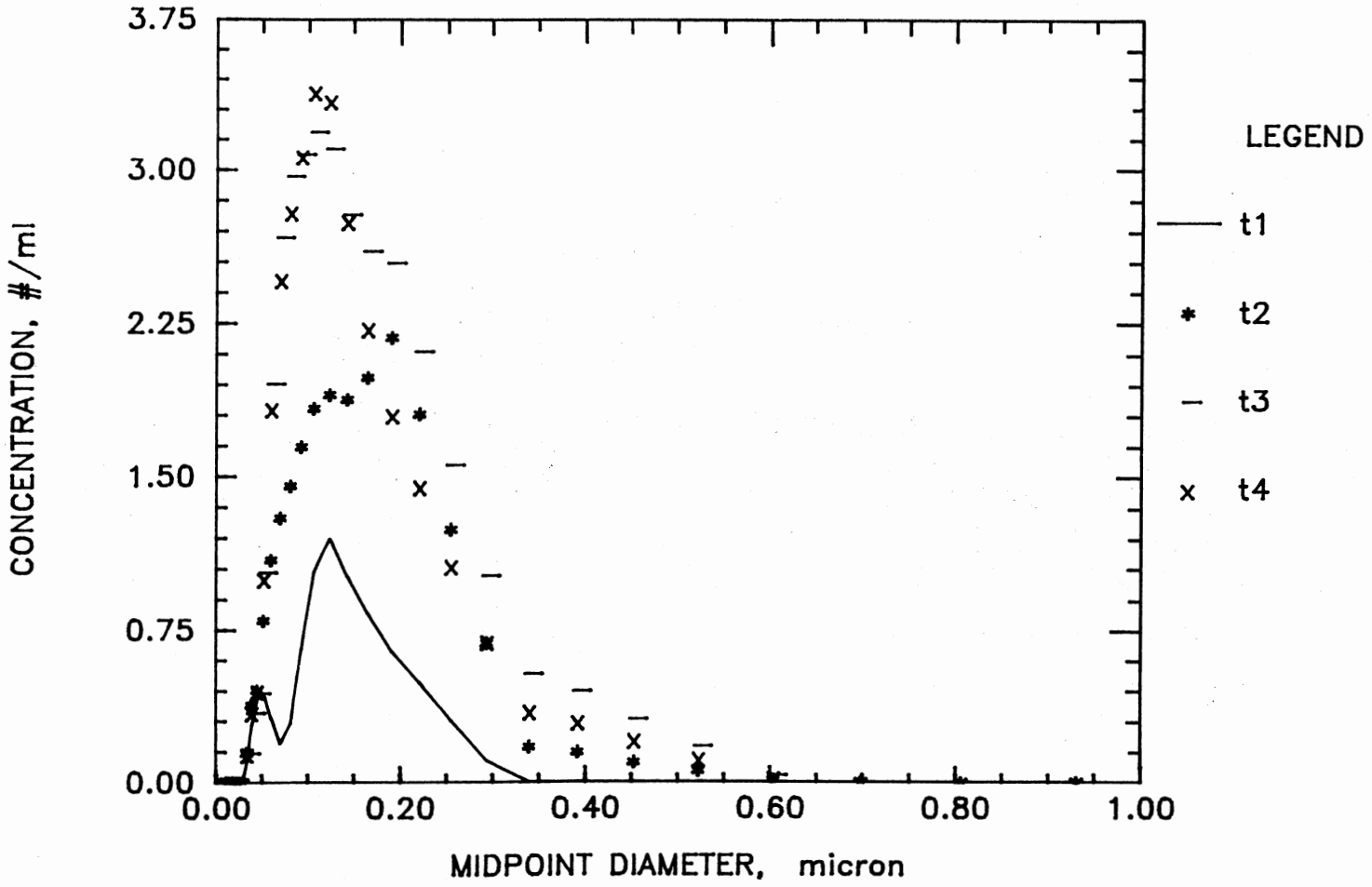

Figure 43. Evolution of Size Distribution of Experiment 63 $[NH_3] = [NO_2] =$ 0.5 ppm, RT. = 10 s and T = 10 °C (Time Progresses From t1 to t4)

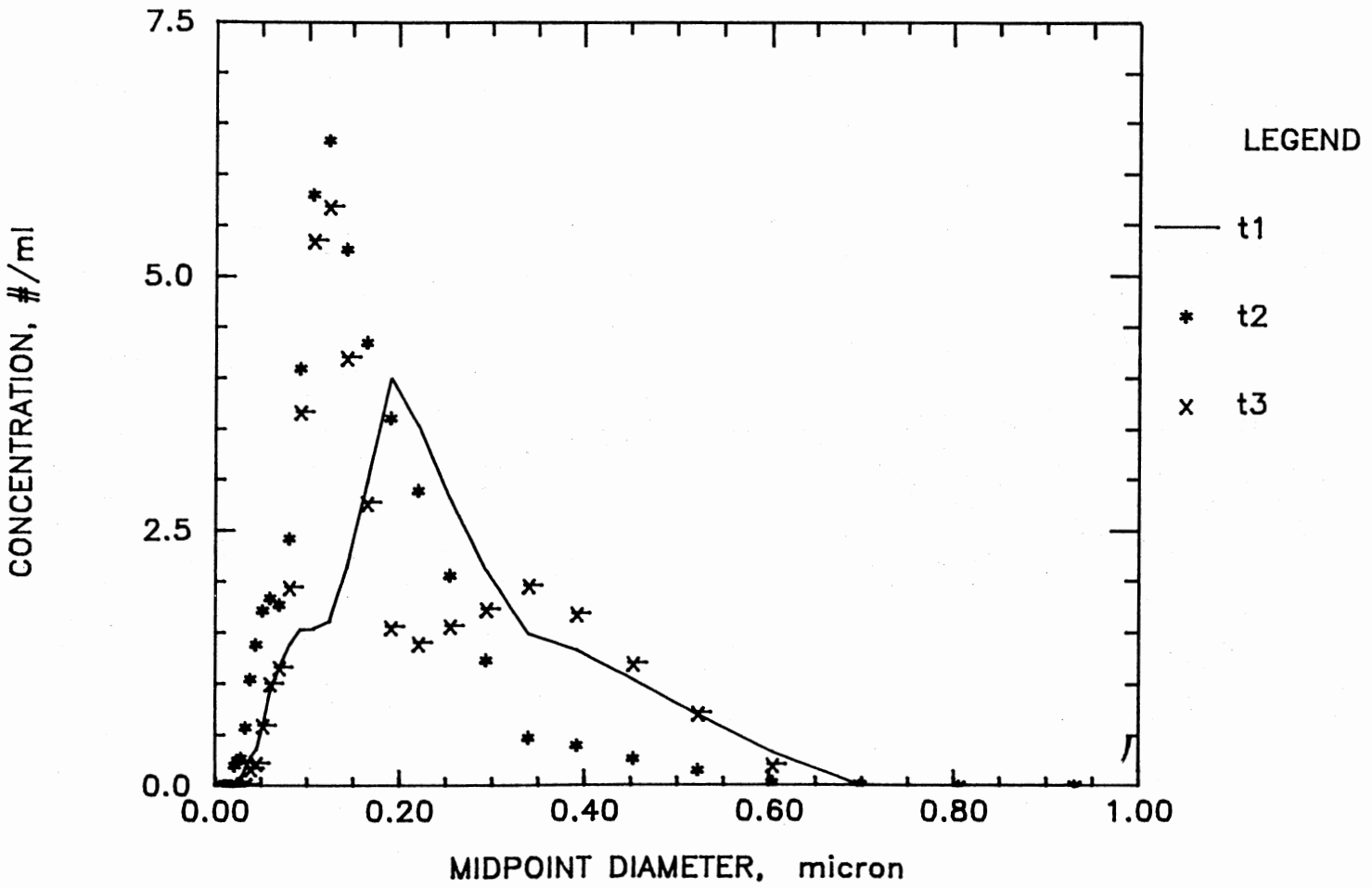

Figure 44. Evolution of Size Distribution of Experiment 58 $[NH_3] = [NO_2] =$ 0.5 ppm, RT. = 10 s and T = 4 °C (Time Progresses From t1 to t3)

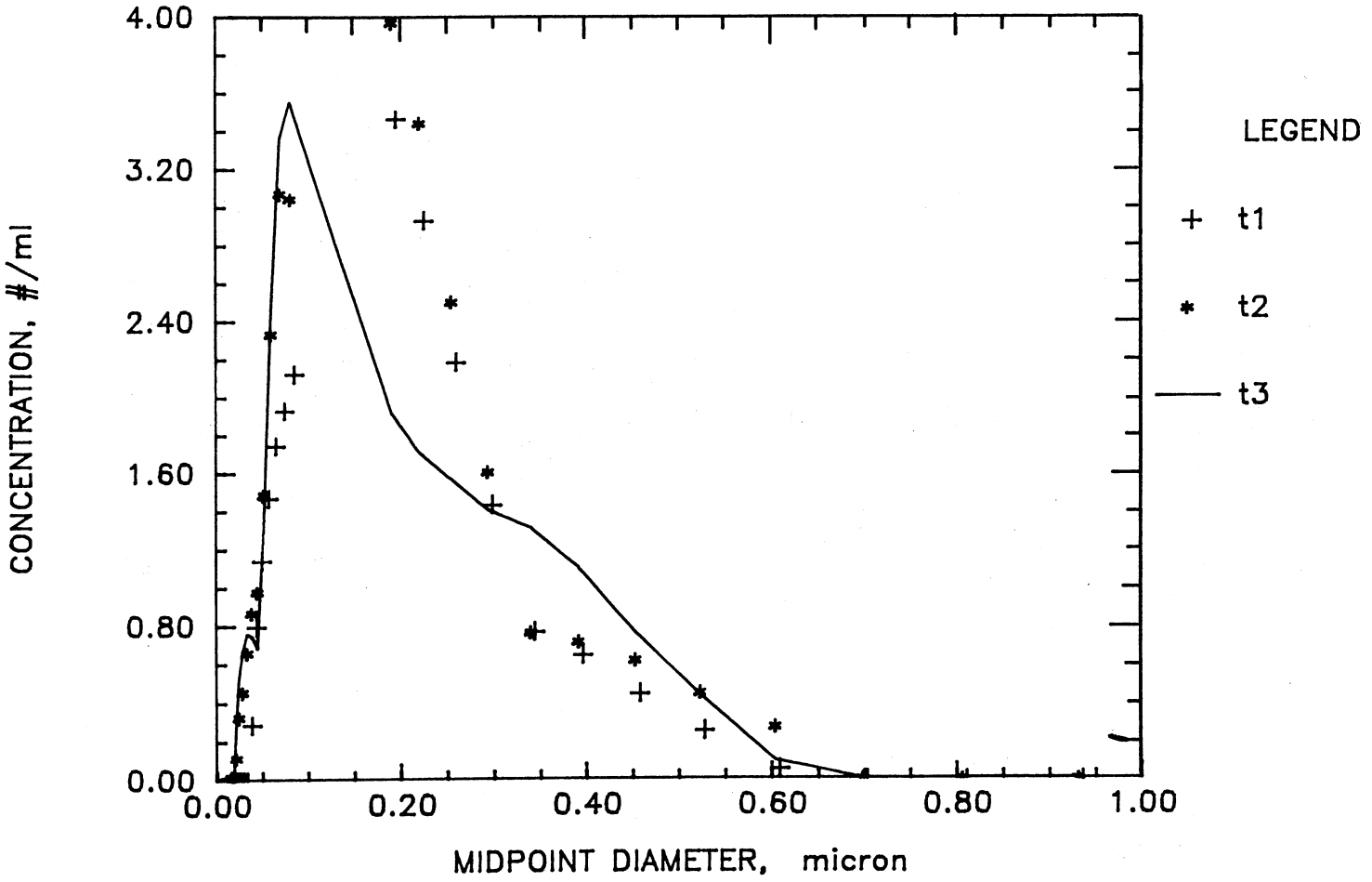

Figure 45. Evolution of Size Distribution of Experiment 60 $[NH_3] = [NO_2] =$ 0.5 ppm, RT. = 10 s and T = 4 °C (Time Progresses From t1 to t3)

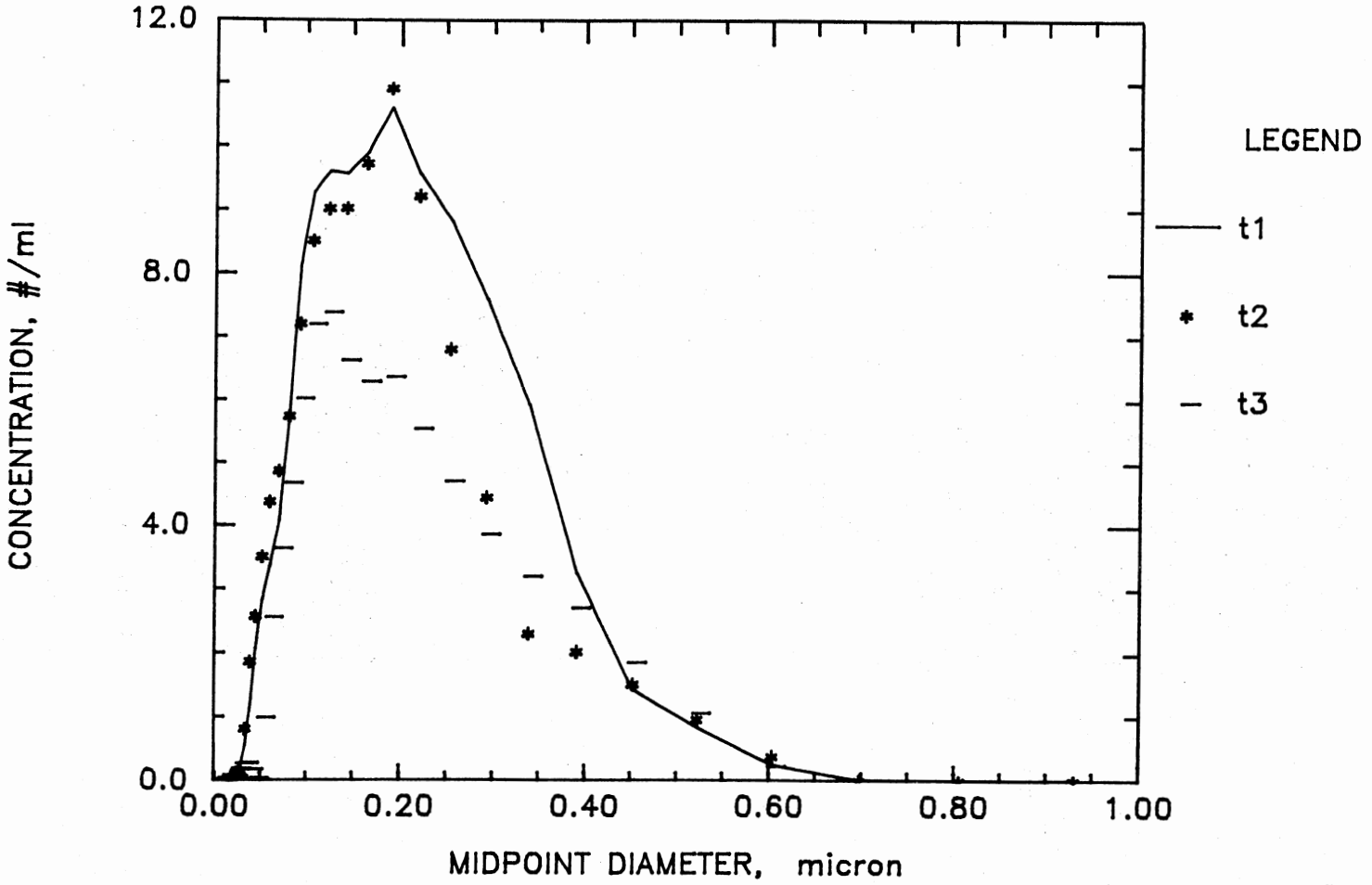

Figure 46. Evolution of Size Distribution of Experiment 59 $[NH_3] = [NO_2] =$ 1 ppm, RT. = 10 s and T = 4 °C (Time Progresses From t1 to t3)

not match, hence, they are not considered as accurate size distributions.

An investigation of the coagulation process includes the examination of the development of the total number and total volume of the particles with time for some reaction conditions. The results of this study are summarized in Table XVIII which are obtained by taking the first size distribution measurement at a very early stage of the reaction, followed by later measurements each at about 5 to 10 minutes apart. Most of these results show that the total number of particles starts to increase and then reach a steady state value while the total particle volume continues to grow. This result again proves that the dominant growth mechanism is condensation and the particle coagulation is insignificant.

In summary, the results of this study show that ammonium nitrate particles form by homogeneous nucleation and grow by adsorption of vapor gases such as NH_3 and HNO_3 followed by a surface reaction and by the condensation of monomeric NH_4NO_3, with the latter being the dominant process. It is also concluded that particle coagulation is not important for the reaction conditions under study. The nucleation occurs in a burst due to a rapid increase in the supersaturation ratio of the monomer. The use of the reaction rate constants (k_a and k_b) reported by Falk, 1955 gives a better prediction of the total number concentrations than those reported by Mearns and Ofosu-Asiedu, 1984a. The experimental and theoretical results show that as the concentration of NO_2 decreases, more induction time and less particles are detected. This finding agrees with the findings of Mearns and Ofosu-Asiedu, 1984a,b about the effect of the partial pressure of NO_2 on the threshold

pressure of NH_3 and on the onset formation of the solid ammonium nitrate. This indicates that equation [10] is the rate controlling step at very low concentrations of NO_2. The variation in the total number concentrations and the size distributions with temperature agrees with the findings of the atmospheric studies.

5.2.4 Effect of Independent Parameters

The effects of the independent parameters on the total number concentration and the size distribution are studied and presented here. The purpose of this section is to examine the importance of these parameters on the processes of formation and growth of ammonium nitrate aerosols.

5.2.4.1 Effect of Reaction Temperature. Figure 47 shows the effect of temperature on the total number concentration for the case of 1.0 ppm reactant concentration with a residence time of 10 s. At a temperature of 21.0 °C a very negligible number of particles is formed even after about one hour of reaction. When the temperature is decreased to 13.0 °C many more particles start to form with a very short induction time (less than 2 minutes). Further decrease in temperature to 10.0 °C did not show a significant change in the induction time or the total number concentration. However, it shows that at lower temperatures the rate of approach to the steady state is faster. Similar behavior is observed at higher reactant concentrations of 5.0 ppm with a residence time of 10 s at temperatures of 20 °C and 15.5 °C as represented in Figure 48. This finding is explained as a decrease in the critical size and the vapor pressure of ammonium nitrate at lower temperatures which leads to more particle formation at shorter induction

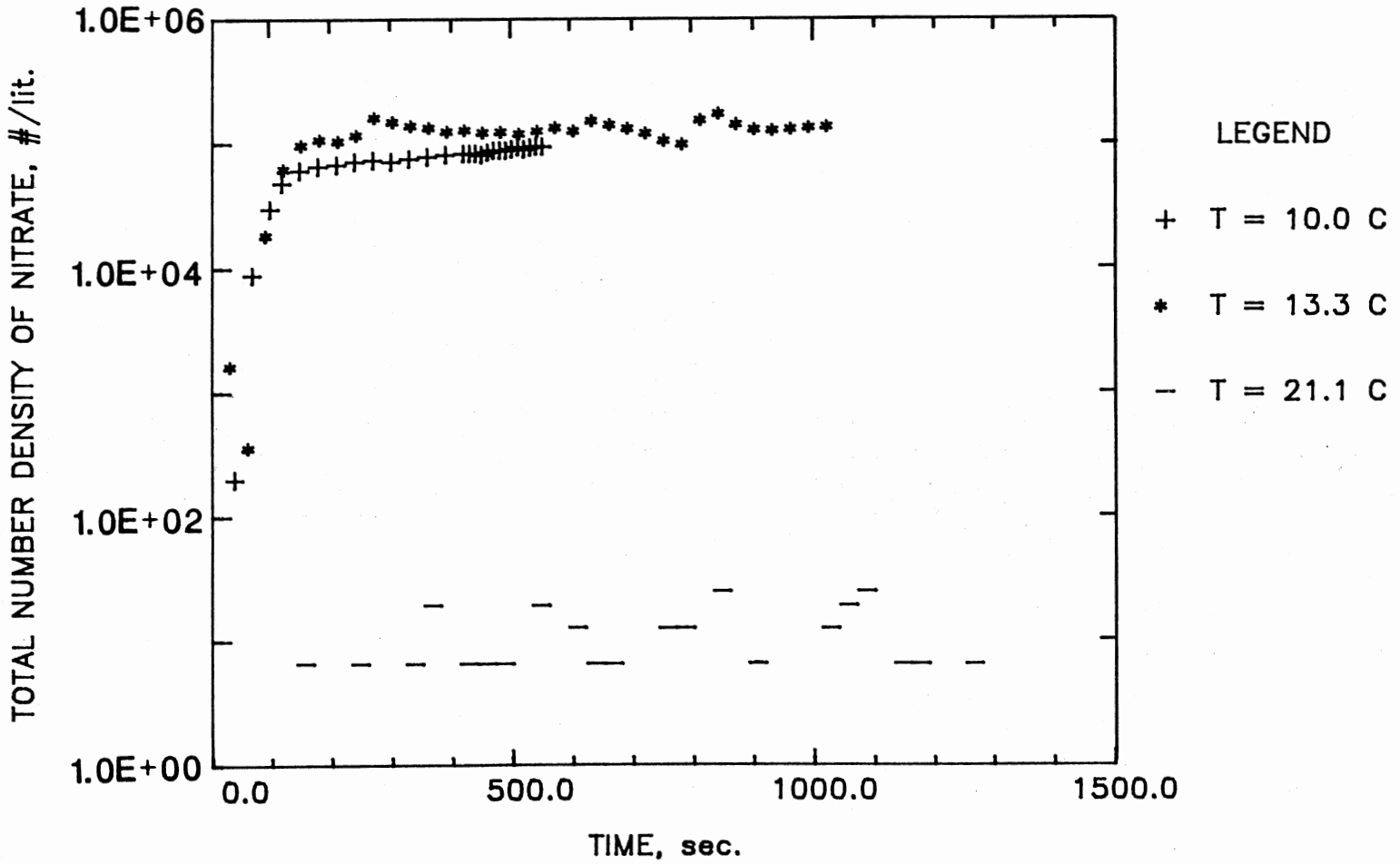

Figure 47. Effect of Temperature on Total Number Concentration for $[NH_3]$ = $[NO_2]$ = 1 ppm and RT. = 10 s (Experiments 29, 51 and 53)

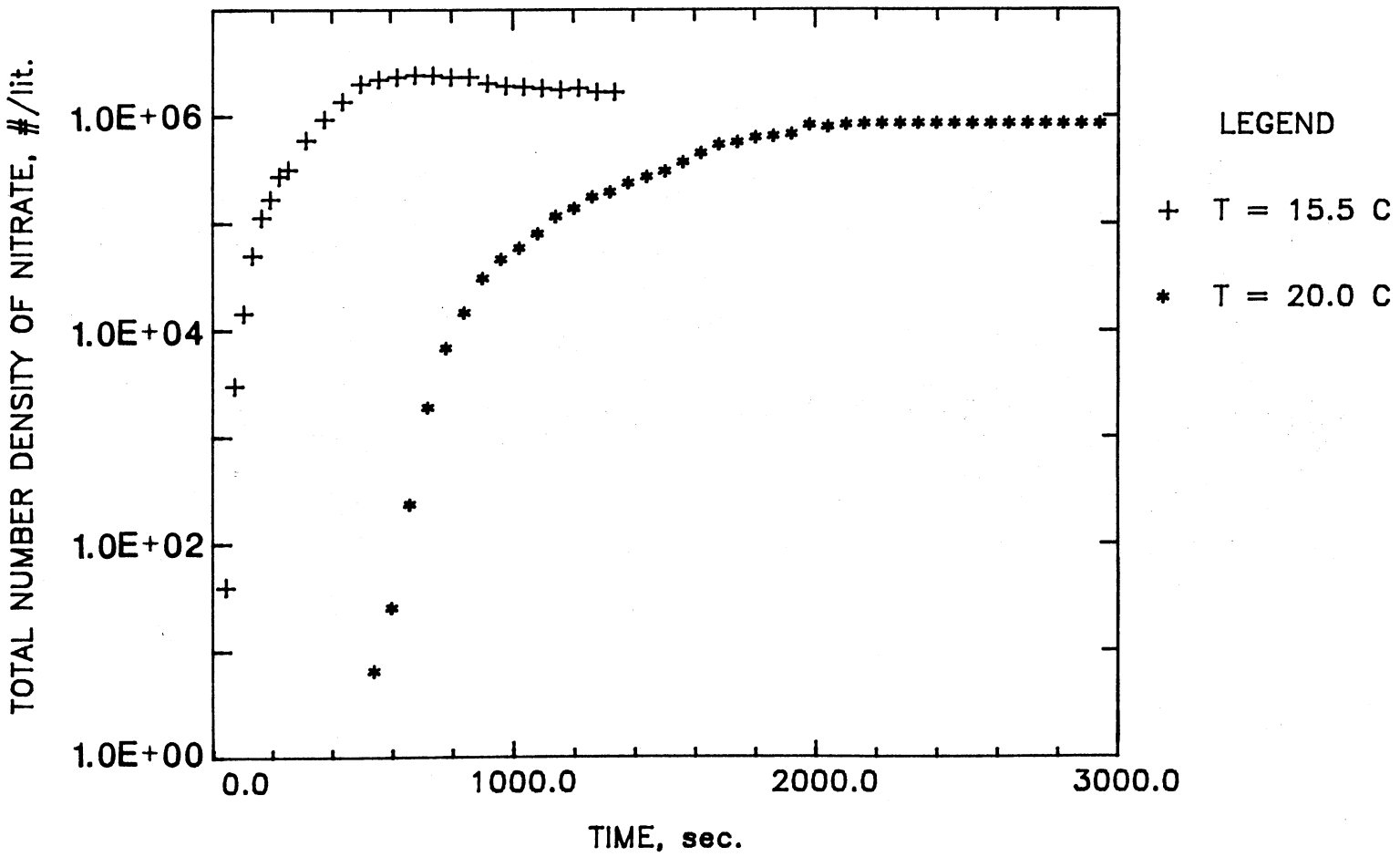

Figure 48. Effect of Temperature on Total Number Concentration for $[NH_3]$ = $[NO_2]$ = 5 ppm and RT. = 10 s (Experiments 26 and 48)

times.

The size distribution as a function of temperature is also studied as shown in Figure 49. For the case of reactant concentration of 0.5 ppm and a residence time of 10 s, a growth in the particle size is observed as the temperature is decreased from 10.0 °C to 4.4 °C. This is also referred to the decrease in the critical particle diameter as the temperature decreases. These results agree with the findings of other researchers in other systems (Su, 1979; and Gonzalez, 1980) as well as the finding of the seasonal variation of the total number concentration and size distributions of atmospheric ammonium nitrate (Cadle, 1982; and Yoshizumi, et al., 1985).

Further discussion of the temperature dependence of the total number, total surface area, and total volume of nitrate aerosol is presented in Section 5.2.5. The implications of these findings on the atmospheric pollution are also discussed in Section 5.2.5.

5.2.4.2 Effect of Initial Reactant Concentrations. Equimolar concentrations of NH_3 and NO_2 are considered at constant temperature and residence time. In general, at a specific temperature and residence time, an increase in the reactant concentrations causes the induction time to become shorter, the total number concentration to increase, the total number concentration to reach the steady state faster, and the size distribution to shift toward the larger particle sizes.

The dependence of the induction time on initial reactant concentration is shown in Figures 50 through 52. At a residence time of 10 s, the induction time decreases from about 90 s to 20 s and from 50 minutes to 15 minutes as the reactant concentrations is increased from 1.0 ppm to 2.5 ppm at temperatures of 13.5 °C and 21.0 °C as shown in Figures 50

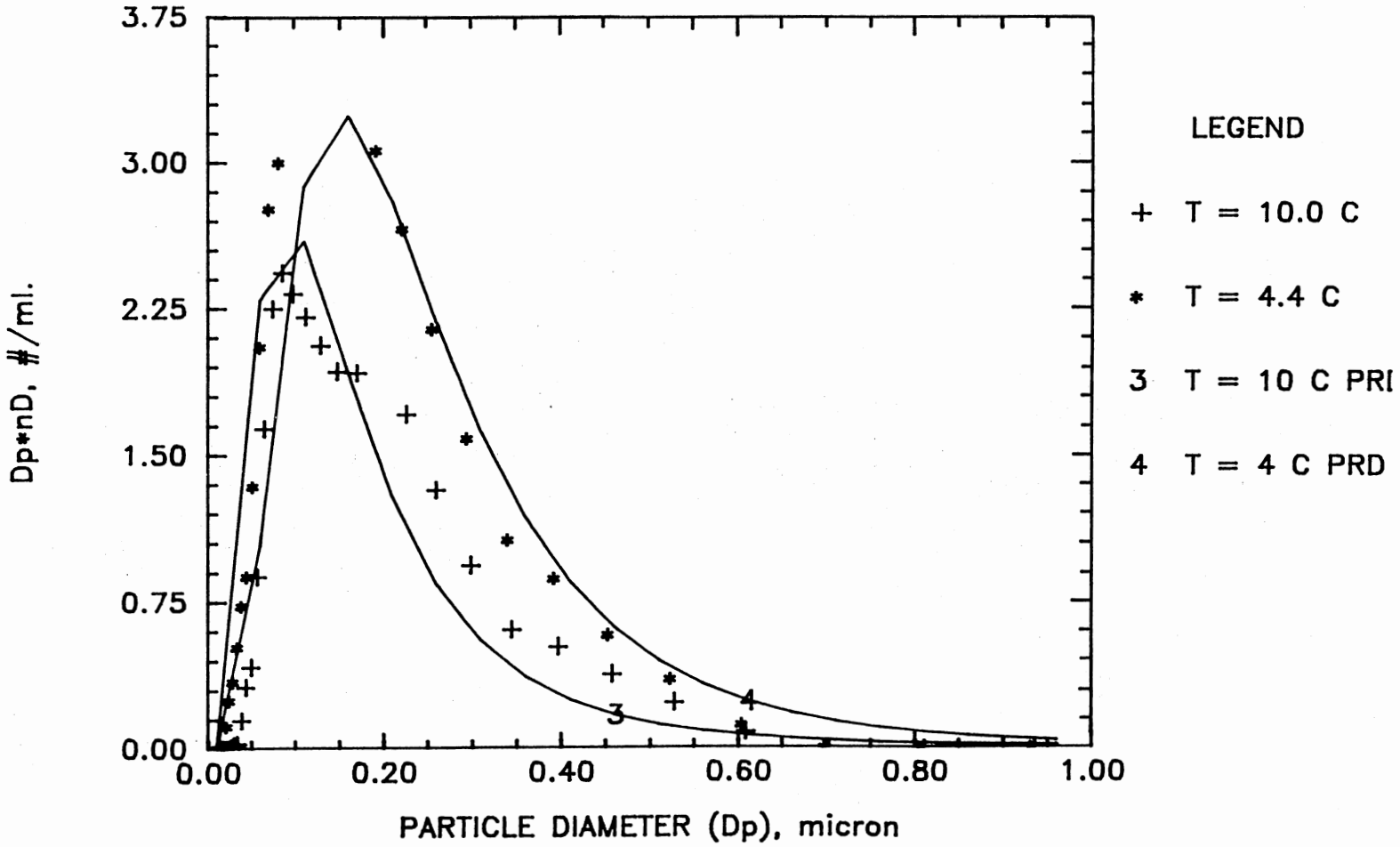

Figure 49. Effect of Temperature on Particle Size Distribution for $[NH_3]$ = $[NO_2]$ = 0.5 ppm and RT. = 10 s (Experiments 60 and 63)

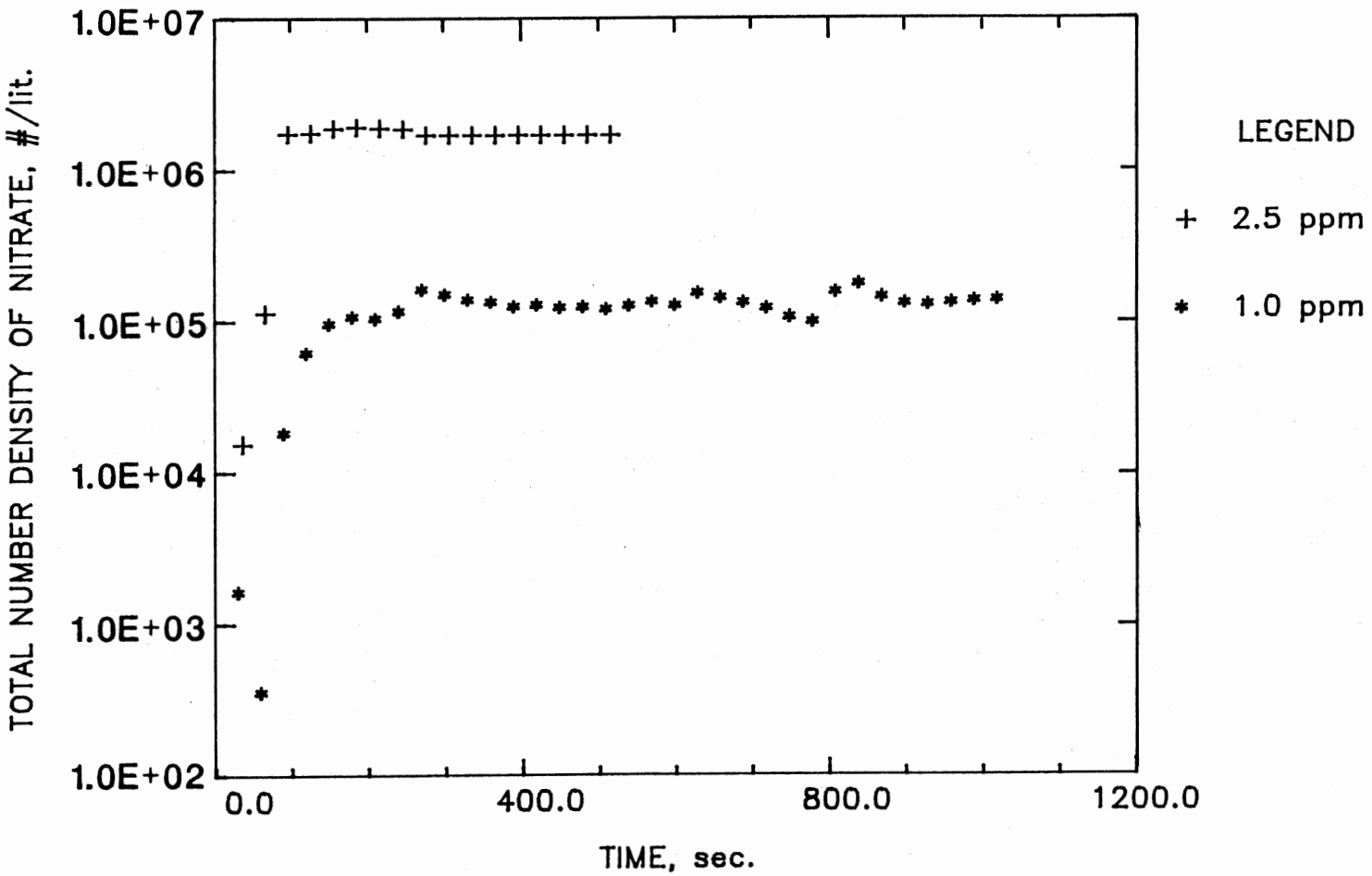

Figure 50. Effect Initial Reactant Concentrations on Total Number Density at T = 13.5 °C and RT. = 10 s (Experiments 50 and 51)

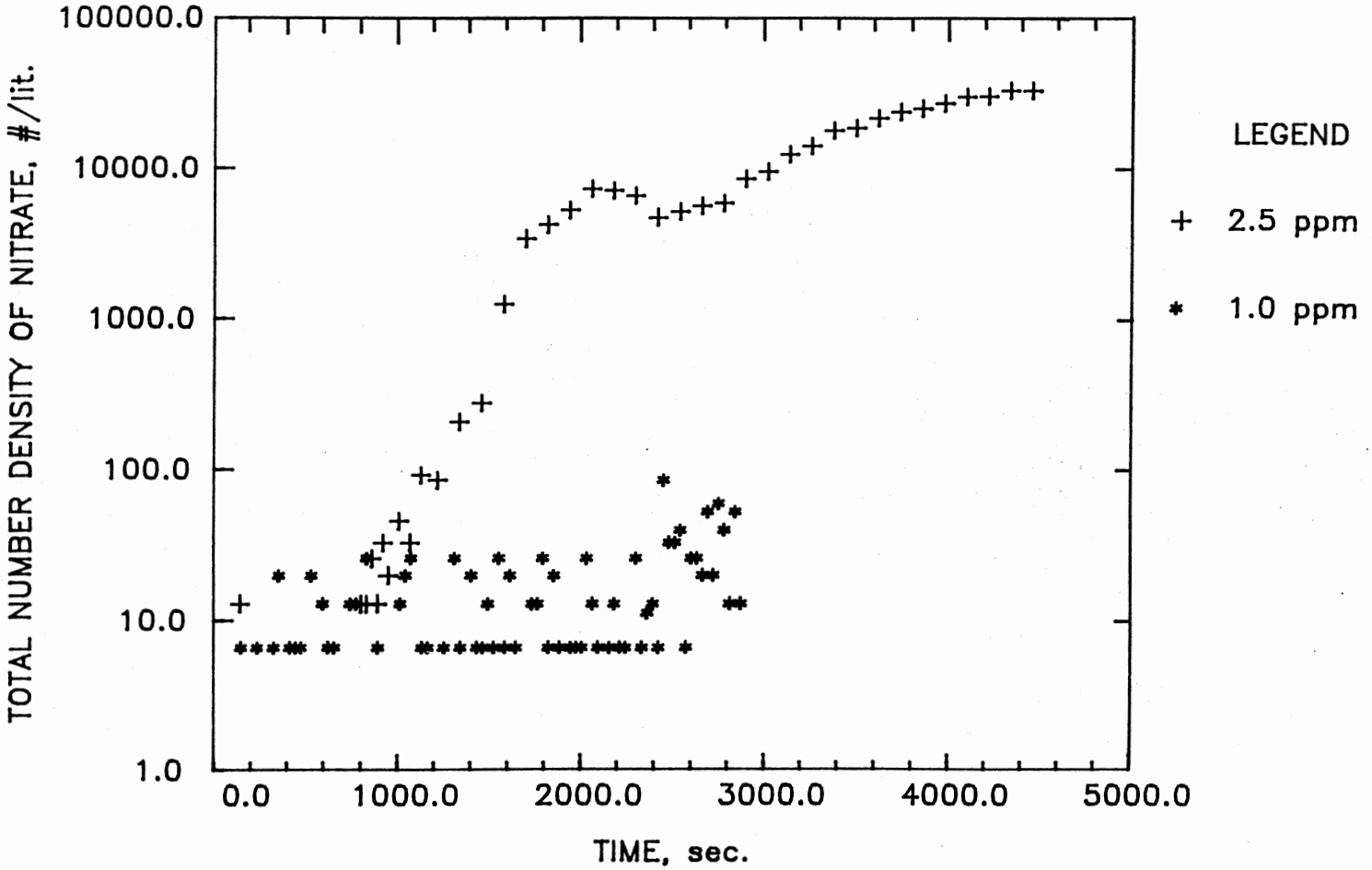

Figure 51. Effect Initial Reactant Concentrations on Total Number Density at T = 21 °C and RT. = 10 s (Experiments 28 and 29)

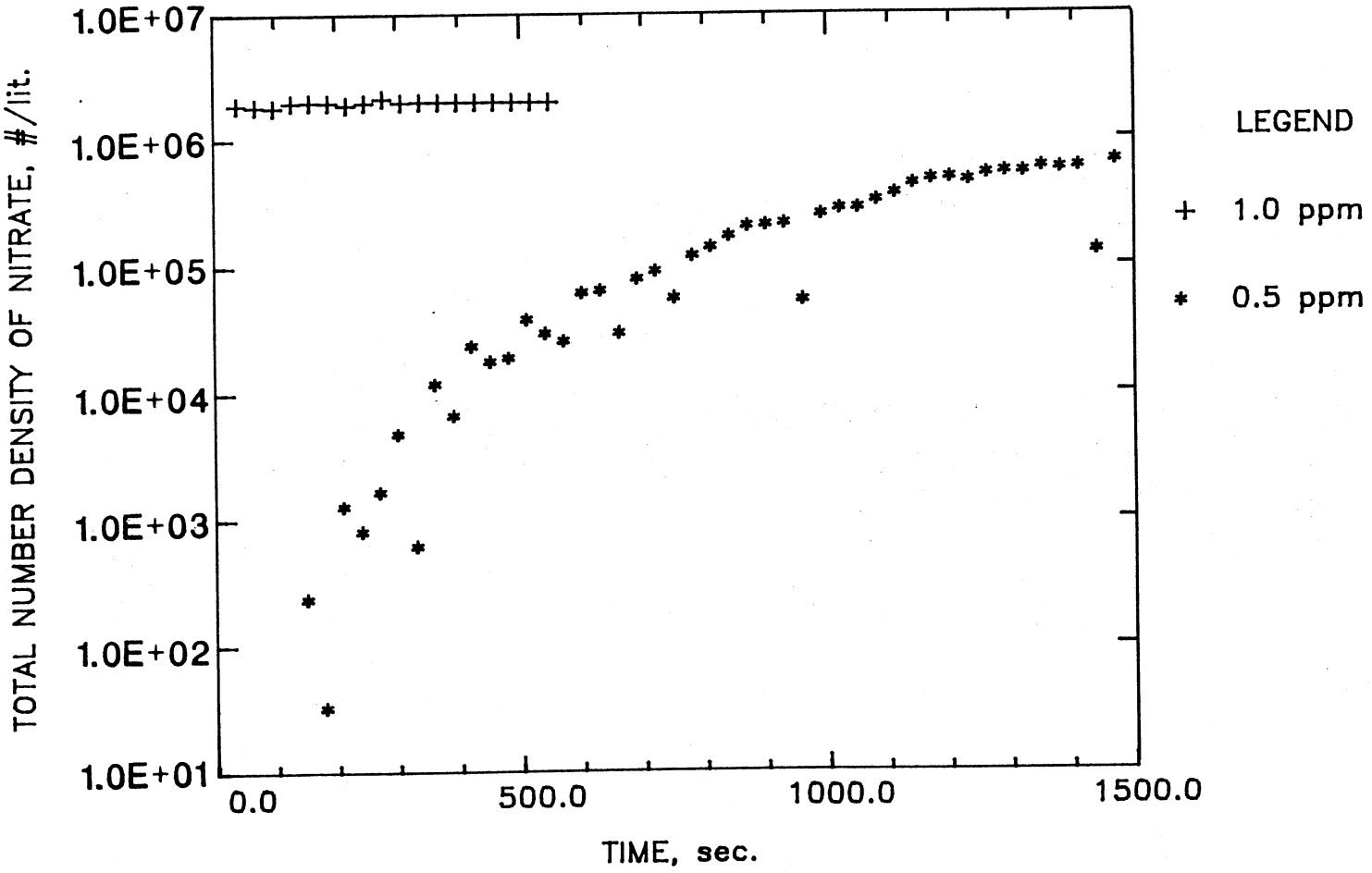

Figure 52. Effect Initial Reactant Concentrations on Total Number Density at T = 4 °C and RT. = 10 s (Experiments 59 and 60)

and 51 respectively. Similarly Figure 52 shows that at a temperature of 4.4 °C and a residence time of 10 s, the induction time changed from 4 minutes to 1 s as the concentrations increased from 0.5 to 1.0 ppm.

The total number concentration increases by a factor of about ten as the reactant concentration is doubled in both cases of temperature of 4.4 °C and 13.5 °C as shown in Figures 50 and 52 respectively. However, at the higher temperature of 21 °C, as shown in Figure 51, the increase in the total number concentration, corresponding to doubling the concentration, is more than two orders of magnitude. In Figures 50 through 52, the rate of approach to the steady state is also shown to be proportional to the reactant concentration. The explanation to these observations is that the supersaturation ratio of the monomer increases as the reactant concentration increases and the critical size decreases, and hence more nucleating species are formed in a shorter time.

The increase in the reactant concentration also causes the particle size to grow as represented in Figure 53. At a temperature of 4.4 °C and a residence time of 10 s, the peak of the size distribution shifts from 0.15 μm to 0.20 μm when the concentration is increased from 0.5 to 1.0 ppm. This observation agrees with the findings of Su, 1979, and Gonzalez, 1980 for the system of NH_3-HCl.

5.2.4.3 Effect of Residence Time. Figures 54 and 55 indicate that particles grow more at longer residence times. For reactant concentrations of 8 ppm each and a temperature of 21 °C, the size spectra show a shift toward the larger sizes, indicating a growth in the particle size, as the residence time is increased from 17.6 to 24 and then to 30 s. Similar behavior is observed for reactant concentrations of 5 ppm at a temperature of 21 °C. These results agree with the

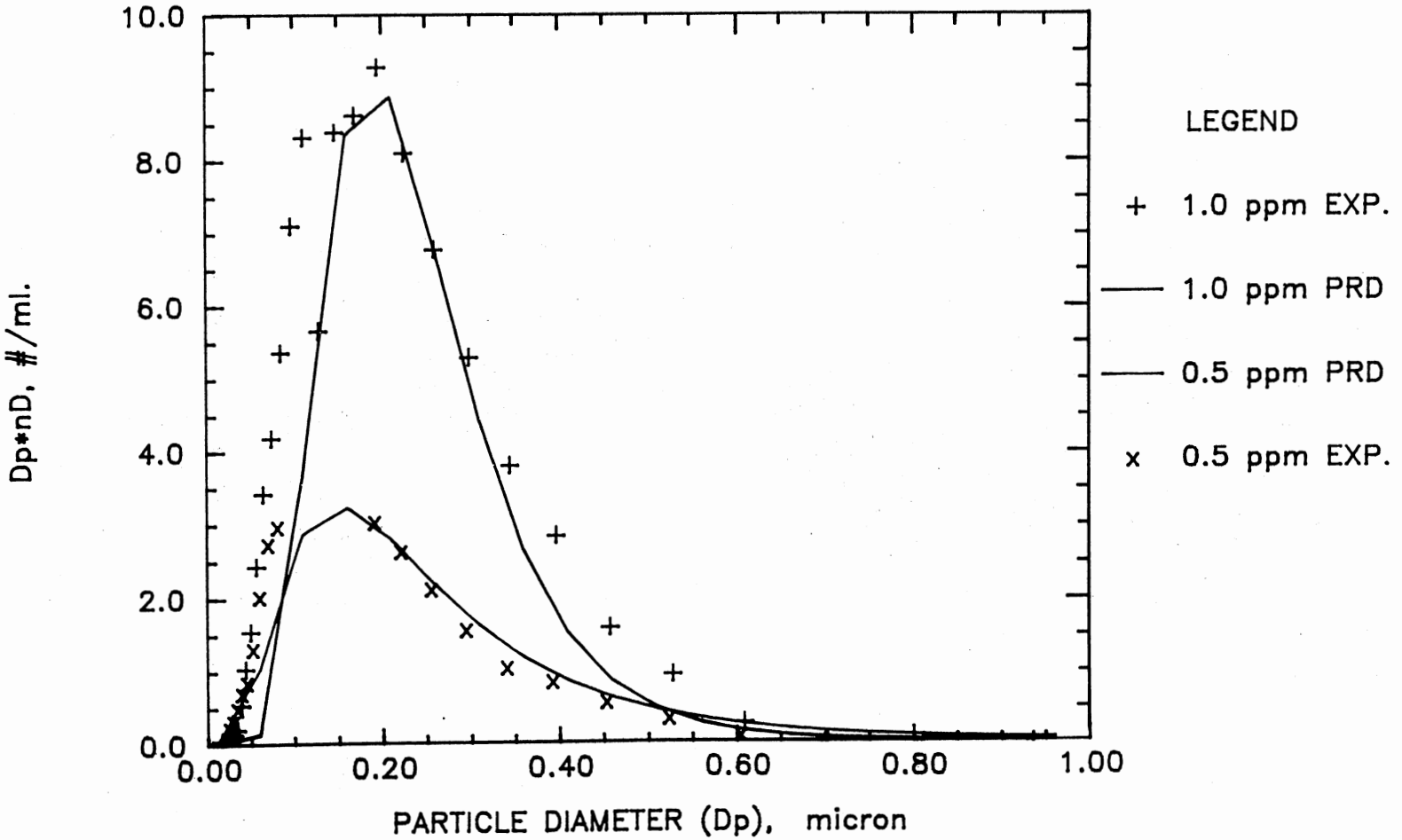

Figure 53. Effect of Initial Reactant Concentrations on Particle Size Distribution at T = 4 °C and RT. = 10 s (Experiments 59 and 60)

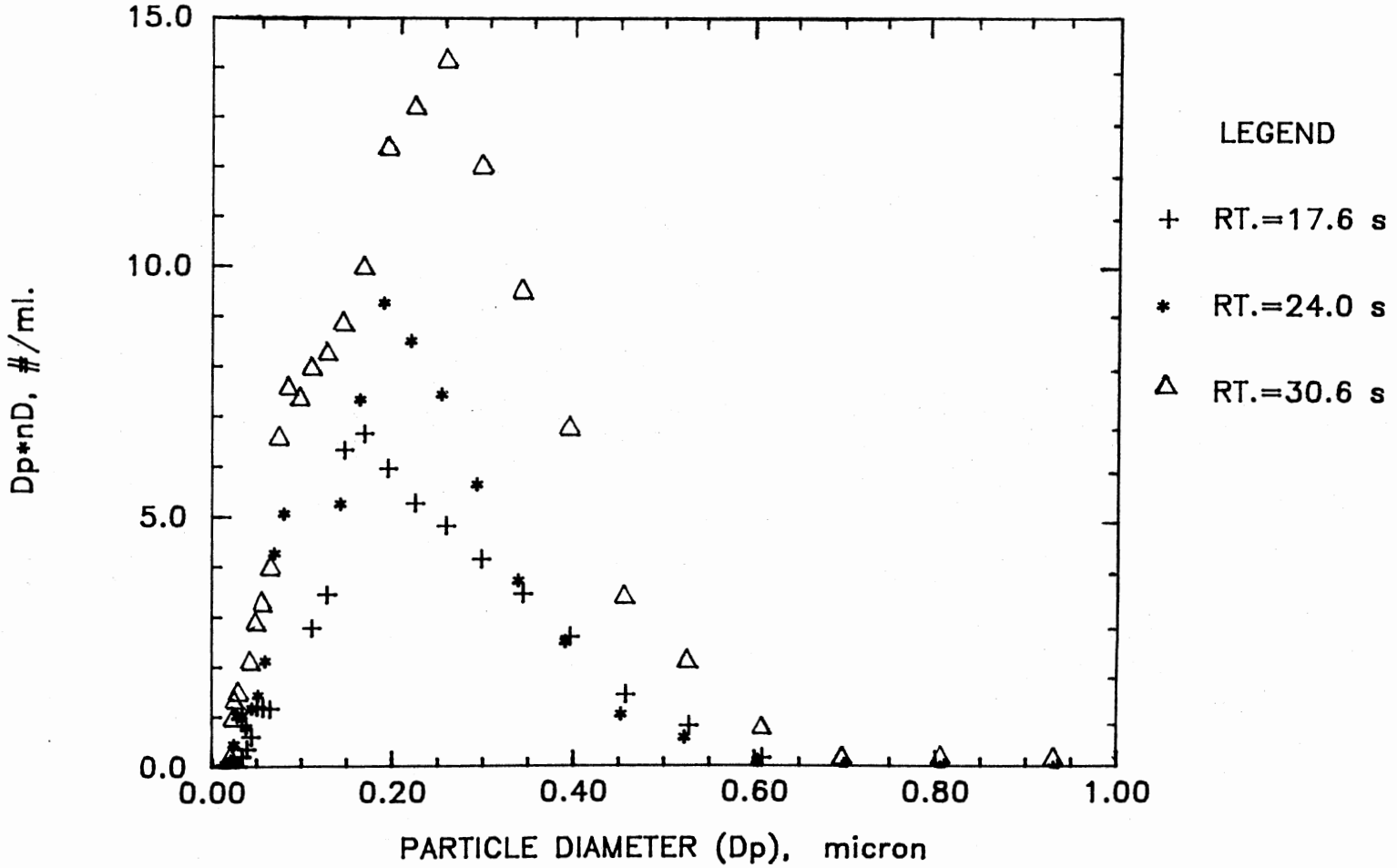

Figure 54. Effect of Residence Time on Particle Size Distribution for $[NH_3]$ = $[NO_2]$ = 8 ppm and T = 21 °C (Experiments 54, 55, and 56)

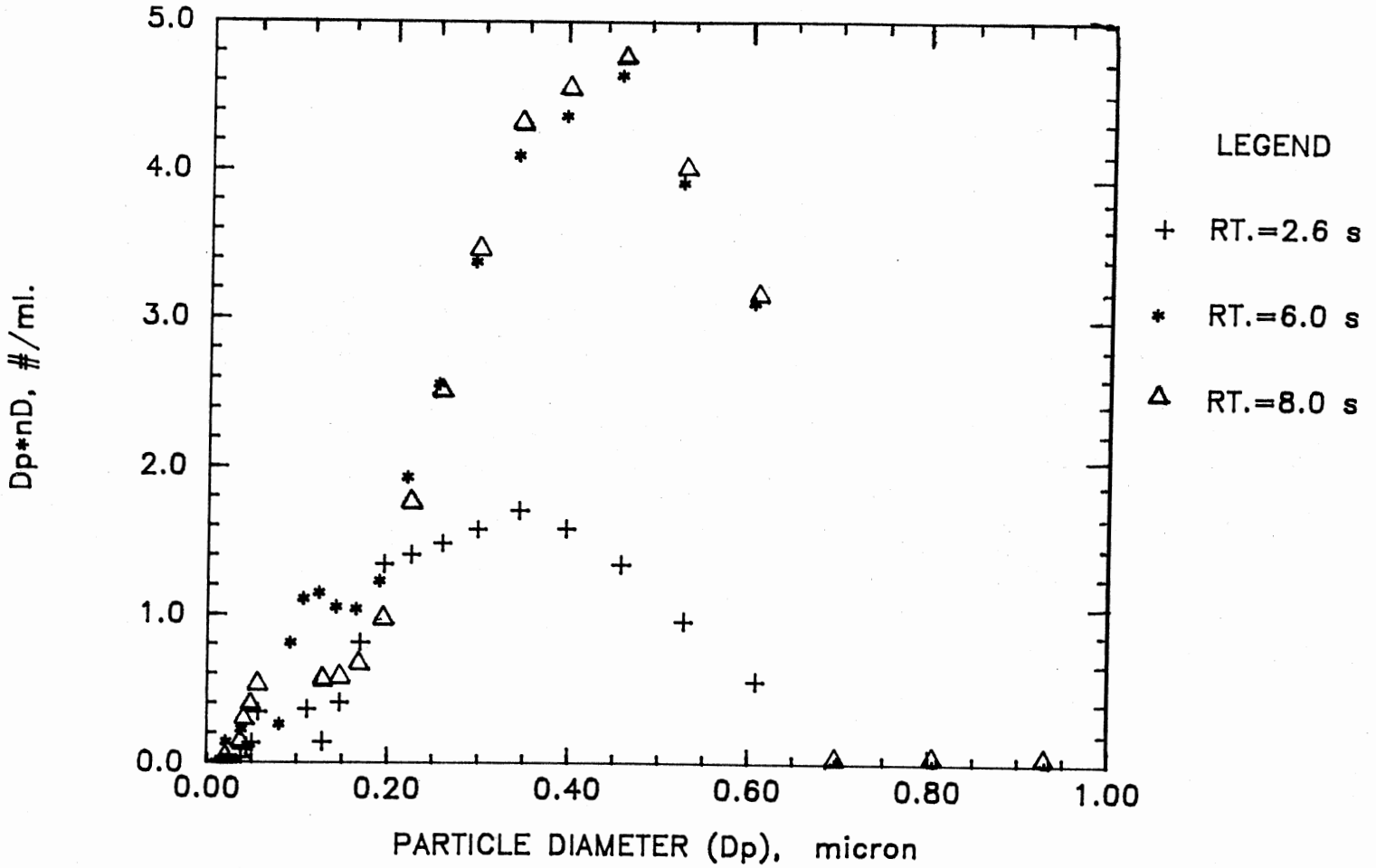

Figure 55. Effect of Residence Time on Particle Size Distribution for $[NH_3]$ = $[NO_2]$ = 5 ppm and T = 21 °C (Experiments 41, 42, and 44)

findings of other investigators of this system and other systems (Kodas, et al., 1986; Su, 1979; and Gonzalez, 1980).

5.2.4.4 Effect of the $[NH_3]/[NO_2]$ Ratio. A ratio (R) of the concentration of ammonia to that of nitrogen dioxide is defined. This ratio is varied in order to see the corresponding change in the number of particles formed and their size. Ratio of 1.0, 0.2 and 0.1 (experiments 34, 47 and 45 respectively) are obtained by fixing the concentration of NH_3 at 5.0 ppm and reducing the concentration of NO_2 correspondingly. A lower ratio of 0.06 is obtained (experiment 46) by fixing the concentration of NH_3 at 0.5 ppm and increasing the concentration of NO_2 to 8 ppm. Figure 56 shows that the total number concentration decreased from about 3.0×10^6 to 5.0×10^4 and then to 50 particles/l. as the ratio decreased from 1.0, to 0.2 and then to 0.1. Further decrease in this ratio to 0.06 shows more particle formation as shown in Figure 56. This is probably because at higher NO_2 concentrations, more HNO_3 is formed, which tend to shift the reaction [4] toward producing more ammonium nitrate.

The model qualitatively predicts the experimental observation of Figure 56 for the same conditions of 20 °C and residence time of 5 s as can be seen in Figure 57. The highest number concentration is obtained when the ratio is unity. This fact agrees with the stoichiometry of the reaction which says that two moles of ammonia react with two moles of nitrogen dioxide to produce one mole of each product species.

The effect of the ratio R on the particle size distribution is shown in Figure 58. A growth in the particle size is observed when the ratio is increased from 0.2 to 1.0 corresponding to an increase in the concentration of NH_3. This growth indicates that higher concentrations

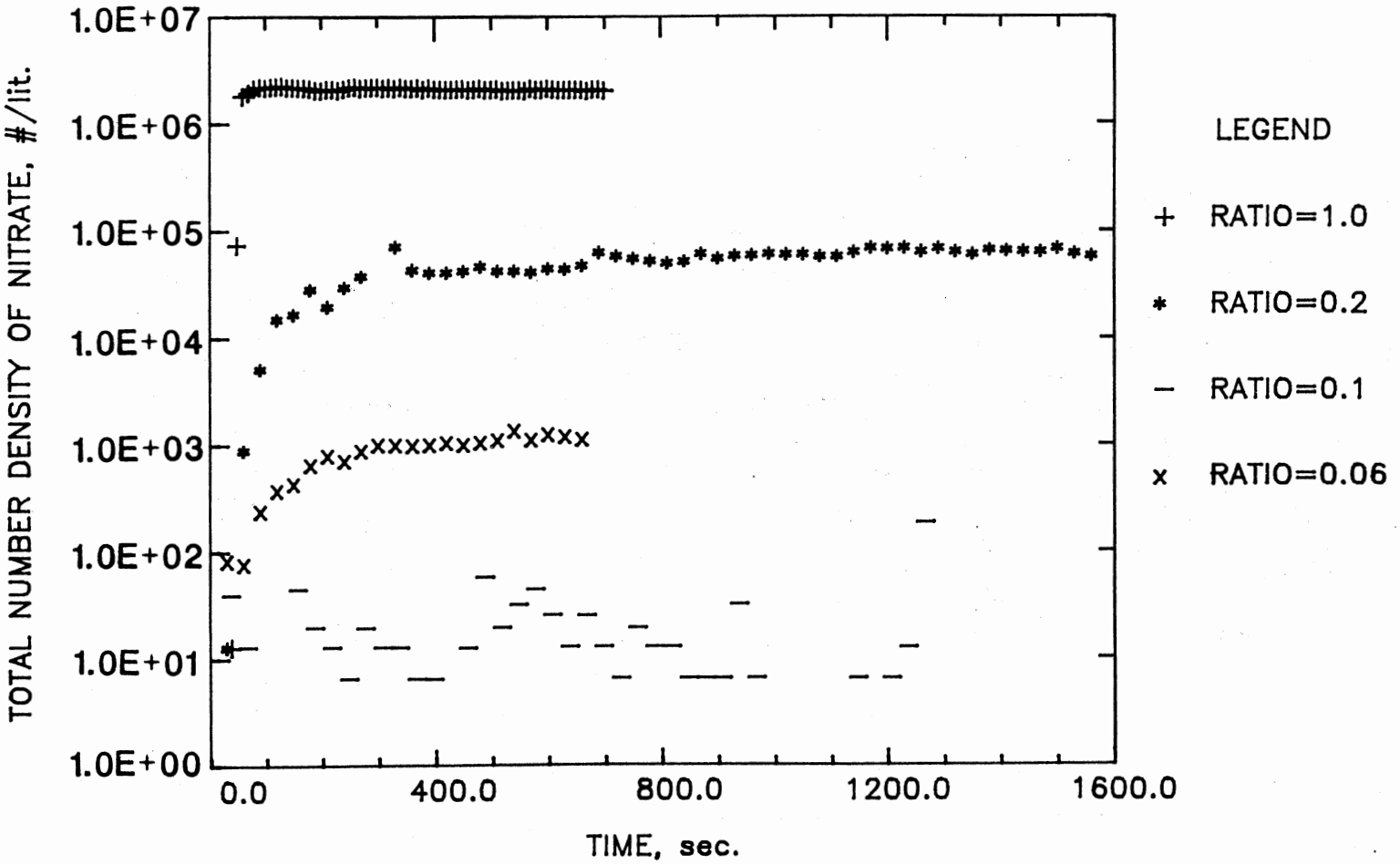

Figure 56 Effect of $[NH_3]/[NO_2]$ Ratio on Measured Total Number Density at T = 20 °C and RT. = 5 s, for Ratio of 1, 0.2, 0.1 and 0.06 Corresponding to Experiments 34, 47, 45 & 46

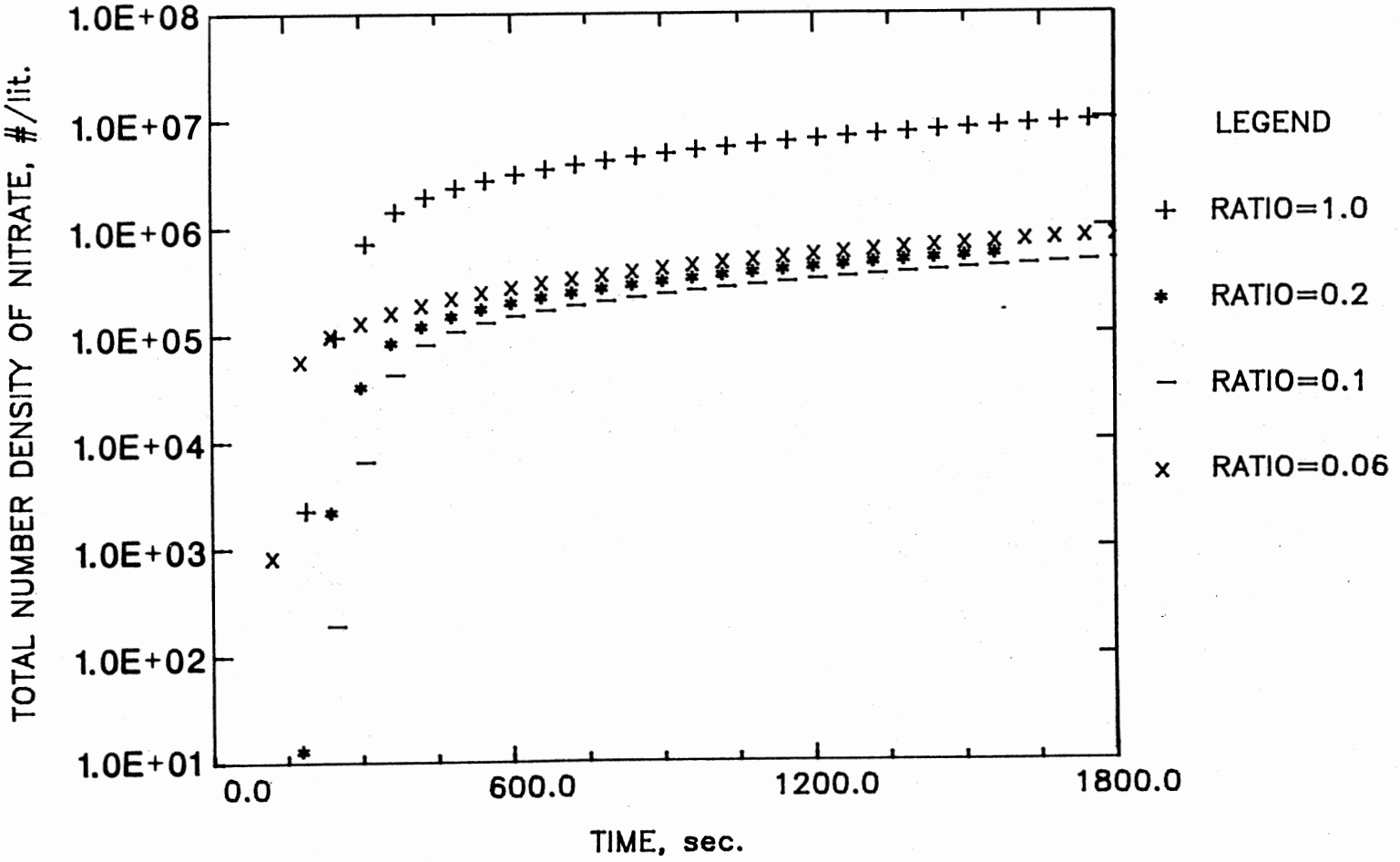

Figure 57. Effect of $[NH_3]/[NO_2]$ Ratio on Predicted Total Number Density at T = 20 °C and RT. = 5 s, for Ratio of 1, 0.2, 0.1 and 0.06 Corresponding to Experiments 34, 47, 45 & 46

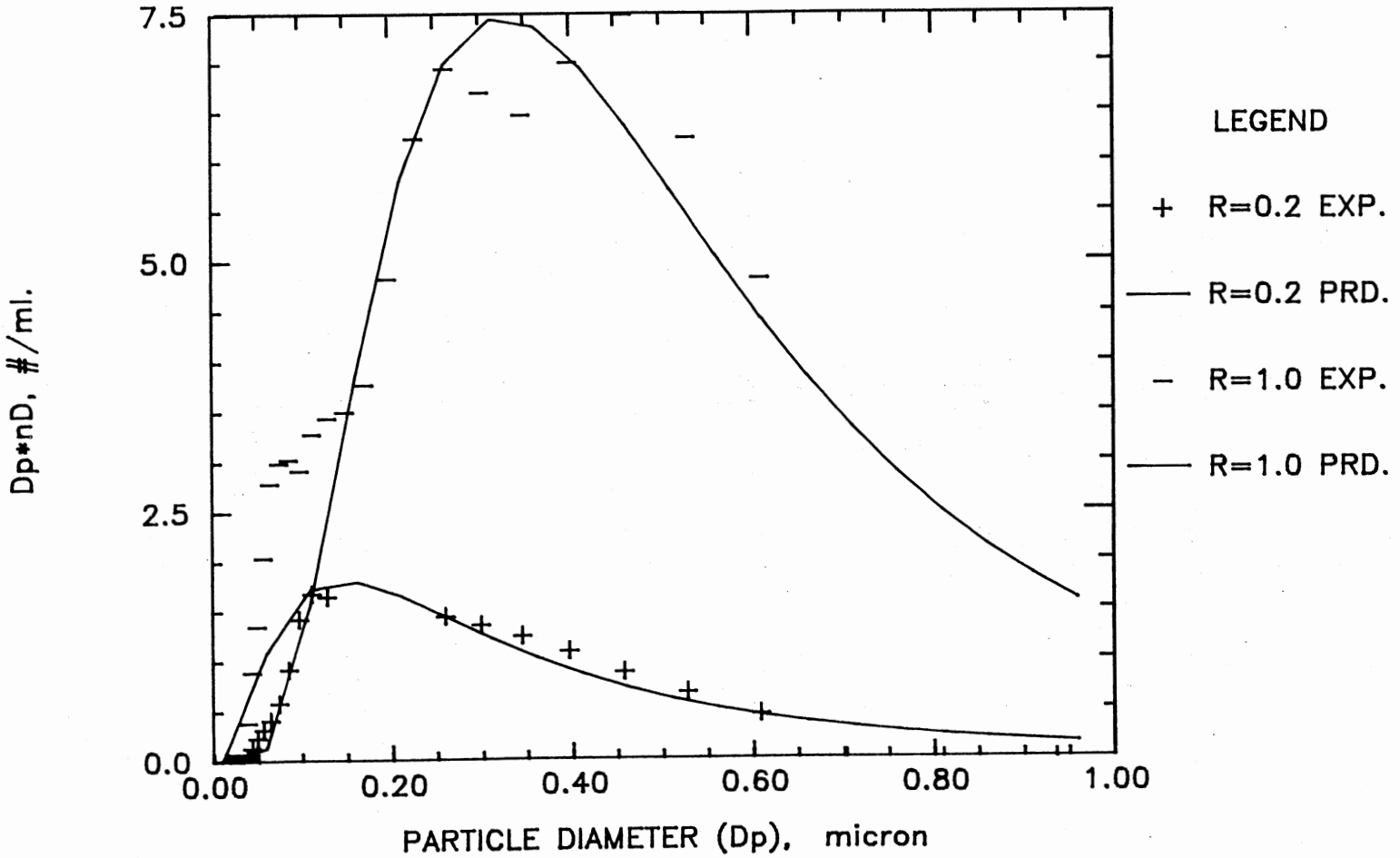

Figure 58. Effect of $[NH_3]/[NO_2]$ Ratio on Particle Size Distribution at T = °C and RT. = 5 s, for Ratio of 1 and 0.2 Corresponding to Experiments 34 and 47

of NH_3, cause the reaction [4] to produce more ammonium nitrate, and hence increase the supersaturation ratio and decrease the critical size of the nitrate particles in the gas-phase.

5.2.5 Dependency of Particle Characteristics on Temperature

Semi-log plots of the total number, total surface area, total volume and critical nuclei size versus temperature at reactant concentrations of 1.0 and 0.5 ppm at a residence time of 10 s are shown in Figures 59 through 64. Except for the total volume, a linear relation is observed for these parameters with the reciprocal of temperature, where they increase as temperature decreases. These graphs indicate that at very low temperatures, (usually the case at high altitude atmospheric environments) high number concentrations can be obtained even for very small concentrations of reactants (1.0 and 0.5 ppm). Figure 59 shows that, for concentrations of 1.0 ppm, the total number density increases by one order of magnitude as the temperature decreases from 20 to 4 °C. For reactant concentrations of 0.5 ppm, the total number density increases by a factor of five with only 6 °C decrease in temperature (from 10 to 4 °C) as shown in Figure 61. Similar behavior is observed for the total surface area and total volume of particles at the two reactant concentrations mentioned above. As the temperature decreases, the critical particle size decreases as can be seen from Figures 63 and 64.

The theoretical prediction shows qualitatively the same behavior of the total number, surface area, and volume with temperature. It shows a good fit, within the accuracy limit of the data, to the experimental

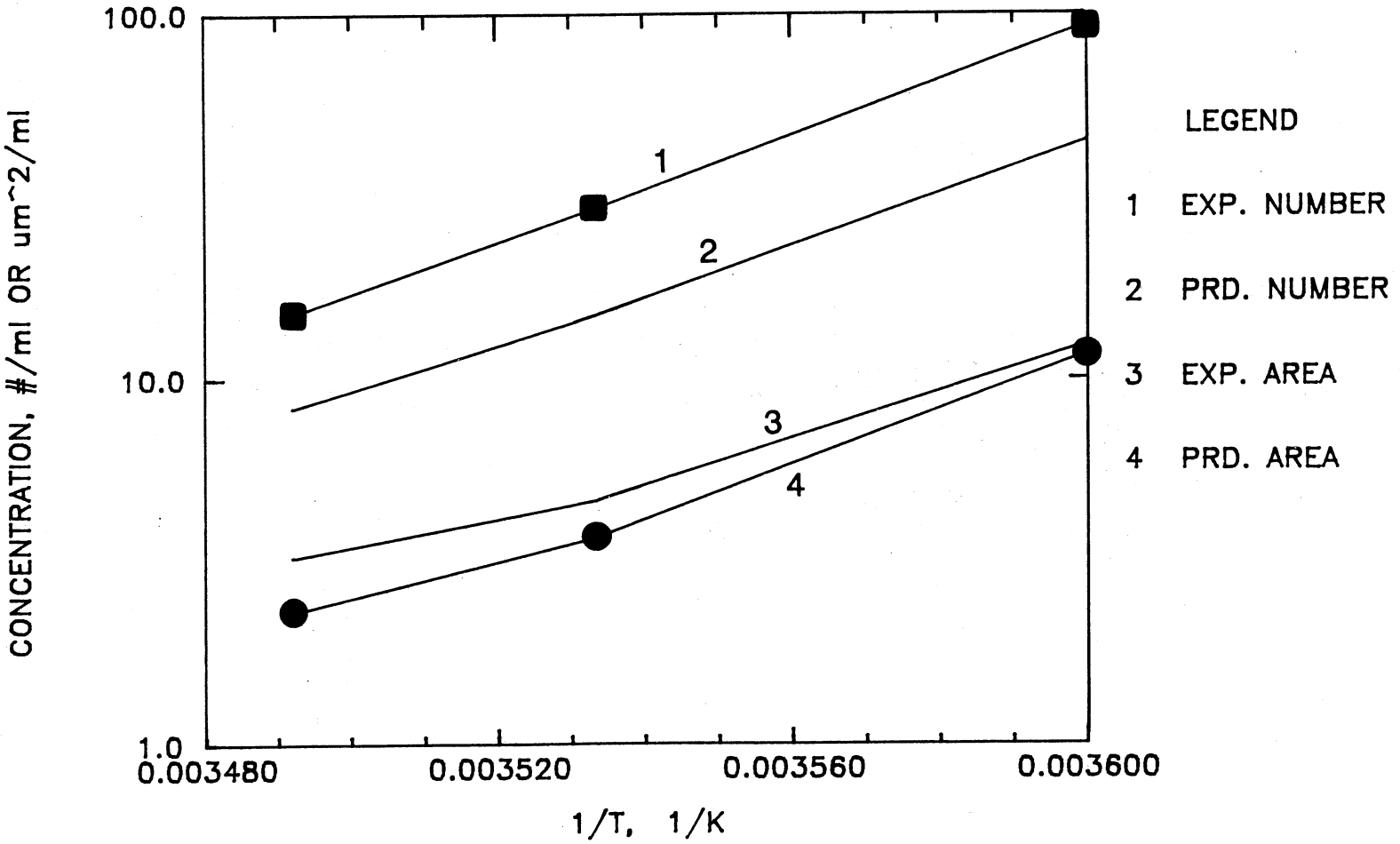

Figure 59. Temperature Dependence of Total Number and Total Surface Area of Particles for $[NH_3] = [NO_2] = 1$ ppm and RT. = 10 s (Experiments 29, 51, 53 and 59)

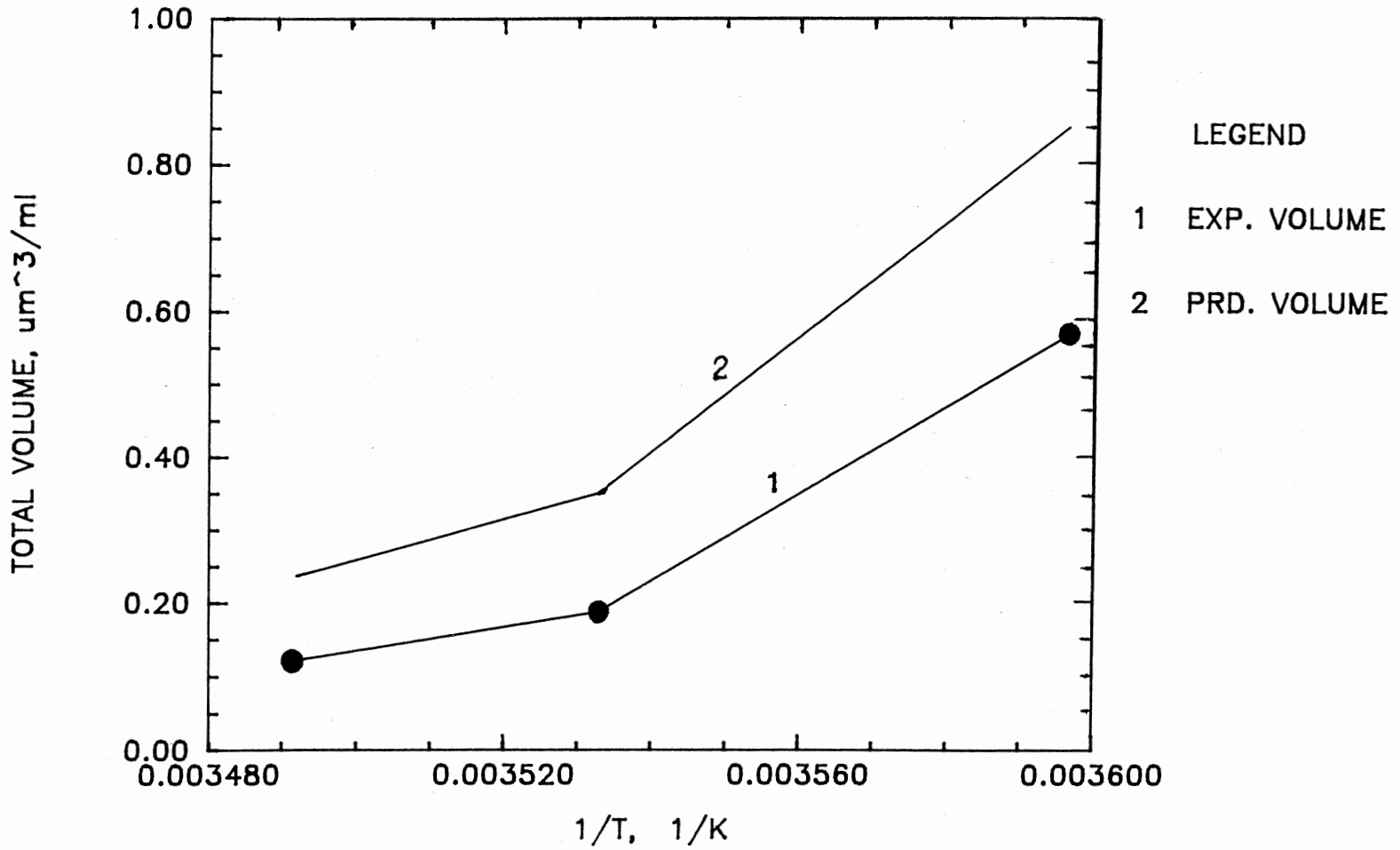

Figure 60. Temperature Dependence of Total Volume for $[NH_3]$ = $[NO_2]$ = 1 ppm and RT. = 10 s (Experiments 29, 51, 53 and 59)

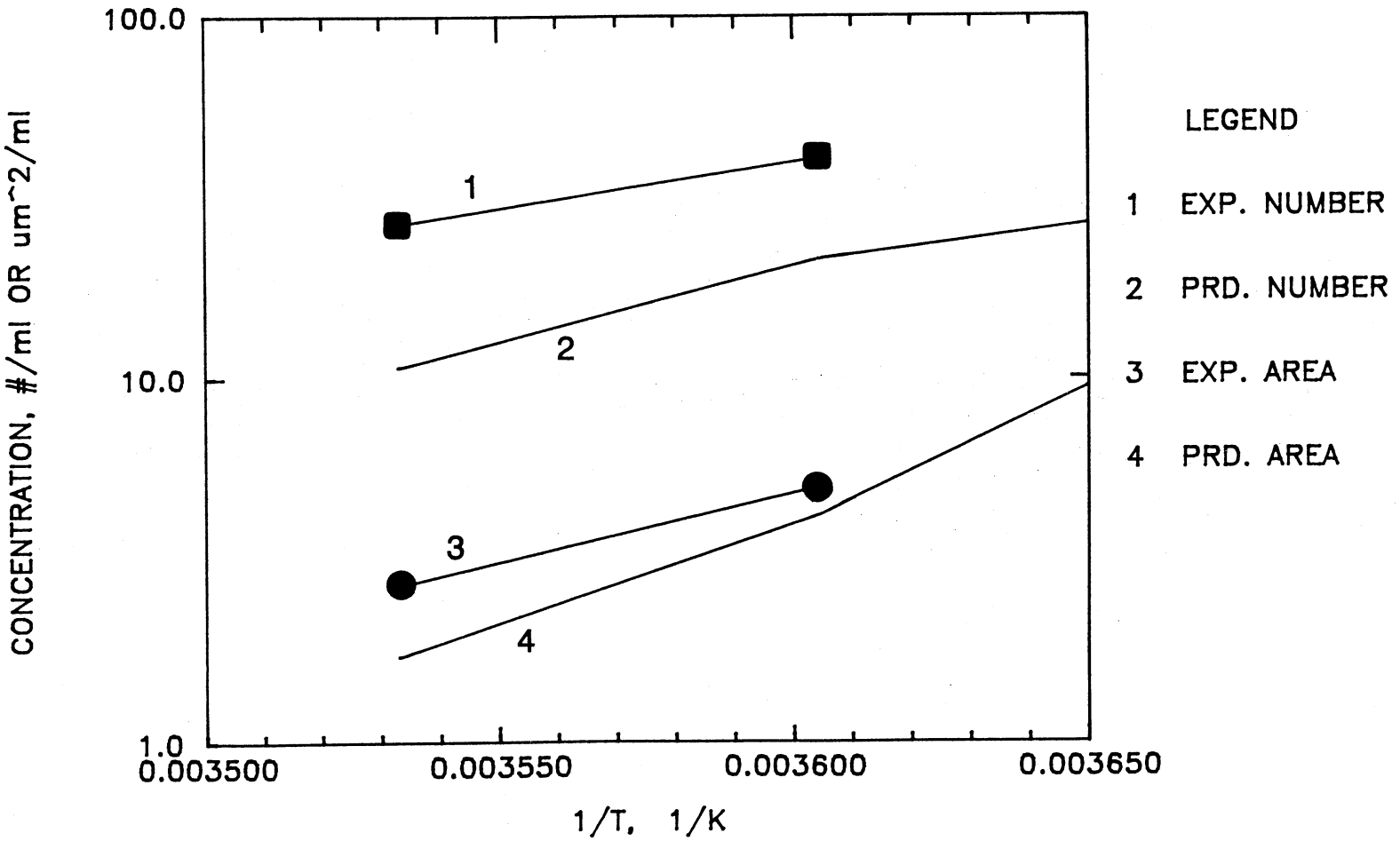

Figure 61. Temperature Dependence of Total Number and Total Surface Area of Particles for $[NH_3] = [NO_2] = 0.5$ ppm and RT. = 10 s (Experiments 52, 58, 60 and 63)

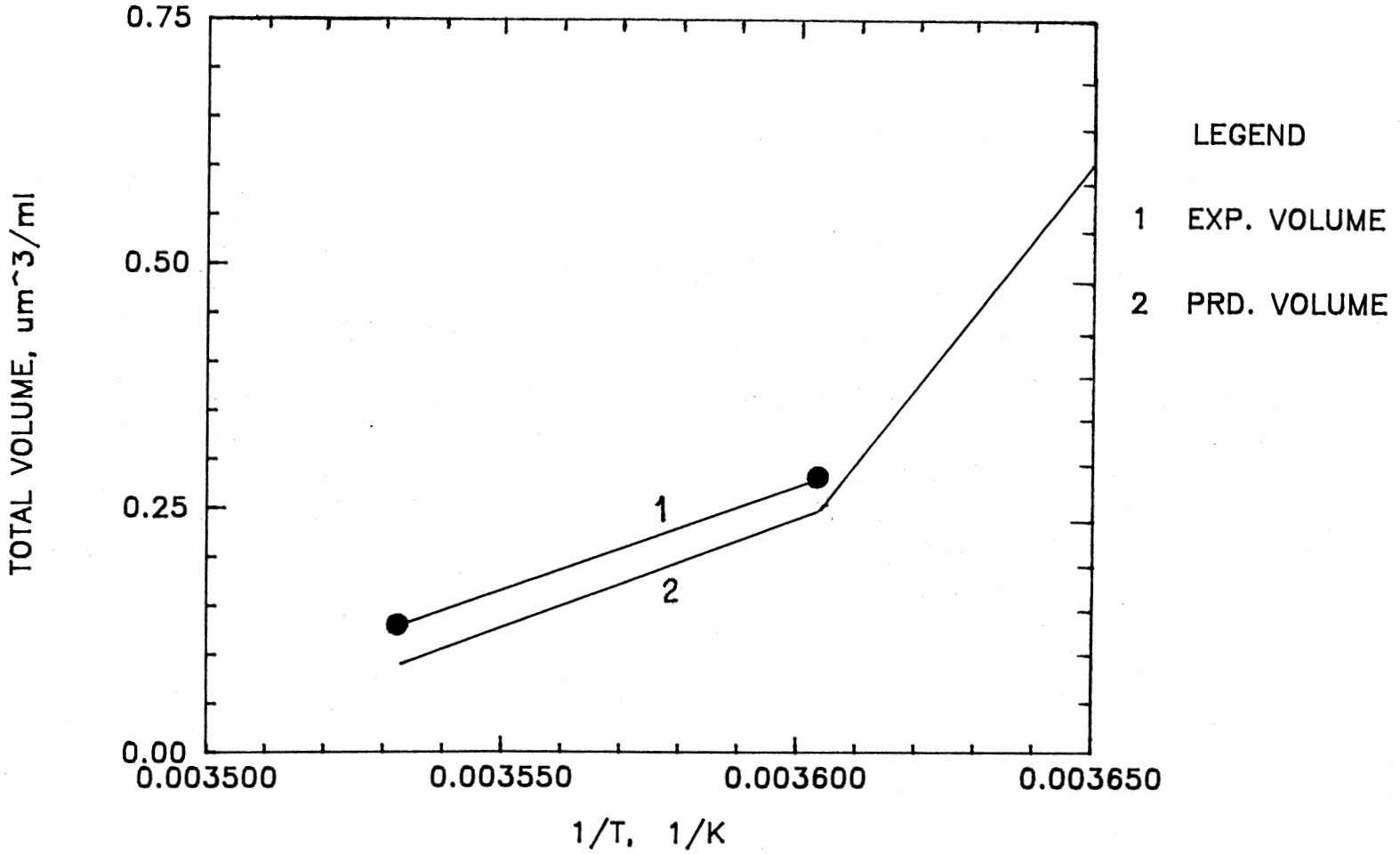

Figure 62. Temperature Dependence of Total Volume for $[NH_3]$ = $[NO_2]$ = 0.5 ppm and RT. = 10 s (Experiments 52, 58, 60 and 63)

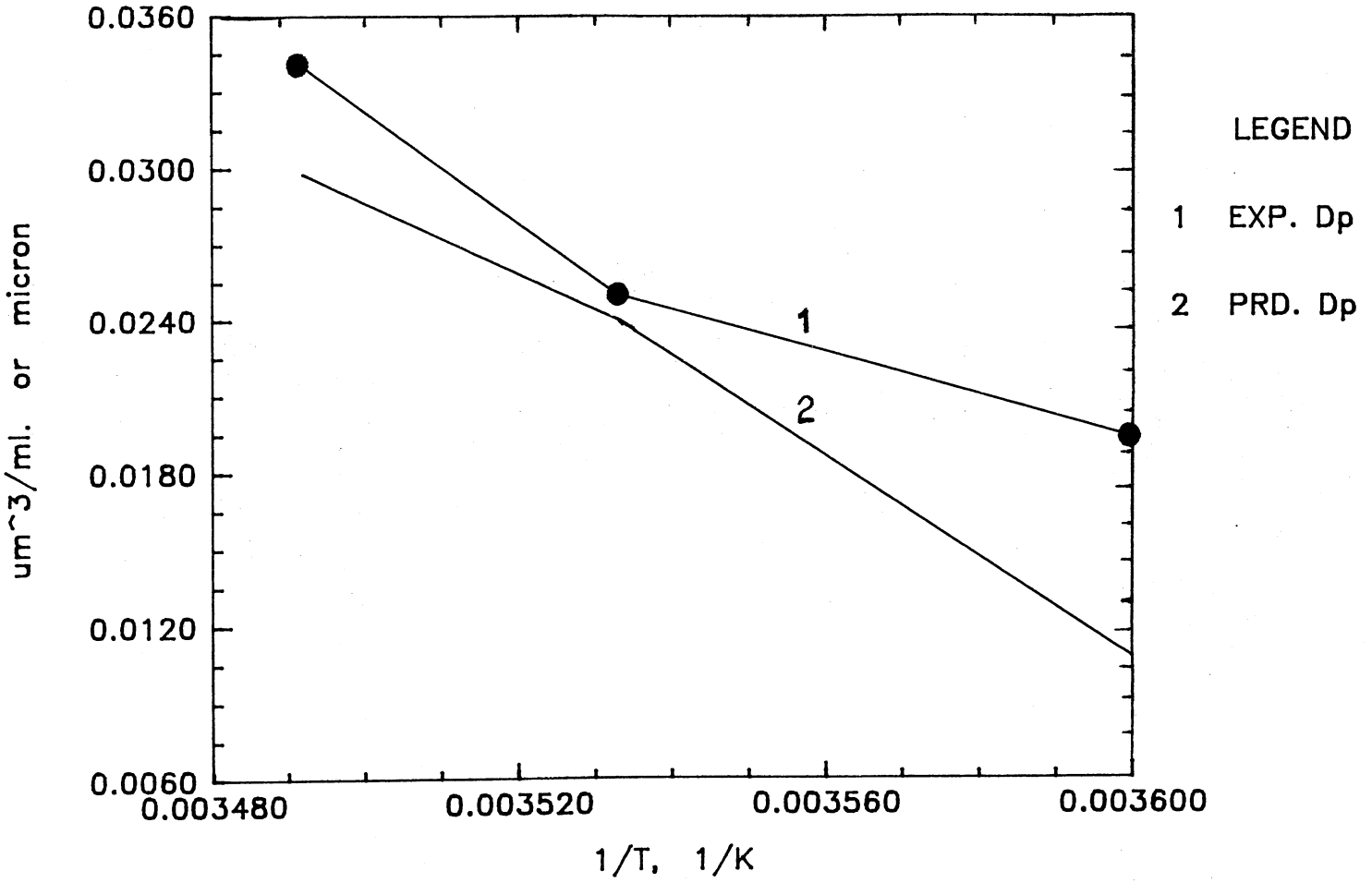

Figure 63. Temperature Dependence of Critical Size of Particles for $[NH_3]$ = $[NO_2]$ = 1 ppm and Reaction Time = 10 s Experiments 29, 51, 53, and 59)

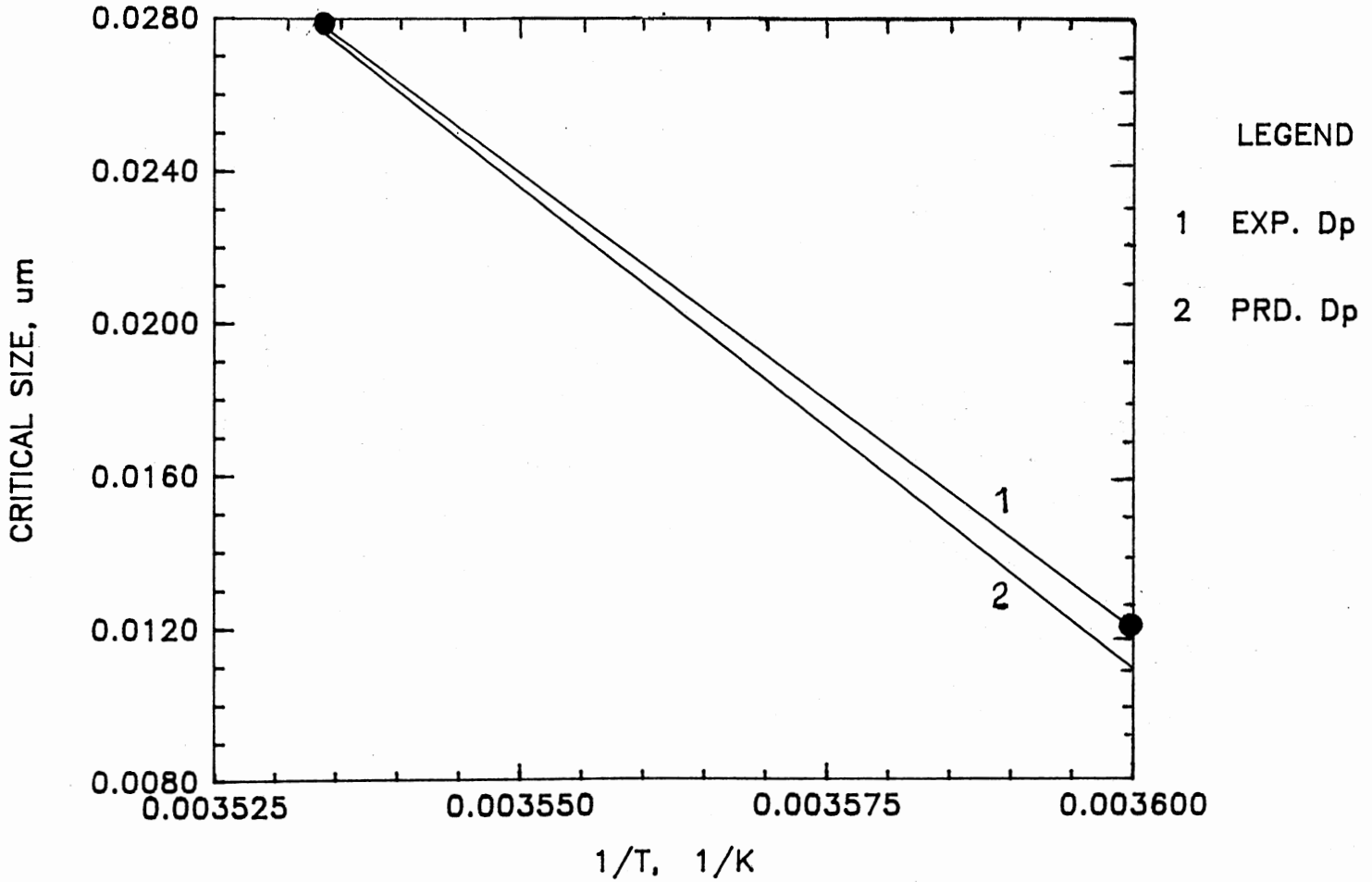

Figure 64. Temperature Dependence of Critical Size of Particles for $[NH_3]$ = $[NO_2]$ = 0.5 ppm and Reaction Time = 10 s Experiments (52, 58, 60 and 63)

results of the critical size. The critical size is estimated by considering the diameter of the smallest observed particle, measured by the DMPS. At a temperature of 20 °C, a residence time of 5 s, and initial reactant concentrations of 5 ppm each (experiment 34), the measured and predicted critical particle diameters are 0.035 μm and 0.0346 μm respectively. At a temperature of 10 °C, a residence time of 10 s, and initial reactant concentrations of 1.0 ppm each (experiment 53), the measured and predicted critical sizes are 0.028 μm and 0.0247 μm respectively. At the low temperature of 4 °C, a residence time of 10 s, and initial reactant concentrations of 1.0 ppm, (experiment 59), the measured and predicted critical sizes are 0.018 μm and 0.0010 μm respectively. This good agreement between the experimentally estimated and theoretically predicted critical sizes assures the validity of the assumption used in experimentally estimating the critical sizes as described above.

The conclusion drawn from this part of the study is that ammonium nitrate aerosols can form in the atmospheric environments of very cold regions and very elevated areas in very large numbers even at very low concentrations of NO_2, NH_3 and HNO_3. This increases atmospheric pollution and global environmental impact of nitrogen oxide emissions in the upper atmospheres.

5.2.6 Variation of Reactant Partial Pressures With Time

The kinetic model is used to predict the variation in the partial pressures of nitrogen dioxide, ammonia, and ammonium nitrate as the reaction progresses. Figure 65 shows this prediction for initial

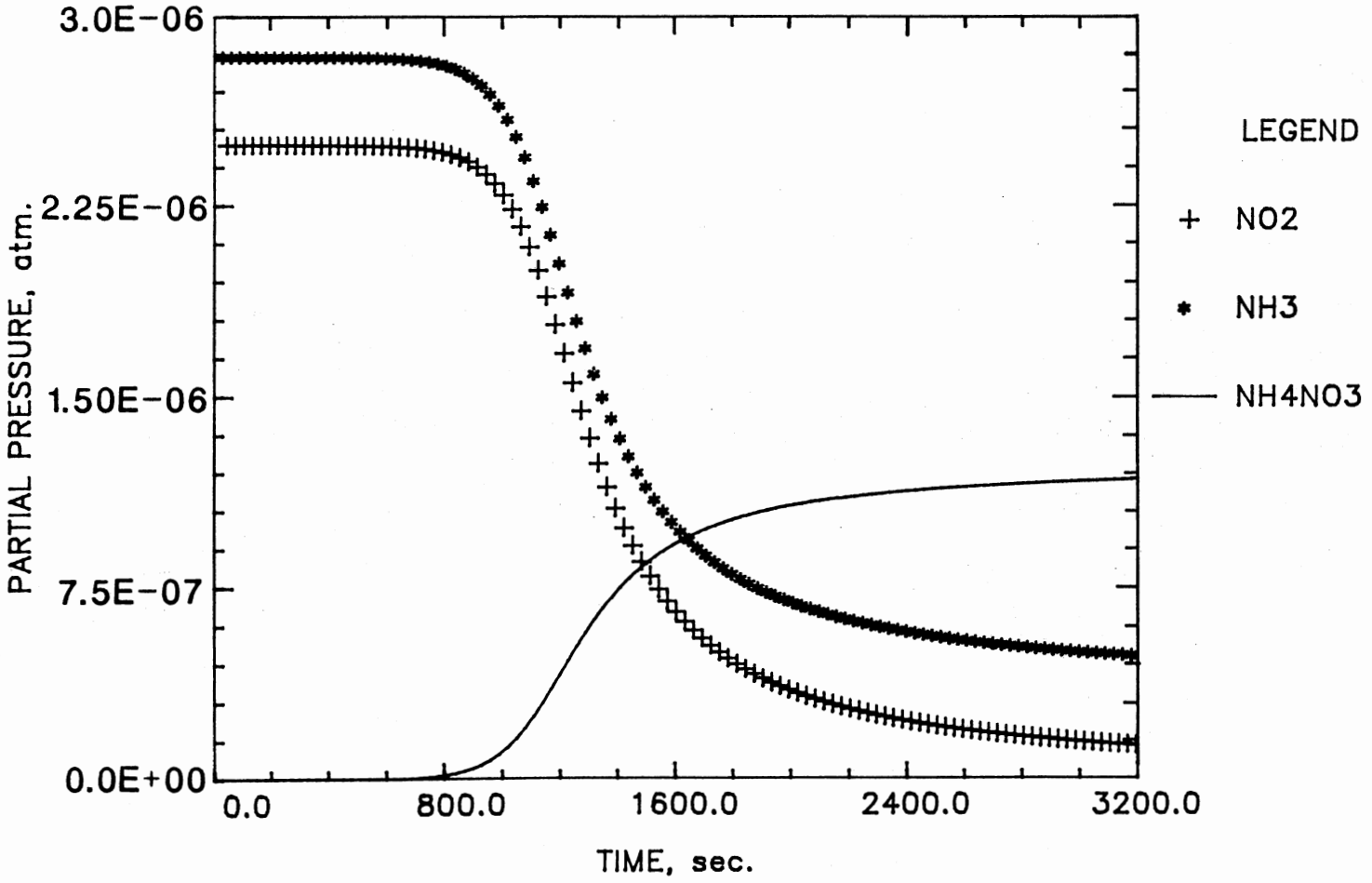

Figure 65. Variation of Partial Pressures of NO_2, NH_3 and NH_4NO_3 With Reaction Time for $[NH_3] = [NO_2] = 2.5$ ppm, RT. = 10 s and T = 21 °C (Experiment 28)

nitrogen dioxide and ammonia concentrations of 2.5 and 2.8 ppm respectively, a residence time of 10 s, and a temperature of 21.0 °C. For the case of a nitrogen dioxide concentration of 5.0 ppm and ammonia concentration of 1.13 ppm at a temperature of 20 °C and a residence time of 5 s, the prediction is shown in Figure 66.

The results of the numerical solution used in this work was checked against the analytical solution represented in equations [45] and [47], at different reaction times (t). The two solutions showed a good agreement (within 2% error) which validates the results of the model incorporated in this study.

Figure 65 shows that the production of ammonium nitrate starts after 13 minutes (800 s), while Figure 66 shows that ammonium nitrate is produced after 3 minutes (200 s). This induction time, for ammonium nitrate partial pressure to build up, is not necessarily the same induction time for the particles to be formed. This is because more time is needed for the supersaturation of ammonium nitrate to become large enough to allow for the nucleation of particles.

5.2.7 Experimental Error and Reproducibility

The error in taking the total number concentration, the total surface area, the total volume, and the size distribution measurements is estimated. As represented in Tables VI through XVII, the experimental errors, expressed as the ratio of the standard deviation to the mean values of the total number, area, and volume of particles are in the range of 0.02-1.13 (or 0.01-81 S.D.). Each size distribution measurement, taken by the DMPS, consists of 40 data points, corre-

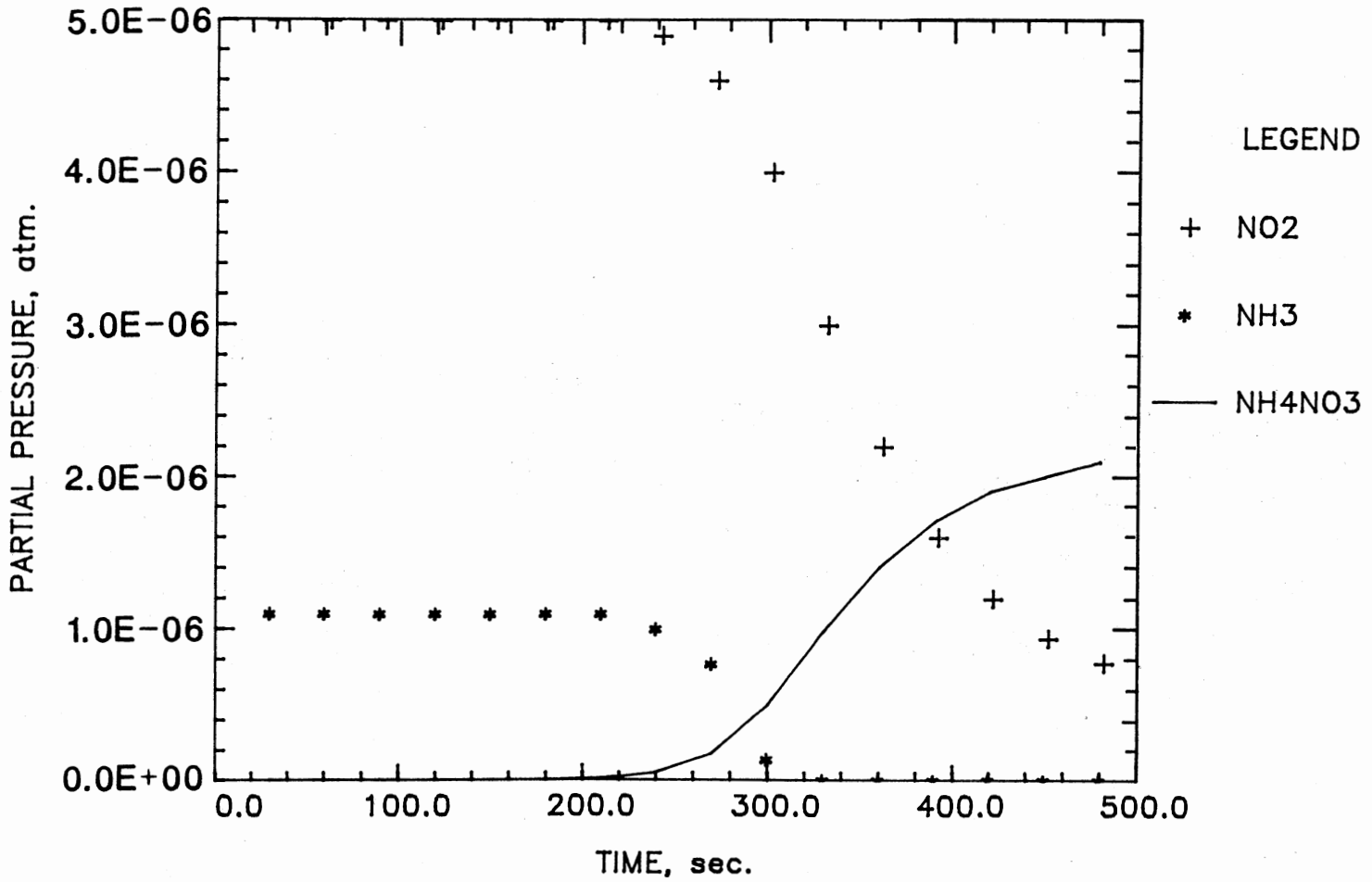

Figure 66. Variation of Partial Pressures of NO_2, NH_3 and NH_4NO_3 With Reaction Time for $[NH_3] = [NO_2] = 1$ ppm, RT. = 5 s and T = 20 °C (Experiment 47)

sponding to the 40 channels of the DMPS. The experimental error in each data point of the size distribution measurements is estimated in terms of the standard deviation and found to be in the range of 0.01-20. The experiments conducted at the very low temperatures (4 °C) show the smallest error and the experiments conducted at higher temperatures (15-20 °C) show a larger error.

Figures 67 and 68 represent the reproducibility of results in both the total number concentration and the size distribution measurements for the two sets of experiments (34 and 40) and (58 and 60), respectively. These two figures show that the system is very capable of reproducing the experiments.

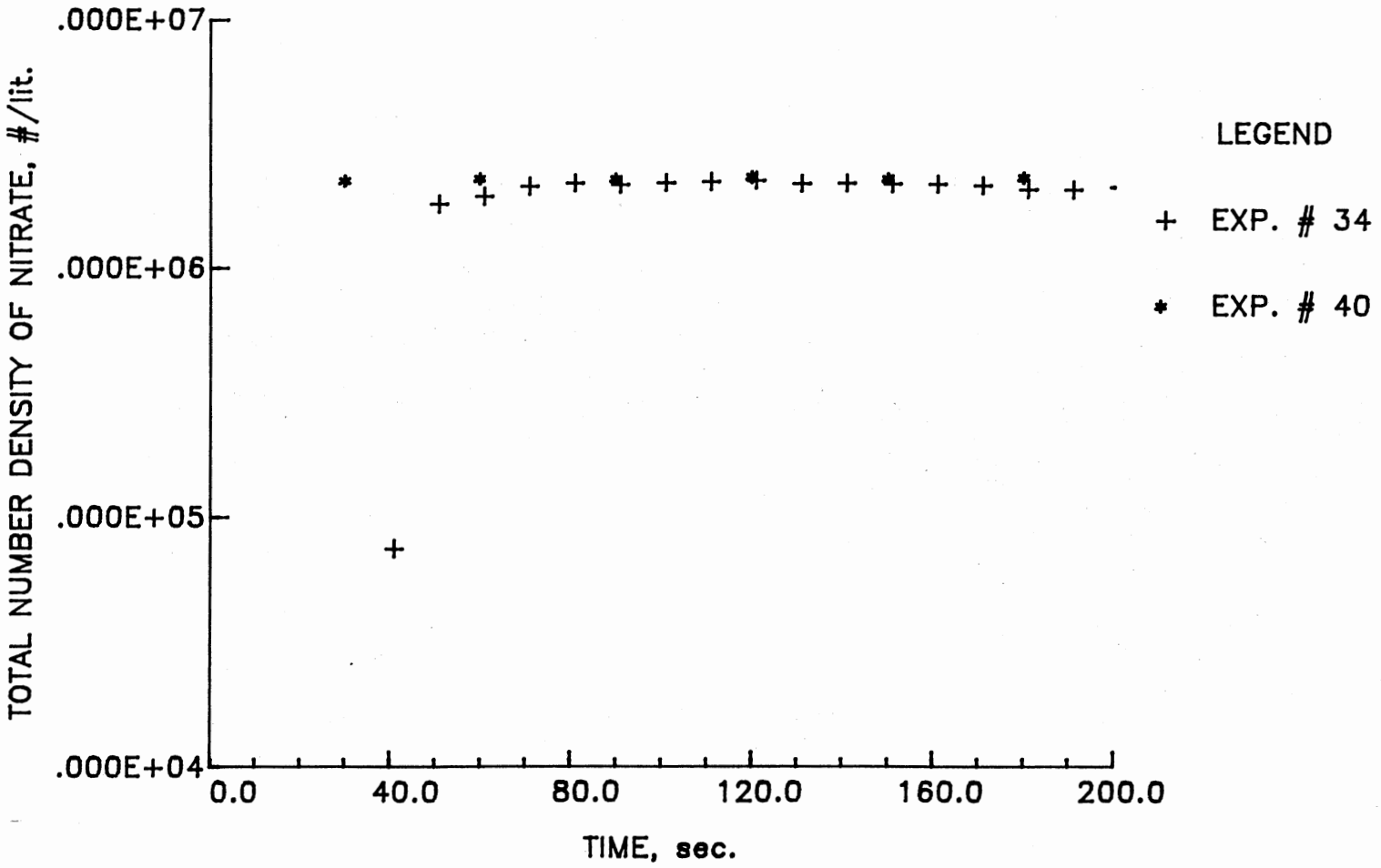

Figure 67. Reproducibility of the Total Number Concentration of Particles Measured by the DMPS for $[NH_3] = [NO_2] = 0.5$ ppm, RT. = 10 s and T = 4 °C (Experiments 58 and 60)

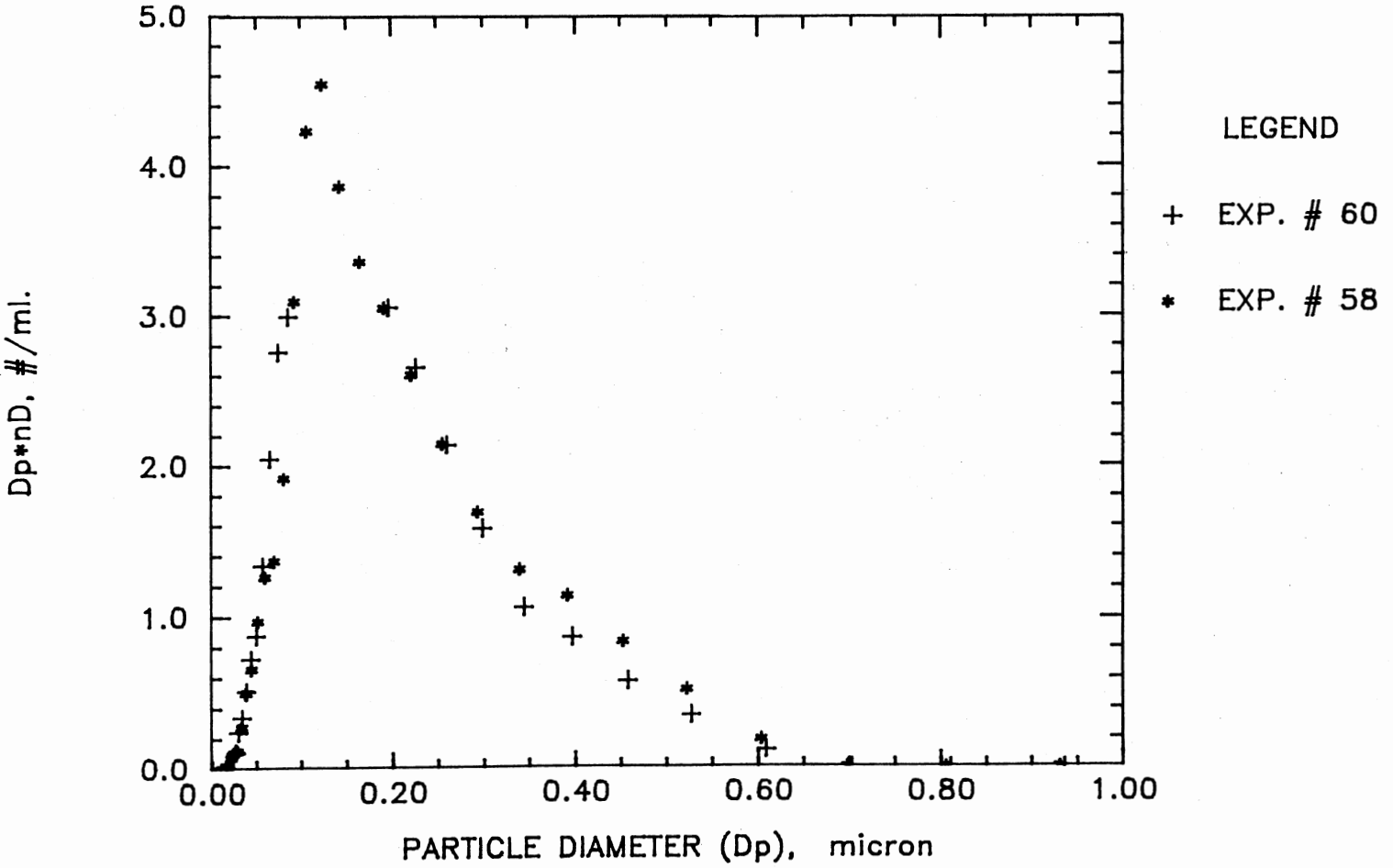

Figure 68. Reproducibility of the Particle Size Measured by the DMPS for $[NH_3] = [NO_2] = 0.5$ ppm, RT. = 10 s and T = 4 °C (Experiments 58 and 60)

CHAPTER VI

CONCLUSIONS AND RECOMMENDATIONS

6.1 Conclusions

From the results of this work, the following conclusions are drawn:

1. Ammonium nitrate aerosols form by homogeneous nucleation and grow predominantly by condensation of the monomeric NH_4NO_3. Adsorption of NH_3 and HNO_3 vapors on the particle surface followed by the surface reaction of NH_3 and HNO_3 also contributes to the particle growth, but their contribution is expected to be one order of magnitude smaller than the condensation of NH_4NO_3.

2. The growth controlling step is the diffusion of ammonium nitrate vapor to the surface of the particles.

3. A good fit, within the limits of the accuracy of the data, of the theoretical size distributions to the experimental data verified that the condensation of the NH_4NO_3 monomer is the dominant growth process.

4. Particle coagulation was found to be insignificant for the ranges of the reaction conditions under study.

5. High total number concentrations (more than 1.5×10^6 particle/l) could be formed at lower temperatures (~ 4 °C), even from very low initial reactant concentrations (~ 0.5 ppm).

6. The estimated critical size, from the experimental measurements of the DMPS, was in the range of 0.018-0.052 μm. The median diameter

and the geometric standard deviation used to fit the size distribution data were in the ranges of 0.1-0.35 μm and 1.5-2.0, respectively.

6.2 Recommendations

Recommendations for the scope of work and for the modification of instrumentation used in this study are offered here for the future investigators in this field:

6.2.1 Recommendations for the Scope of Work

1. In order to make the results of this study more applicable to the atmospheric conditions, it is recommended to conduct this study at very low temperatures ($\leq$ 0 °C), very long residence times and pressures lower than 1 atm. This will give a better representation of the actual atmospheric conditions.

2. It is also recommended to consider intermediate to high relative humidities. Since it is possible that under high humidity the do inant growth mechanism may change and condensation of water vapor or HNO_3 may become a significant growth mechanism.

6.2.2 Recommendations for the Instrumentations

1. It is recommended to use thermocouples to monitor the reaction temperature inside the reactor at the inlet and outlet ports. This is because the reaction is very sensitive to temperature and an accurate temperature measurement is needed for accurate documentation.

2. Instead of controlling the room temperature, it is recommended to use a heating/cooling jacket around the reactor with a good insulation. This will provide a more flexible system for very high and

very low temperature experiments.

3. Before taking any further size distribution measurements with DMPS system, it is recommended to find out and solve the discrepancy between the total number concentration measurements of the CNC and the DMPS.

BIBLIOGRAPHY

Appel, B. R., Wall, S. M., Tokiwa, Y., and Haik, M. (1980). Simultaneous Nitric Acid, Particulate Nitrate and Acidity Measurements in Ambient Air. Atmos. Environ. 14: 549-554.

Appel, B. R., Tokina, Y., and Haik, M. (1981). Sampling of Nitrates in Ambient Air. Atmos. Environ. 15:283-289.

Becker, R., and Doering, W. (1935). Kinetische Behandlung der Keimbildung in Ubersattigten Dampfen. Ann. Phys. (Leipzig). 24:719-752.

Besson and Rosset (1906). Compt. rend. 142:633.

Brander, J. D., Junk, N. M., Lawrence, J. W., and Robins, J. (1962). Vapor Pressure of Ammonium Nitrate. J. Chem. Engng. Data. 7:227-228.

Cadle, S. H., Countess, R. J., and Kelly, N. A. (1982). Nitric Acid and Ammonia in Urban and Rural Locations. Atmos. Environ. 16:2501-2506.

Dahlin, R. S., Su, J. and Peters, L. K. (1981). Aerosol Formation in Reacting Gases: Theory and Application to the Anhydrous NH_3-HCl System. AIChE J. 27:404-418.

de Pena, R. G., Olszyna, K., and Heicklen, J. (1973). Kinetics of Particle Growth. I. Ammonium Nitrate from the Ammonia-Ozone Reaction. J. Phys. Chem. 77:438-443.

Denbigh, J. (1971). The Principles of Chemical Equilibrium. 3rd Edn. Cambridge University Press. London.

Falk, F., and Pease, R. N. (1954). An Initial Report on the Stoichiometry and Kinetics of the Gas Phase Reaction of Nitrogen Dioxide and Ammonia. J. Am. Chem. Soc. 76:4746-4747.

Falk, F. (1955). Stoichiometry and Kinetics of the Gas Phase Reaction of Nitrogen Dioxide and Ammonia. Ph. D. Dissertation.

Farkas, L. (1927). Keimbildungsgeschwindigkeit in ubersattigten dampfen. Z. Phys. Chem. 125:236-242.

Fissan, H. J., Helsper, C., and Thielen, H. J. (1982). Determination of Particle Size Distributions by Means of an Electrostatic Classifier. Proceedings of 10th Annual Conference, Gesellschaft für Aerosolforschung, Bologna, Italy.

Forrest. J., Tanner, R. L., Spandau, D., D'Ottavio, T., and Newman, L. (1980). Atmos. Enviro. 14:137.

Forrest. J., Spandau, D., Tanner, R. L., and Newman, L. (1982). Atmos. Enviro. 16:1473.

Frenkel, J. (1955). Kinetic Theory of Liquids. Dover, New York.

Friedlander, S. K., (1977). Smoke, Dust, and Haze. Wiley, New York.

Friedlander, S. K., (1983). Dynamics of Aerosol Formation by Chemical Reaction. Ann. New York Acad. Sci., 404:354-364.

Gelbard, F., and Seinfeld, J. H. (1978). Numerical Solution of the Dynamic Equation for Particulate Systems. J. Comp. Phys. 28:357-375.

Gelbard, F., and Seinfeld, J. H. (1979). The General Dynamic Equation for Aerosols: Theory and Application to Aerosol Formation and Growth. J. Colloid Interface Sci. 68:363-382.

Gelbard, F., and Seinfeld, J. H. (1980). Simulation of Multicomponent Aerosol Dynamics. J. Colloid Interface Sci. 78:485-501.

Gonzalez, A. (1980). Aerosol Formation in the NH_3-HCl System, M.S. thesis, University of Kentucky.

Grennfelt, P. (1980). Investigation of Gaseous Nitrates in an Urban and Rural Area. Atmos. Environ. 14:311-316.

Henry, J. G., Gonzalez, A., and Peters, L. D. (1983). Dynamics of NH_4Cl Particle Nucleation and Growth at 253-296 K. Aerosol Sci. Technol. 2:321-339.

Hoppel, W. A. (1978). Determination of the Aerosol Size Distribution From the Mobility Distribution of the Charged Fraction of Aerosols. J. Aerosol Sci. 9:41-54.

Kadowaki, S. (1977). Size Distribution and Chemical Composition of Atmospheric Particulate Nitrate in the Nagoya Area. Atmos. Environ. 11:671-675.

Kaischew, R. and Stranski, I. N. (1934). Zur Kinetischen ableitung der Keimbildungsgeschwindigkeit. Z. Phys. Chem., Abt. B 26:317-326.

Keady, P. B., Quant, F. R., and Sem, G. J. (1983). Differential Mobility Particle Sizer: A New Instrument for High-Resolution Aerosol Size Distribution Measurement Below 1 μm. TSI Quarterly. Issue 2, IX:3-11.

Keady, P. B. (1988). TSI. St. Paul, Minnesota. Personal communications on August 4, 1988.

Kodas, T. T., and Friedlander, S. K. (1988). Design of Tubular Flow Reactors for Monodisperse Aerosol Production. AIChE J. 34:551.557.

Kodas, T. T., Pratsinis, S. E., and Friedlander, S. K. (1986). Aerosol Formation and Growth in a Laminar Core Reactor. J. Colloid Interface Sci. 111:102-111.

Lothe, J., and Pould, G. M. (1962). Reconsiderations of nucleation theory. J. Chem. Phys. 36:2080-2085.

Mearns, A. M., and Ofosu-Asiedu, K. (1984a). Kinetics of Reaction of Low Concentration Mixtures of Oxides of Nitrogen, Ammonia and Water Vapor. J. Chem. Tech. Biotechnol. 34A:341-349.

Mearns, A. M., and Ofosu-Asiedu, K. (1984b). Ammonium Nitrate Formation in Low Concentration Mixtures of Oxides of Nitrogen, Ammonia and Water Vapor. J. Chem. Tech. Biotechnol. 34A:350-354.

Middleton, P., and Brock, J. (1976). Simulation of Aerosol Kinetics. J. Colloid Interface Sci. 54:249-264.

Moskowitz, A. H. (1977). Particle Size Distribution of Nitrate Aerosols in the Los Angeles Air Basin. U. S. Environmental Protection Agency, EPA-600/3-77-053.

Olszyna, K. J., DePena, R. G., Luria, M., and Heicklen, J. (1974). Kinetics of Particle Growth-IV: NH_4NO_3 from the NH_3-O_3 Reaction Revisited. J. Aerosol Sci. 5:421-434.

Pilinis, C. and Seinfeld, J. H. (1987). Mathematical Modeling of the Dynamics of Multicomponent Atmospheric Aerosols. Atmos. Environ. 21:943-955.

Plomp, A., ten Brinck, H. M., Spoelstra, H., and van der Vate, J. F. (1982). A High Resolution Electrical Mobility Aerosol Spectrometer (MAS). Proceedings of 10th Annual Conference, Gesellschaft für Aerosolforschung, Bologna, Italy.

Pratsinis, S. E., Kodas, T. T., Dudukovic, M. P., and Friedlander, S. K. (1986). The Effect of Aerosol Reactor Residence Time Distribution on Product Aerosol Characteristics. Chem. Eng. Sci. 41:693-700.

Russell, A. G., McCue, K. F., and Cass, G. R. (1988). Mathematical Modeling of the Formation of Nitrogen-Containing Air Pollutants. 1. Evaluation of an Eulerian Photochemical Model. Environ. Sci. Technol. 22:263-271.

Seapan, M., Selman, D., Seale, F., Siebers, G., and Wissler, E. H. (1982). Aerosol Characterization Using Molecular Beam Techniques. J. Colloid Interface Sci. 87:154-166.

Seinfeld, J. H. (1986). Atmospheric Chemistry and Physics of Air Pollution. John Wiley & Sons. New York.

Seinfeld, J. H., and Bassett, M. (1982). "Effect of the Mechanism of Gas-to-Particle Conversion on the Evolution of Aerosol Size Distributions," in Heterogeneous Atmospheric Chemistry, Schryer, D. R. (Ed.), American Geophysical Union, Washington, D.C., 6-12.

Shaw, R. W., Jr., Stevens, R. K., Bowermaster, J. (1982). Atmos. Environ. 16:845.

Springer, G. S. (1978). "Homogeneous Nucleation," in Advances in Heat Transfer, Vol. 14, Academic Press, New York, 281-346.

Stelson, A. W., Friedlander, S. K., and Seinfeld, J. H. (1979). A Note on the Equilibrium Relationship Between Ammonia and Nitric Acid and Particulate Ammonium Nitrate. Atmos. Environ. 13:369-371.

Stelson, A. W., and Seinfeld, J. H. (1982). Relative Humidity and pH Dependence of the Vapor Pressure of Ammonium Nitrate-nitric Acid Solutions at 25 °C. Atmos. Environ. 16:993-998.

Su, J. (1979). Experimental Studies on Aerosol Formation in the NH_3-HCl and NH_3-SO_2 Systems at ppm Concentration Levels. M.S. thesis, University of Kentucky.

Thomson, W. (1870). On the Equilibrium of Vapor at a Curved surface of Liquid. Proc. R. Soc. Edinburgh. 7:63-68.

Tran, T. T., and Seapan, M. (1984). Formation of NH_4NO_3 By NH_3 + NO_2 Reaction. Proceedings of the First International Aerosol Conference, Minneapolis, Minnesota, U.S.A.

Vega, E., and Peters, L. K. (1983). Dydnamics of Cluster Growth During Homogeneous Nucleation of Supersaturated Vapor. Aerosol Sci. Technol. 2:513-529.

Volmer, M., and Weber, A. (1926). Keimbildung in Ubersattigten Gebilden. Zeitschrift Phys. Chem. 119:277-301.

Volmer, M., (1929). Uber Keimbildung und keimwirkung als specialfalle der heterogenen katalyse. Z. Elektrochem. 35:555-561.

Volmer, M. (1939). Kinetic der Phasenbildung. Steinkoph, Dresden.

Warren, D. R., and Seinfeld, J. H. (1984). Nucleation and Growth of Aerosol From a Continuously Reinforced Vapor. Aerosol Sci. Technol. 3:135-153.

Warren, D. R., and Seinfeld, J. H. (1985). Simulation of Aerosol Size Distribution Evolution in Systems With Simultaneous Nucleation, Condensation, and Coagulation. Aerosol Sci. Technol. 4:31-43.

Weiss, G. (Ed.) (1986). Hazardous Chemicals Data Book. Noyes Data Corporation, N. J.

Yoshizumi, K., and Hoshi, A. (1985). Size Distributions of Ammonium Nitrate and Sodium Nitrate in Atmospheric Aerosols. Environ. Sci. Technol. 19:258-261.

Zeldovich, J. (1942). Theory of Nucleation and Condensation. Sov. Phys.-JETP (Engl. Transl.) 12:525.

Zettlemoyer, A. C. (Editor) (1969). Nucleation. Marcel Dekker, Inc. New York.

APPENDIX A

CALIBRATION DATA FOR THE FLOWMETERS

The four rotameters used in this project were calibrated three times during this study by using a 250 ml bubblemeter. The measured data indicated that the minimum standard deviation is in the order of 0.01 at low flowrates, and the maximum standard deviation is in the order of 2.0 at very high flowrates. A summary of the measured and fitted calibration data is presented in Tables XXI and XXII, respectively.

TABLE XXI

SUMMARY OF THE MEASURED CALIBRATION DATA FOR THE FOUR ROTAMETERS

Date	Rotameter #6		Rotameter #7		Rotameter #8		Rotameter #9	
	Setting	Flow ml/s	Setting	Flow ml/s	Setting	Flow ml/s	Setting	Flow ml/s
1-9-87	0.55	0.0	0.45	0.0	0.60	0.0	0.65	0.0
	1.30	10.8	1.30	10.9	1.30	13.0	1.30	12.5
	1.80	16.0	1.80	15.9	1.80	19.7	1.80	18.1
	2.20	21.5	2.20	21.5	2.20	24.4	2.20	23.2
	2.90	30.2	2.90	30.0	2.90	33.3	2.90	32.8
	4.00	44.7	4.00	44.0	4.00	46.3	4.00	46.5
	5.00	54.5	5.00	57.4	5.00	61.1	5.00	60.0
	5.60	64.7	5.60	62.6	5.60	68.7	5.60	66.3
	5.90	66.1	5.90	70.7	5.90	72.6	5.90	73.8
	7.00	81.8	7.00	83.5	7.00	87.0	7.00	91.6
	7.90	95.5	7.90	99.8	7.90	100.3	7.90	104.5
	8.50	101.2	----	----	8.50	110.3	----	----
8-10-87	0.55	0.0	0.45	0.00	0.60	0.00	0.65	0.0
	1.10	6.6	1.00	6.5	1.00	8.7	0.90	7.7
	1.80	15.8	1.50	15.0	1.75	18.4	1.30	11.9
	2.50	24.6	2.30	22.8	2.45	27.4	1.65	17.4
	3.00	32.2	2.95	30.9	3.00	35.3	2.40	26.4
	3.70	41.4	4.00	46.9	4.55	54.8	2.90	33.4
	4.40	50.5	4.70	54.8	----	----	3.80	44.6
	5.00	58.6	5.30	60.8	----	----	4.10	52.0
	----	----	----	----	----	----	5.90	71.6
11-8-87	0.55	0.00	0.45	0.00	0.60	0.00	0.65	0.0
	1.15	7.8	1.75	15.7	2.90	34.1	2.00	20.8
	3.10	32.5	2.90	29.3	4.65	58.0	3.00	34.5
	4.50	53.9	3.60	39.5	6.05	76.8	4.50	53.8
	5.80	71.9	4.10	45.9	7.60	99.5	5.75	73.6
	7.80	94.2	5.50	65.2	----	----	7.00	85.9
	8.55	119.7	7.00	84.7	----	----	----	----

TABLE XXII

SUMMARY OF THE FITTED CALIBRATION DATA FOR THE FOUR ROTAMETERS

Rotameter	Rotameter Setting	Flowrate, ml/sec		
		Date: 1-9-87	Date: 8-10-87	Date: 11-8-87
# 6	1.00	5.9	5.46	4.7
	1.50	12.3	12.0	11.8
	2.00	18.6	18.7	18.9
	2.50	25.0	25.3	26.0
	3.00	31.3	31.9	33.1
	3.50	37.7	38.6	40.2
	4.00	44.0	45.2	47.3
	4.50	50.3	51.8	54.4
	5.00	56.7	58.5	61.5
	5.50	63.0	56.1	68.6
	6.00	69.4	71.7	75.7
	6.50	75.7	78.3	82.8
	7.00	82.0	85.0	89.9
	7.50	88.4	91.6	97.0
	8.00	94.7	98.2	104.1
	8.50	101.1	104.9	111.2
# 7	1.00	5.8	7.1	6.0
	1.50	12.3	13.5	12.5
	2.00	18.9	19.8	19.0
	2.50	25.4	26.2	25.5
	3.00	32.0	32.6	32.0
	3.50	38.5	38.9	38.6
	4.00	45.1	45.3	45.1
	4.50	51.6	51.7	51.6
	5.00	58.2	58.0	58.1
	5.50	64.7	64.4	64.6
	6.00	71.3	70.8	71.1
	6.50	77.8	77.1	77.7
	7.00	84.4	83.5	84.2
	7.50	90.9	89.9	90.7
	8.00	97.5	96.2	97.2
	8.50	104.0	102.6	103.7

TABLE XXII (Continued)

Rotameter	Rotameter Setting	Flowrate, ml/sec		
		Date: 1-9-87	Date: 8-10-87	Date: 11-8-87
# 8	1.00	7.4	7.5	6.2
	1.50	14.1	14.2	13.3
	2.00	20.8	21.0	20.3
	2.50	27.6	27.8	27.4
	3.00	34.3	34.6	34.5
	3.50	41.0	41.4	41.5
	4.00	47.8	48.2	48.6
	4.50	54.5	55.0	55.6
	5.00	61.2	61.8	62.7
	5.50	68.0	68.6	69.7
	6.00	74.7	75.4	76.8
	6.50	81.4	88.1	83.9
	7.00	88.2	88.9	90.9
	7.50	94.9	95.7	98.0
	8.00	101.6	102.5	105.0
	8.50	108.4	109.3	112.1
# 9	1.00	5.9	7.6	6.3
	1.50	12.9	14.3	13.1
	2.00	19.9	21.1	20.0
	2.50	26.9	27.8	26.8
	3.00	33.8	34.5	33.6
	3.50	40.8	31.2	40.4
	4.00	47.8	47.9	47.3
	4.50	54.8	54.6	54.1
	5.00	61.7	61.4	60.9
	5.50	68.7	68.1	67.7
	6.00	75.7	74.8	74.6
	6.50	82.7	81.5	81.4
	7.00	89.6	88.2	88.2
	7.50	96.6	94.9	95.0
	8.00	103.6	101.6	101.9
	8.50	110.5	108.4	108.7

APPENDIX B

DETAILED EXPERIMENTAL PROCEDURE

Procedure for the Particle Measuring System

There are two different operating modes for the Differential Mobility Particle Sizer System (DMPS): the overpressure mode, which can be used when the pressure of the aerosol flow system is high enough, and the underpressure mode, which is used when the aerosol stream has low pressure. Different apparatus setup and different operating procedures are used for each mode. These are described in the DMPS operating manual. In this study the underpressure mode is used because the experiments were done at atmospheric pressure. This procedure includes preparing the Condensation Nucleus Counter (CNC), calculating the proper flowrates of the Electrostatic Classifier, and setting the parameters of the DMPS program.

1. Make sure that the butanol bottle in the rear of the CNC is filled to at least 2/3 level.
2. Set the butanol drain switch on the rear panel of the CNC to the closed position, and turn on the power to the CNC. After a few minutes, check that the alcohol has filled the reservoir and that the indicator lights are reading properly. The heater light should flash on and off. The condenser light and alcohol level light should be on continuously. Allow the CNC a full 20 minutes to warm-up.
3. Before making the measurement, calculate the flowrates needed for the Electrostatic Classifier (EC).
4. Reduce the Analyzer Voltage to zero by turning the Analyzer Voltage Knob counter-clockwise to stop, and then turn on the power to the EC.
5. Prior to turning any pumps, adjust the valves as follows:

Sheath air valve 13	--	fully open
Monodisperse aerosol valve 14	--	fully open
Excess air valve 15	--	fully closed
External metering valve 16	--	fully closed

6. Turn on the power to both the external vacuum pump (3103) and the CNC pump.
7. Turn the meter selection switch on the EC to the Excess Air Flowmeter.
8. Turn the Meter Selection switch to the Monodisperse Air flowmeter. Slowly open the external metering valve 16 so the monodisperse aerosol is at the proper flowrate. The voltage will first decrease and then will increase due to a flow reversal. Be sure air is flowing out of the monodisperse aerosol exit. Leave the monodisperse aerosol valve 14 to the fully open position.
9. Turn the Meter Selection switch to the Sheath Air flowmeter. Adjust the Sheath Air valve 13 to the correct flow.
10. Check to see that the impactor pressure drop agrees with its flow calibration.
11. Repeat steps (7) through (10) until all flowrates are properly set. The CNC pump must be on while setting the flows.
12. Check to see that the CNC flowmeter is reading in the null position.
13. Remove the impactor head screw. Place a light coating of grease on the impaction surface. Replace the head screw.
14. Perform the final system check as follows:
    Make pre-sampling check on the system by measuring the aerosol concentration coming out of the monodisperse aerosol port with zero

voltage potential on the center rod. If the system has perfectly laminar flow and is leak tight, there will be no particles measured by the CNC. The external filter on the sheath air inlet in the under pressure mode (which is the mode used in this work) helps to eliminate all particles from the sheath air. Recheck and fine tune the system flowrates to eliminate any turbulence (i.e. have the CNC read zero particles). Check all fittings and filters for possible leaks. Do not take size distribution measurements if the concentration measured by the CNC exceeds a few tenths of a particle/cc.

15. If the DMPS software is to be used to take the measurements, then turn on the power to the computer and to the DMPS interface box and boot up the DMPS program.
16. To record the total number density of the aerosol as a function of time, use the "COUNT" program.

Procedure for the Particle Generating System

1. Calculate the required flowrates of air, NH_3-air, and NO_2-air gases corresponding to the desired concentrations of NH_3 and NO_2.
2. Turn off the power to both vacuum pumps.
3. Connect the reactor outlet to the CNC through valve 12, and make sure that valves 4, 5, 6, 7, 8, 9, 11, 12 and 18 are open, while valves 1, 2, 3, 10 and 17 are closed (see Figure 2.)
4. Open valve 1 to allow air to flow through the system, and adjust for the desired flow in flowmeters 7 and 9 by using valves 1, 4 and 5, and turn on the vacuum pump in the CNC. Check for foreign particles by monitoring the reading of the CNC display. For a

clean system the CNC should read zero particle/cm^3.

5. Open valve 2 to allow NO_2 to flow through the system, and adjust for the desired flowrate by using valves 2 and 8. Check for foreign particles.
6. Have the program COUNT ready if the computer is to be used to record the change in the total number of particles with time.
7. Open valve 3 to allow NH_3 to flow into the system, and quickly adjust for the desired flowrate by using valves 3 and 6.
8. Start the program COUNT immediately after allowing the NH_3 to flow, and wait until steady state is reached.
9. After the total number of particles reaches steady state, turn off the vacuum pump in the CNC.
10. Open valve 10 and close valve 12 to allow gases to flow through the electrostatic classifier (make sure that valves 13 and 14 are fully open while valves 15 and 16 are fully closed).
11. Turn on the vacuum pump in the CNC and the external vacuum pump and adjust for the desired excess air, sheath air and monodisperse flowrates by using valves 15, 13 and 16 respectively.
12. Add a very thin layer of grease to the impactor head, and adjust the EC flowrates so that the CNC reads zero particles. (See Step 12 in the particle measuring system procedure.)
13. Start taking the reading from the DMPS. If the computer is to be used to take the measurements, then the Analyzer Voltage toggle switch (on the front panel of the EC) needs to be on the EXTERNAL PROGRAM position and the Average Time switch (on the front panel of the CNC) needs to be at the SHORT position.

APPENDIX C

HEALTH HAZARDS OF REACTING SPECIES

TABLE XXIII

HEALTH HAZARDS OF REACTING SPECIES, WEISS (1986)

ITEM	NO_x	NH_3	NH_4NO_3
Personal Protective Equipment	Robber gloves, safety goggles and face shield; protective clothing; acid gas canister respirator or self-contained breathing apparatus.	Gas-tight chemical goggles, self-contained breathing apparatus, rubber boots, rubber gloves, emergency shower and eye bath.	Wear self-contained breathing apparatus.
Symptoms Following Exposure	Very concentrated fumes causes coughing, choking, headache, nausea, pain in chest and abdomen; otherwise few symptoms appear at time of exposure.	700 ppm causes eye irritation, and permanent injury may result if prompt remedial measures are not taken, 5000 ppm can cause immediate death from spasm.	Irritation of eyes and mucous membranes. Absorption via ingestion or inhalation causes irritation and acid urine.
Treatment of Exposure	Inhalation: remove patient to fresh air and have him breathe as deeply as possible; call a doctor, enforce complete rest for 24-48 hours. Keep warm, give oxygen if coughing starts. Eyes and Skin: flush with water for 15 minutes.	Inhalation: move victim to fresh air and give artificial respiration if necessary. Oxygen may be useful. Skin and Eyes: flood immediately with water for 15 minutes. Treat subsequently as thermal burn.	Remove from exposure - symptoms reversible
Threshold Limit Value	3 ppm	25 ppm	Not pertinent
Short Term Inhalation Limits	25 ppm for 5 minutes	50 ppm for 5 minutes	Not pertinent
Toxicity by Ingestion	Data not available	Not pertinent	Data not available
Late Toxicity	Data not available	Not pertinent	Data not available
Vapor Irritant Characteristics	Vapor causes severe irritation to eyes and throat and can cause eye and lung injury.	Vapor causes severe eye or throat irritation and may cause eye or lung injury.	Not pertinent
Liquid or Solid Irritant Characteristics	Severe skin irritant, causes second and third-degree burns on short contact and is very injurious to the eyes.	Causes smarting of the skin and first-degree burn on short exposure.	None
Odor Threshold	5 ppm	46.8 ppm	Not pertinent

VITA

Walid Saleh Bou-Hamra

Candidate for the Degree of

DOCTOR OF PHILOSOPHY

Thesis: FORMATION OF AMMONIUM NITRATE AEROSOLS BY GAS-PHASE REACTION OF AMMONIA AND NITROGEN DIOXIDE

Major Field: Chemical Engineering

Biographical:

Personal Data: Born in Kuwait City, Kuwait, 1958, the son of Saleh and Shaika Bou-Hamra. Married to Hanan A. Gaith on July 9, 1979.

Education: Graduated from Edayliyah High School, Kuwait, in 1976; received Bachelor of Science Degree in Chemical Engineering from Kuwait University in 1981; received Master of Science Degree in Chemical Engineering from Oklahoma State University in December, 1985; completed requirements for the Doctor of Philosophy Degree at Oklahoma State University in December, 1988.